Regulation and functions of burst firing: the role of KCNQ3 potassium channels *in vivo*

DISSERTATION

zur Erlangung des akademischen Grades
doctor rerum naturalium
(Dr. rer. nat.)
im Fach Biologie

eingereicht an der
Lebenswissenschaftlichen Fakultät
Humboldt-Universität zu Berlin

von
Frau M.Sc. Xiaojie Gao

Präsidentin der Humboldt-Universität zu Berlin:
Prof. Dr.-Ing. Dr. Sabine Kunst
Dekan der der Lebenswissenschaftlichen Fakultät:
Prof. Dr. Bernhard Grimm

Gutachter/in: 1. Prof. Dr. Andrew Plested
2. Prof. Dr. Susanne Schreiber
3. Prof. Dr. Tatiana Korotkova

Tag der mündlichen Prüfung: 12.12.2019

The experimental and analytical work of this thesis was performed from 2013 to 2018 under supervision of Dr. Alexey Ponomarenko and Dr. Tatiana Korotkova at the Leibniz Institute for Molecular Pharmacology (FMP), Berlin, Germany.

Abstract

Ion channels conduct ion flows across neuronal membrane whereby action potential is generated and propagated. They play a central role in regulating the excitability and firing behavior of a neuron. Among them, the KCNQs present a prominent family of voltage-gated potassium channels. Dysfunction of KCNQ2–5 channels can lead to varied neurological diseases including early onset epilepsy and deafness. In cortex and hippocampus, KCNQ2 and KCNQ3 have been demonstrated to underlie the non-inactivating M-current critical for controlling the repetitive firing of pyramidal cells. However, the functional significance of KCNQ3, unlike that of KCNQ2, remains elusive. Here, by applying *in vivo* extracellular electrophysiology in *Kcnq3* constitutive knockout mice and the wild-type littermates, we find that hippocampal pyramidal cells lacking KCNQ3 exhibit increased burst firing. Moreover, the spike frequency adaptation of their bursts is diminished, and the burst propensity during two different field oscillations – theta versus non-theta – becomes indistinguishable. During theta oscillations, *Kcnq3* knockout pyramidal cells no longer display unimodal phase preference and do not coordinate their burst firing. But phase advancement along successive theta cycles continues to occur at times of transiently intensified firing. The selective firing of place cells is largely preserved in the knockout while mainly relying on bursts. These results suggest that KCNQ3 channels indeed play a significant and specific role in regulating the neurons' excitability and information processing, thus providing crucial mechanistic insights into the relevance of the KCNQ3 channels in neurological disorders.

Keywords: KCNQ3, *in vivo* electrophysiology, burst firing, network oscillations

Zusammenfassung

Ionenkanäle leiten Ionenströme über neuronale Membranen, wodurch Aktionspotentiale erzeugt und weitergeleitet werden. Sie spielen eine zentrale Rolle bei der Regulierung der Erregbarkeit und des Aktivierungsverhaltens von Neuronen. KCNQs sind eine wichtige Familie von spannungsgesteuerten Kaliumkanälen; ihre Dysfunktion kann zu verschiedenen neurologischen Krankheiten führen, einschließlich Erkrankung an Epilepsie und Taubheit. Es wurde gezeigt, dass KCNQ2 und KCNQ3 den M-Strom verantwortlich sind. Letzterer ist für die Regulierung des repetitiven Feuerns von Pyramidenzellen entscheidend. Im Gegensatz zu KCNQ2, ist die funktionelle Bedeutung von KCNQ3 noch nicht aufgeklärt. In dieser Arbeit zeigen wir mittels extrazellulärer Elektrophysiologie *in vivo*, dass bei konstitutiven *Kcnq3* Knockoutmäusen die hippokampalen Pyramidenzellen vermehrt burstartig feuern. Außerdem weisen diese Tiere eine verminderte Spike-Frequenz-Anpassung auf und die Wahrscheinlichkeit des Burst-Feuerns während zwei verschiedener Oszillationen – Theta gegen Nicht-Theta – kann nicht mehr unterscheiden werden. Des Weiteren zeigen *Kcnq3*-Knockout-Pyramidenzellen während der Theta-Oszillation weder eine dominante Phasenpräferenz, noch eine Koordination ihrer Burst-Feuerung. Die Thetawellen Phasenpräzision tritt weiterhin bei dem vorübergehend verstärkten Feuern auf. Das räumliche selektive Feuern von mutmaßlichen Ortszellen blieb auch bei den Knockout-Mäusen erhalten, aber es ist hauptsächlich vom Burst-Feuern abhängig. Diese Studie zeigt, dass der KCNQ3-Ionenkanal eine wichtige Rolle bei der Regulierung der neuronalen Erregbarkeit und der Informationsverarbeitung spielt, und gibt damit Einblicke in die Bedeutsamkeit der KCNQ3-Ionenkanäle bezüglich der neurologischen Störungen.

Schlagwörter: KCNQ3, *in vivo* Elektrophysiologie, Burst Feuerung, Netzwerk Oszillationen

Acknowledgement

First of all, I would like to thank Tatiana Korotkova and Alexey Ponomarenko for their co-supervision. Their enthusiasm for neuroscience has been inspiring. I have learnt a lot from their expertise on *in vivo* electrophysiology. I truly appreciate the freedom I have to explore the research subject and my own scientific interests. I also thank my colleagues Maria Gorbati, Marta Carus and Franziska Bender for their friendly help in the lab.

I am greatly indebted to Thomas J. Jentsch, Sebastian Schütze and Matthias Heidenreich. During our collaboration on the KCNQ3 project, they provided insightful feedbacks and stimulating discussion on the experiments as well as direct inputs on the writing for the publication.

I am also grateful to Lisa Marshall and Sonja Binder. It was a valuable experience to collaborate with them and to gain knowledge on the more clinical aspects of the brain oscillations.

Additional thanks go to Marina Spors who offered me kind encouragement alongside her competent administrative support.

I gratefully acknowledge the financial and academic support from the Leibniz-Forschungsinstitut für Molekulare Pharmakologie and Deutsche Forschungsgemeinschaft (SPP1665).

Finally, my deepest gratitude goes to my family and friends for their continuous, unconditional love and support.

Contents

1 Introduction 4

1.1 Hippocampus 6

1.1.1 The anatomy and organization 6

1.1.2 Hippocampal theta oscillations 8

1.1.3 The function of hippocampus in spatial memory 11

1.2 The burst firing of neurons 13

1.2.1 Burst as a distinct mode of action potentials 14

1.2.2 The mechanisms of burst generation in hippocampal pyramidal cells 15

1.2.3 Functional implications of burst firing 19

1.3 KCNQ3 potassium channels 21

1.3.1 The structure of KCNQ3 channels 21

1.3.2 The expression of KCNQ3 channels 22

1.3.3 The role of KCNQ3 in neuronal excitability 23

1.3.4 KCNQ3 in human diseases and related animal models 26

1.4 In vivo extracellular electrophysiology 28

1.4.1 Recording extracellular field potentials 29

1.4.2 Unitary recordings 30

2 Methods 32

2.1 Animals 32

2.2 Electrophysiology *32*

2.2.1 Electrodes 32

2.2.2 Surgical implantation 33

2.2.3 Data acquisition 34

2.2.4 Behavioral paradigms 34

2.3 Analysis of in vivo electrophysiological data *35*

2.3.1 Local field potential analysis 35

2.3.2 Spike sorting 36

2.3.3 Characterization of recorded units 37

2.3.4 Analysis of burstiness 38

2.3.5 Cross-correlation of unit pairs 40

2.3.6 Place cell analysis 40

2.3.7 Theta phase and phase precession analysis 41

3 Results 43

3.1 Firing rate of Kcnq3$^{-/-}$ pyramidal cells *43*

3.2 The burst firing of Kcnq3$^{-/-}$ pyramidal cells *43*

3.2.1 Increased burst firing and diminished frequency accommodation 43

3.2.2 Recent spiking reduced burst probability 46

3.2.3 The distribution of burst probability in the pyramidal cells 47

3.2.4 Decreased dependence of burst firing on the network state 50

3.3 The neuronal firing during theta oscillations *52*

3.3.1 The theta modulation of burst firing 52

3.3.2 The patterns and condition of theta phase precession 54

3.4 Spatial signaling by bursts and single spikes 59

3.5 Reduced gamma and ripple oscillations in Emx1-ΔKcnq3 mice 63

4 Discussion 65

4.1 The implications of increased burstiness of Kcnq3$^{-/-}$ pyramidal cells 65

4.2 The discrepancy between in vitro and in vivo findings regarding the functions of KCNQ3 channels 67

4.3 The relevance of KCNQ3 channels for the functions of hippocampus 68

4.3.1 Enabling spatial representation in both bursts and single spikes 68

4.3.2 Controlling theta phase preference but not phase precession 69

4.3.3 Contributing to local high frequency oscillations 70

4.3.4 Implications for protection against over-excitability 71

4.4 Different roles of KCNQ2 and KCNQ3 in the neuronal excitability 73

4.5 Clinical implications 74

4.6 Future studies 75

4.7 Concluding remarks 76

5 Appendix 77

5.1 Table 2: Properties of place cells 77

6 References 78

7 Abbreviation 98

1 Introduction

> "We consider diseases not as something personal and special, but only a manifestation of life under modified conditions, operating according to the same laws as apply to the living body at all times, from the first moment until death."
>
> — Rudolf Virchow, Die Epidemien von 1848.

The mother cried out, her hands pressing against the window. Inside the intensive caring unit, a baby was hitting his arms and legs repeatedly. His face twisted and went red. For a second, he stopped breathing. The EEG monitor first displayed dramatic waves and spikes, which eventually subsided when the baby resumed his breathing and the jerking ceased. This was the third time in a week; the first occurred six days after birth, the mother recalled. She was not entirely unprepared. It was something in the family that surfaced occasionally with the arrival of a new member. Her mother and a cousin had it. Nor was she devastated since the doctor had reassured her that the seizure was of a benign nature and most of the affected newborns could overcome it and grow up normally. But she could not help worrying. The moments of her cousin having seizure attacks in his schoolyears were always in her mind[1].

This could be a typical scenario in families beset by benign familial neonatal convulsions (BFNC). Occurring in the first days after birth and often disappearing within weeks or months, the seizure syndrome is unprovoked, with no identifiable causes. Instead, like many idiopathic epilepsies, BFNC has a hereditary predisposition. Genetic analysis in large pedigrees with BFNC has pinpointed the disease-causing mutations in two genes, *KCNQ2* and *KCNQ3*. The genes encode respectively the KCNQ2 and KCNQ3 ion channel subunits that belong to a subfamily of voltage-gated potassium channels and are predominantly expressed in the nervous system. The discovery of the potassium channels underlying this form of idiopathic epilepsy has raised the hope that by understanding the functions of these KCNQ channels we will eventually understand the mechanism of the epileptogenesis and develop treatments.

Multiple lines of studies have suggested a shared role of KCNQ2 and KCNQ3 channels in regulating neuronal excitability. Their expression in adult human brains largely overlap (Cooper

[1] The scene is based on a case of benign familianl neonatal epilepsy reported in a family carrying *KCNQ3* mutation; source: Maljevic S, Vejzovic S, Bernhard MK, Bertsche A, Weise S, et al. 2016. Novel *KCNQ3* mutation in a large family with benign familial neonatal epilepsy: a rare cause of neonatal seizures. *Molecular Syndromology* 7: 189-96.

et al 2000). They form heteromeric channels that yield current manifold of that by their homomers (Selyanko et al 2001, Wang et al 1998) . The current mediated by the KCNQ2/3 channels underlies the functionally important “M-current” (Wang et al 1998), a slow, non-inactivating potassium current that controls the neuron membrane potential and restrains neurons from repetitive firing (Cooper & Jan 2003).

However, studies at cellular and network levels have so far mainly recognized the functional significance of KCNQ2 channels but not of KCNQ3. Defects of KCNQ2 channels, by conditional knockout in cortical principal cells or dominant-negative mutation, result in aberrant electrocorticogram activity and increased excitability of hippocampal pyramidal cells in rodents (Peters et al 2005, Soh et al 2014). In contrast, deleting the KCNQ3 channels conditionally from cortical principal cells does not affect cellular or network excitability examined in slice (Soh et al 2014). The hippocampi of *Kcnq3* mutant mice are also spared from neuronal loss and mossy fiber sprouting that are often associated with seizure pathogenesis (Singh et al 2008). For the KCNQ3, a link between an inadequate ion channel and the brain inclined to seizure remains missing.

The present study sets out to re-examine the role of KCNQ3 channels in neuronal and network excitability, not in slice as previous studies, but in awake behaving mice. To this end, I employed the *in vivo* extracellular recordings of field potential and of single unit activity in the hippocampal CA1 area in *Kcnq3* constitutive knockout mice. Before reporting the findings, I will introduce the most relevant background knowledge in this section that concerns the anatomy and functions of the hippocampus, the burst firing pattern and its implications, and what we know so far about the KCNQ3 channels.

1.1 Hippocampus

In this thesis, I investigate the neuronal activities in hippocampal CA1 area. There have been a number of comprehensive reviews on hippocampal anatomy and physiology (Andersen et al 2007, O'Keefe & Nadel 1978). Here I summarize the most important anatomical features of rodent hippocampus before delving into its physiology and functions, focusing on the local field potential oscillations and spatial memory that are most relevant in my study.

1.1.1 The anatomy and organization

Lying beneath the cortex and as part of the limbic system in rodents, the hippocampal formation includes adjoining and interconnected structures of dentate gyrus (DG), hippocampus proper, subiculum, perisubiculum, parasubiculum and entorhinal cortex (Andersen et al 2007) . The hippocampus proper, also called CA areas, is further divided into three subfields — CA1, CA2 and CA3.

Entorhinal cortex (EC), as a gateway, relays cortical inputs to other hippocampal areas. Via performant path, EC layer II neurons project to dentate gyrus and CA3 while layer III projecting to CA1 and subiculum. Receiving inputs from EC and other afferents from septal nuclei and brain stem, the DG granule cells innervate the CA3 pyramidal cells through the mossy fibers. The CA3 pyramidal cells project collateralized axons to CA3, CA2 and CA1; the projections to CA3 itself and CA2 form associational connections which forward recurrent excitation (Rapp & Gallagher 1996). In CA1, extensive collateralized projections are absent. Upon receiving its major inputs from the CA3 Schaffer collaterals, CA1 pyramidal cells give rise to projections targeting subiculum and deep layers of entorhinal cortex. The subiculum does not project back to CA fields but connects reciprocally with EC (Fig. 1.1). It serves a major output station from hippocampal to other cortical and subcortical regions including neocortex, septal nuclei and hypothalamus. Many axons from CA1 and subiculum reach back to EC, closing a largely unidirectional information loop throughout the hippocampal formation. The path—from entorhinal cortex to dentate gyrus, dentate gyrus to CA3, CA3 to CA1—is the classical hippocampal tri-synaptic pathway (Andersen et al 1971). Other intrahippocampal and extrahippocampal connections subsist, adding further complexity to the circuit.

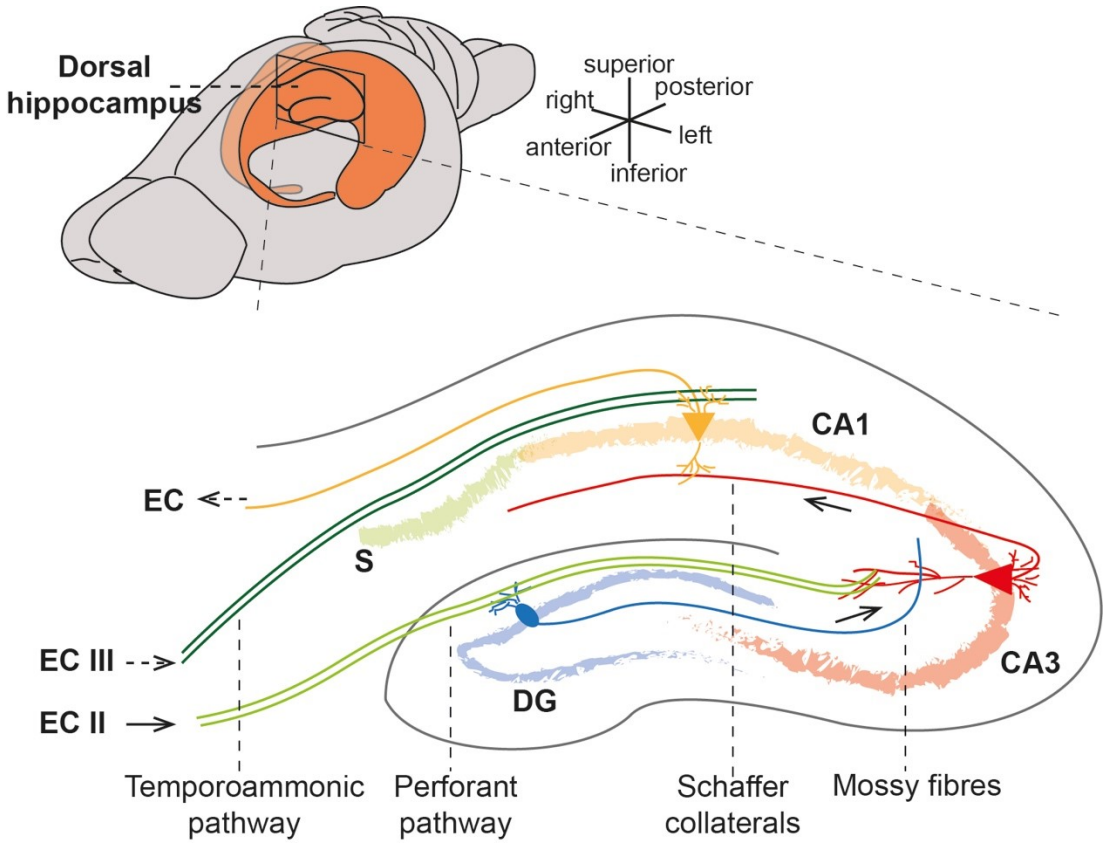

Figure 1.1: Location and basic circuit of the mouse hippocampus. *Upper: the anatomical position of the dorsal hippocampi in the mouse brain. Lower: sub-regions and circuitry of the hippocampus on transverse axis. The black solid arrows show the canonical tri-synaptic pathway. Input from layer II entorhinal cortex (EC) reaches dentate gyrus (DG) via the perforant pathway. Granule cells in DG then project to CA3 pyramidal cells through mossy fibers. From CA3, the Schaffer collaterals innervate CA1 pyramidal cells which further relay information to subiculum (S). In addition to the tri-synaptic pathway, there are projections from EC II to CA3 via perforant pathway and from EC layer III to CA1 pyramidal cells via temporoammonic pathway. Axons of CA1 pyramidal cells also project back to deep-layers of the EC.*

Distinct from the six-layered EC, the dentate gyrus (DG), CA fields and subiculum have a three-layer appearance: a superficial, almost cell-free layer, a middle layer populated by principal cells and interneurons, and a deep polymorphic cell layer occupied by fibers and interneurons. In CA1, the molecular layer is subdivided into stratum radiatum and the most superficial stratum lacunosum-moleculare. Below the stratum pyramidale is the polymorphic layer termed stratum oriens. The principal cells of the CA1 area, pyramidal cells, are characterized by their triangular soma packed within stratum pyramidale. Their basal dendrites branching into stratum oriens and apical dendrites into stratum radiatum are innervated by CA3 Schaffer collaterals while most axons from EC arrive at distal apical dendrites in stratum lacunosum-moleculare (Fig. 1.1). Beside the pyramidal cells, a diverse population of

interneurons reside across all CA1 strata. They are exclusively inhibitory (GABAergic) and mainly target neurons within hippocampus. Highly heterogeneous in the morphology, neurochemical properties, afferents and targets, they exert a complex regulation on pyramidal cells and network functions such as oscillatory activities (Freund & Buzsáki 1996). For example, baskets cells form inhibitory synapses on pyramidal cells' peri-somatic area while Chandelier cells only innervate the axon initial segments of pyramidal cells. Another group of interneurons, the O-LM cells, selectively target the most distal dendrites of pyramidal cells in stratum lacunosum-moleculare. Importantly, many interneurons receive local excitatory inputs from pyramidal cells.

1.1.2 Hippocampal theta oscillations

When electrodes are placed in the hippocampus, they record electric signals that originate from synaptic transmembrane currents, intrinsic membrane oscillation and other electrical events. This composite signal, referred as "local field potential" (LFP), is postulated to inform the collective activities of the neuron aggregates at high temporal resolution (Buzsáki et al 2012, Herreras 2016). Varied oscillatory patterns have been observed in hippocampal LFP. Based on their dominant frequency ranges, oscillations are defined as theta (6–10 Hz), beta (12–30 Hz), gamma (40–100 Hz), ripple (140–200 Hz) and fast ripple (>200 Hz) (Fig. 1.2). Non-rhythmic patterns, on the other hand, are denoted as large irregular activity (LIA). Oscillatory patterns are generated through the synchronized activation of a large neuron aggregate and are often associated with certain functional states of the network. In rodent, theta oscillations are prominent during voluntary locomotion and rapid eye movement (REM) sleep (Vanderwolf 1969). Beta has been associated with the interaction of hippocampus and olfactory bulb during odor learning in rodents (Martin et al 2007). Gamma oscillations in the hippocampus are often nested within theta rhythms during a variety of behaviors. Ripples are frequently present together with another signal pattern called sharp waves during slow wave sleep (Buzsáki 1986). Higher-frequency oscillations are rare and some are likely pathological (Engel Jr et al 2009).

Theta waves were first found in rabbit hippocampus by Jung and Kornmuller (Jung & Kornmüller 1938) and later in many other cortical and subcortical structures (Popa et al 2010, Steriade 2000, van der Meer & Redish 2011). The large amplitude potentials in these structures are generated through the parallel aligned dendrites and their afferents. Within the hippocampus, theta waves are most apparent in CA1 and dentate gyrus during voluntary movements and REM sleep (Vanderwolf 1969) .

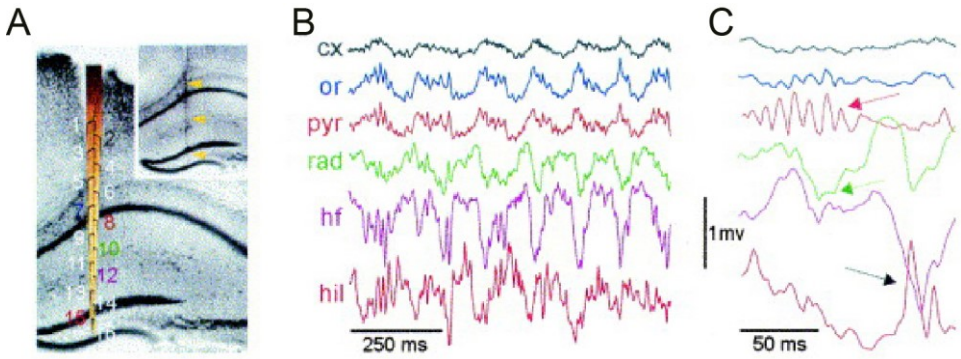

Figure 1.2: Theta rhythms and sharp-wave ripples in hippocampal LFP of the mouse (from Buzsáki et al, 2003; with permission from Elsevier). *(A) 16-site silicon probe implanted along the CA1– dentate gyrus axis for local field potential recording. Numbers indicate recording sites with spacing of 100 μm. Inset: arrowheads indicate the probe track. (B) Theta–gamma oscillation recorded during wheel running. Color-coded traces correspond to locations in A (cx, neocortex; or, stratum oriens; pyr, pyramidal layer; rad, stratum radiatum; hf, hippocampal fissure; hil, hilus). (C) Ripples (red arrow) in the pyramidal cell layer associated with a negative sharp wave in stratum radiatum (green arrow). A dentate field spike (DS) is also shown (black arrow).*

The generation of theta oscillations. LFP depth versus voltage profile of theta oscillations in the CA1 area has a characteristic phase and amplitude shift along strata (Fig. 1.2A, B). As the extracellular field potential is thought to arise from post-synaptic potentials at the somas and dendrites of the pyramidal cells, the profile reflects the interplay of different current generators in hippocampus (Buzsáki 2002). Dendritic excitation by afferents from entorhinal cortex and CA3 (Bragin et al 1995, Brankačk et al 1993, Buzsáki 1986) and the somatic inhibitory postsynaptic potentials from the rhythmic discharge of local interneurons (Fox 1989, Kamondi et al 1998, Ylinen et al 1995) have been suggested to give rise to the theta waves in the CA1 area. In addition, hippocampal neurons possess varied voltage-dependent conductances that contribute to intrinsic membrane potential oscillation at theta frequency (Alonso & Llinás 1989, Kamondi et al 1998).

The generation of theta rhythms critically involves medial septal nucleus and the nucleus of diagonal band of Broca (MSDBB) (Petsche et al 1962, Winson 1978). Lesion or inactivation of medial septum has been shown to disrupt the hippocampal theta wave (Green & Arduini 1954, Mizumori et al 1990, Petsche et al 1962). One putative pacemaker are the septal GABAergic neurons. These neurons discharge rhythmically to the hippocampal theta (Hangya et al 2009, King et al 1998) and their projections to hippocampus innervate all known subtypes of hippocampal interneurons, which in turn leads to the disinhibition of hippocampal pyramidal

cells (Freund & Antal 1988, Takács et al 2008). Interestingly, projections from hippocampus back to MSDBB originate exclusively from hippocampal interneurons and target mainly the GABAergic neurons in the medial septum (Takács et al 2008, Toth et al 1993). Modelling studies suggest that this reciprocal inhibitory circuit between medial septum and hippocampus is essential for the theta generation (Denham & Borisyuk 2000, Wang 2002).

The cholinergic neurons in the MSDBB also project to hippocampus but diffusively innervate both pyramidal cells and interneurons (Teles-Grilo Ruivo & Mellor 2013). Selective lesion of septal cholinergic neurons reduces the power of hippocampal theta by several folds (Lee et al 1994). The septal cholinergic projection primarily contributes to the "atropine-sensitive" type of theta oscillations that occurs during anesthesia or behavior immobility (Kramis et al 1975). Direct excitation of hippocampal pyramidal cells via muscarinic receptors activation is deemed too slow to be responsible for generating the oscillations. Instead, the role of cholinergic inputs in the theta generation may rely more on their modulation of interneurons in hippocampus and septum (Buzsáki et al 1983, Stewart & Fox 1990). Moreover, activation of septal cholinergic neurons is shown to indirectly enhance theta oscillations in behaving mice by suppressing slow wave ripples and peri-theta field activity (Vandecasteele et al 2014).

Alongside the drive from MSDBB, theta rhythms can also be generated through the interaction of components within local hippocampal circuits. Studies on the coherence of theta oscillations across all layers in CA1 reveal that the recurrent circuitry of CA1 and hilar mossy cells can function as an intrahippocampal theta oscillator independent of extrahippocampal (entorhinal) rhythmic inputs (Bragin et al 1995, Kocsis et al 1999). An *in vitro* study on an isolated hippocampus further demonstrated that multiple theta oscillators existed along the septotemporal axis of CA1 and were sufficient to generate theta oscillations even when the CA3 was removed (Goutagny et al 2009).

The functions of theta oscillations. Theta rhythm presumably functions as a temporal reference for neurons to correlate with each other (Buzsáki 2002, Colgin 2016). In hippocampus, place cells systematically advance their phases within theta cycles during transversal of place fields ("theta precession") (O'Keefe & Recce 1993). The varied theta phases of neurons from a cell ensemble can be organized into an experience-dependent order called "theta sequence" that correlates with certain physical attributes such as the animal's trajectory in the explored space (Dragoi & Buzsáki 2006, Skaggs et al 1996). Theta also provides a timing and plasticity mechanism for neurons to integrate and segregate multiple inputs (Hölscher et al 1997). For

hippocampal neurons, theta has been suggested to facilitate the coding of multimodal sensory information in task-related memory (Kepecs et al 2007, Macrides et al 1982).

1.1.3 The function of hippocampus in spatial memory

Notwithstanding its broad implications in cognition, behavior inhibition and stress regulation, theories of hippocampus functions have been largely focusing on memory owing to two influential discoveries. One is of the severe amnesia in patient H.M. after the removal of his medial temporal robe to relieve intractable epilepsy (Scoville & Milner 1957) and the other is of the hippocampal "place cells" that fire selectively in accordance with animal's location in a space (O'Keefe 1976, O'Keefe & Nadel 1978). They have inspired a growing body of research that recognize hippocampus as a unique cognitive system for declarative memory whereby people remember daily facts and events, and for spatial memory whereby animals navigate in physical world (Bird & Burgess 2008, Buzsáki & Moser 2013, O'Keefe & Nadel 1978). Followed is a brief review on some most important discoveries in rodent hippocampus in support of the "spatial memory" thesis, and theoretical proposals that attempt to integrate the mechanisms for navigation with the more general functions for memory.

Place cells. In the 1970s, O'Keefe and Ranck started applying extracellular unit recording in hippocampus of freely moving rats (O'Keefe & Dostrovsky 1971, Ranck 1973). Based on firing rate, spike waveforms and the relation of spike with LFP, they distinguished two classes of neurons: "theta cells" and "complex spike cells". The later which were likely to be pyramidal cells (Henze et al 2000), selectively increased firing when the animal was in a certain location of the environment and were coined "place cells". The "place field" of each place cell locates differently such that a sufficient population of place cells can represent the whole place that the animal has explored (O'Keefe 1976, Wilson & McNaughton 1993). The spatial map derived from the place cell firing is primarily shaped by the geometric properties of the space such as its boundary (O'Keefe & Burgess 1996). Distal cues rather than the proximal ones appear of predominant influence (Muller & Kubie 1987, O'Keefe & Burgess 1996). For instance, rotating the distal, extra-maze landmarks caused the entire map to rotate accordingly while in an already familiar environment, the firing map of the animal pertained even in the absence or displacement of proximal landmarks (Muller & Kubie 1987).

The firing map of a place cell is not merely shaped by external physical environment, but also by the navigation executed by the animal itself. One example is the directionality of place

cell. When the animal was restricted to travel in one direction along a narrow linear track and another direction back to the starting point, most place cells only appeared in one direction (McNaughton et al 1983a, Muller & Kubie 1987). The path-integration theory postulates that the hippocampal firing map relies on information generated through self-motion like direction and distance (Etienne et al 1996). Apart from place cells, path integration also involves two other types of cells: head direction (HD) cells and grid cells. HD cells are found in the dorsal presubiculum and entorhinal cortex. They prefer firing when the animal's head points in a certain direction (Taube et al 1990). The relation between two HD cells hold constant across environments. When the whole HD cells constellation rotates, the place cell map rotates (Taube et al 1990). Grid cells in the layer II and layer III of the medial entorhinal cortex are more like a metric system for distance (Hafting et al 2005). Each grid cell has multiple firing fields in a space. These fields generate a periodic triangular pattern like a grid imposing on the space. The spacing, orientation and the phase of the pattern against external reference vary from one cell to another (Hafting et al 2005, Solstad et al 2006). Theoretical and computational studies suggest that place field of a place cell can be generated through linear combination of the activity of multiple grid cells with varied grid spacing (O'Keefe & Burgess 2005, Solstad et al 2006).

Theta phase precession and sequence-coding. Not only encoding a spatial representation, the firing of place cells also conveys temporal information through their sequential activation. During the transversal of place fields, the firing of a place cell often starts at certain phase of the ongoing LFP theta and advances progressively toward earlier phases in subsequent theta cycles. This phenomenon is called "theta phase precession" (Huxter et al 2008, O'Keefe & Recce 1993). Computational model suggests that phase shift encodes additional spatial information than firing rate (Burgess et al 1994). Moreover, when the animal travels across several overlapping place fields, the corresponding place cells will be activated in a compressed, shifted sequence in each ongoing theta cycle (Dragoi & Buzsáki 2006, Skaggs et al 1996). The sequential activation repeated at such time scale is hypothesized to facilitate the spike-timing dependent plasticity between discrete place cells in forming the memory trace (Buzsáki & Moser 2013, Dan & Poo 2004). The sequence of place cells can be reactivated or "replayed" in sharp-wave ripples during sleep or pause between locomotion, which suggests a potential mechanism for memory consolidation (Foster & Wilson 2007, Lee & Wilson 2002, Skaggs et al 1996).

Bridging spatial mapping with memory. Many hippocampal mechanisms for navigation imply a more general memory function: the reliable recall of the firing map when the animal re-enters a previously explored environment (Muller & Kubie 1987), the replay of cell sequences during sleep (Foster & Wilson 2007, Lee & Wilson 2002, Skaggs et al 1996) and the requirement of NMDA-dependent long-term potentiation (LTP) for shaping and stabilizing place fields (McHugh et al 1996, Mehta et al 2002). If both spatial representation and declarative memory share a common structural substrate, do these two hippocampal functions fundamentally employ the same neuronal mechanisms or computational algorithm? The question was first explored in O'Keefe and Nadel's cognitive map theory (O'Keefe & Nadel 1978). They propose that animals primarily use hippocampus as a cognitive map system which represents the absolute space and provides the basis for spatial memory; in human, this structure for representing objects in physical space is extended to represent more abstract, verbal and non-verbal information. According to this thesis, the spatial map evolves to serve a spatial-temporal framework to incorporate objects, events and concepts that provides basis for episodic memory. Drawing on recent advances in recording ensembles of various spatial cells and state-dependent LFP oscillations, Buzsáki and Moser propose that the hippocampus employs two types of navigation mechanisms: map-based and path integration. These two mechanisms, as they suggested, essentially support the two forms of declarative memory in human: the semantic memory which recalls independent objects and facts like the map representing discrete locations, and the episodic memory which recalls subjective experience of events in their context as the path integrating egocentric locomotion (Buzsáki & Moser 2013).

1.2 The burst firing of neurons

In this study I examined the neuronal activities by recording extracellular action potentials. Underlying each action potential is a concerted operation of membrane ion channels with diverse ion selectivity, gating properties and distributions in different neuron types. The vast repertoire of ion channels, on the other hand, endows neurons with action potentials of varied shapes and temporal patterns, which intrinsically determines a neuron's input-output properties (Beck & Yaari 2008). The survey below is dedicated to a special spiking pattern called burst firing.

1.2.1 Burst as a distinct mode of action potentials

The basic form of neuron firing is a solitary spike in response to a brief current injection or synaptic excitation, which is a rapid stroke of membrane depolarization followed by a relatively slower repolarization back to the resting membrane potential. In contrast, "burst" represents a qualitatively different pattern: in response to a just-threshold current injection, a neuron fires a cluster of spikes with a pronounced membrane afterdepolarization (Connors et al 1982, Kandel & Spencer 1961, McCormick et al 1985). The notion of burst derives from "repetitive firing". First described in Sepia nerve by Arvanitaki (Arvanitaki 1939) and later also in mammalian neurons, repetitive firing originally featured a sustained train of action potentials with little adaptation under prolonged current injection (Eccles & Krnjević 1959, Frank & Fuortes 1956, Hunt & Kuno 1959). But subsequent studies in cortical neurons observed a different repetitive pattern: a cluster of action potentials, usually of two to six, with each similar to a single spike

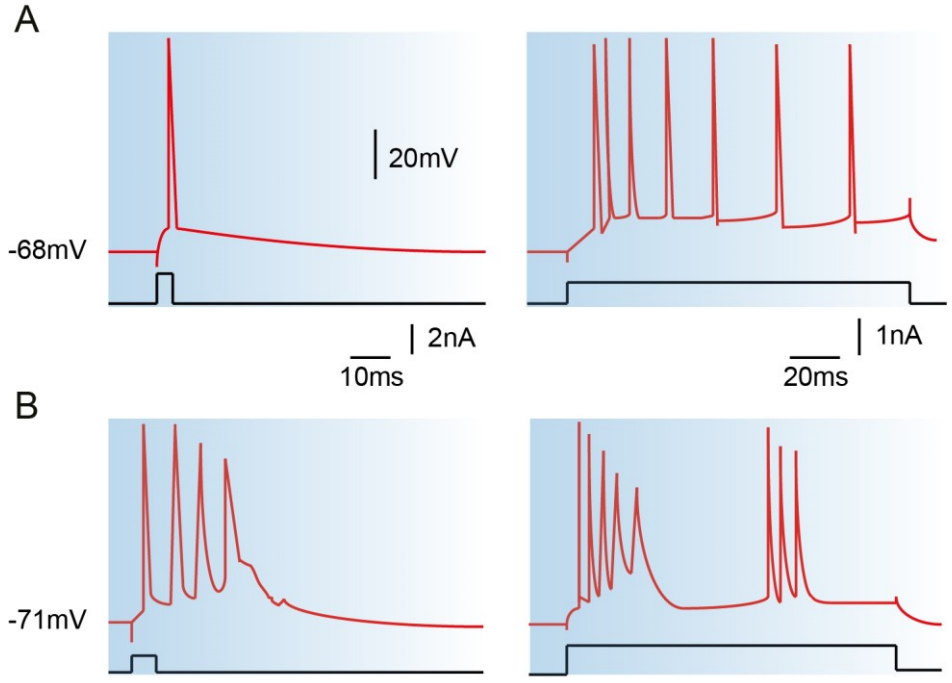

Figure 1.3: Varied firing patterns of CA1 pyramidal cells. *CA1 pyramidal cells of distinct burst propensity showed different firing patterns in response to brief (left panels) and prolonged (right panels) current pulses that were injected through the recording electrode in normal extracellular potassium concentration. Red trace presents the evoked response at the soma of the neuron recorded intracellularly; lower black trace illustrates the corresponding current pulse. (A) Responses of a regular spiking pyramidal cell; the neuron fired a train of independent spikes in response of suprathreshold stimulation (right). (B)Responses of a highly bursty ('Burst grade III') pyramidal cell; the neuron fired spontaneous bursts and responded to stimulation with a stereotyped burst of several spikes. All panels reproduced, with permission from Jensen et al 1994. © (1994) The American Physiological Society.*

but gradually declining in their amplitudes (Mountcastle et al 1957, Tasaki 1954). In their 1960 seminal paper on the electrophysiology of hippocampal neurons, Kandel and Spencer first adopted "burst" to denote such pattern (Kandel & Spencer 1961). Through extracellular single unit recording, Ranck demonstrated the burst firing in hippocampal pyramidal cells *in vivo* and described them as "complex spikes" (Ranck 1973).

The probability and condition for a neuron to fire bursts differ between neuron types. Some neurons are "intrinsically bursting" as they often fire in a burst-or-none manner (Connors & Gutnick 1990). These include a few groups of neurons in certain laminae of neocortex and a subgroup of subicular neurons (Connors et al 1982, McCormick et al 1985, Sharp & Green 1994). Many more neurons, however, fire both bursts and single spikes (Fig. 1.3). The probability of initiating a burst is regulated by the intrinsic and synaptic properties of the neuron and is also related with the functional states (Beck & Yaari 2008). Hippocampal CA1 pyramidal cells, for example, fire bursts much abundantly during slow wave sleep (Vyazovskiy et al 2009), while during active exploration of experiment animals, bursts emerge only transiently but convey information about physical world such as space (Harris et al 2001, Ranck 1973).

1.2.2 The mechanisms of burst generation in hippocampal pyramidal cells

Bursts in hippocampal pyramidal cells are called "complex spike bursts", which emphasizes the frequency and amplitude accommodation of successive spikes within one burst (McNaughton et al 1983b, Ranck 1973). Across hippocampus, pyramidal cells from different subfields show varied propensities to fire complex spike bursts. Although it remains disputable whether the heterogeneity of burst propensity reflects different neuron types with distinct morphologies and physiological properties or a single cell type with varied excitability (Graves et al 2012, Grienberger et al 2014, Jarsky et al 2007, Jensen et al 1994), *in vivo* whole-cell recordings suggest that burst firing can be evoked in all pyramidal cells through synaptic excitation in the intact CA1 area (Grienberger et al 2014). The tendency of a pyramidal cell to fire bursts, proposed by Jensen et al., should be regarded as a continuum of "burstiness" instead of a strict dichotomy between exclusively regular spiking neurons and intrinsic bursting ones. For all cells, the authors postulated, burst firing is generated and modulated through shared mechanisms (Jensen et al 1994, Staff et al 2000).

The ionic mechanisms of complex spike bursts. Featuring a brief, self-limited trains of spikes, the burst in hippocampal pyramidal cells also has a characteristically large, prolonged spike

after-depolarization (ADP) (Kandel & Spencer 1961, Storm 1987, Wong & Prince 1981). Unlike the "passive" ADP following the fast repolarization of a regular single spike which is monotonically declining, the ADP of a burst is an "active" one that is sustained and cumulative, allowing the membrane to re-depolarize above threshold and to trigger further action potentials.

Sustained inward currents that are active in the voltage range of ADP provide the primary ionic drive for membrane depolarization that can outlast a single spike and be summated by successive spikes. Such currents include the persistent Na^+ current (I_{NaP}) from soma (Azouz et al 1996) and slow Ca^{2+} currents from dendrites (Golding et al 1999, Metz et al 2005, Yaari et al 2007). I_{NaP} is activated below action potential threshold and is resistant to inactivation after the fast spike. Blocking I_{NaP} current by applying Tetrodotoxin to the somatic region of CA1 pyramidal cells but not dendrites reduced the size of ADP and suppressed intrinsic bursting initiated by somatic current injection (Azouz et al 1996, Yue et al 2005). Conversely, low extracellular Ca^{2+} concentration that enhanced the I_{NaP} currents promoted burst firing in otherwise regular spiking neurons (Su et al 2001). The slow Ca^{2+} currents, on the other hand, are mediated by dendritic low-voltage activated Ca^{2+} channels such as T-type Ca^{2+} channels (Yaari et al 2007) and R-type Ca^{2+} channels (Metz et al 2005). The dendritic depolarization is constantly opposed by repolarizing conductance like the dendritic A-type K^+ currents. When dendritic Ca^{2+} channels are up-regulated or when the opposition from K^+ currents is lifted, dendritic Ca^{2+} currents grow substantially to amplify the ADP and induce bursts (Hoffman et al 1997, Yaari et al 2007). By applying 4-aminopyridine (a potassium current blocker) at apical dendrites, Magee et al. showed that action potential back-propagation also evoked dendritic Ca^{2+} spikes and facilitated active ADP and bursting (Magee & Carruth 1999). In spite of the potential to build up active ADP by sustained Na^+ or Ca^{2+} currents, majority of pyramidal cells tend to fire single spikes. The size and duration of active ADP are controlled by different types of outward K^+ currents (Storm 1989). A critical one is the M-current mediated by KCNQ channels (Wang et al 1998). This potassium current is non-inactivating, sub-threshold activated and concentrated in axo-somatic compartments of CA1 pyramidal cells, which mirrors that of the I_{NaP} current. Inhibiting M-currents by its selective blocker linopirdine or XE991 dramatically amplifies the spike ADP and promotes bursting in regular spiking pyramidal cells (Gu et al 2005, Yue & Yaari 2004). M-current also contributes to the medium after-hyperpolarization (mAHP), an after-spike potential that often follows a burst or a train of repetitive spikes (Storm 1989). Although the mAHP is too slow for the repolarization of fast

spikes, it is important for the spike frequency adaptation and burst termination (Gu et al 2005, Storm 1989).

The modulation of burst firing by transmitters and receptors. The increased incidence of complex spike bursts during slow wave sleep and consummatory behaviors implies a strong network effect on burst firing (Ranck 1973, Suzuki & Smith 1985). Bursting *in vivo* is most probable after a period of prolonged silence and under large intracellular action potential rising slope, which suggests bursts as "conditional synchrony detectors" (Harris et al 2001, Lisman 1997). Combining whole-cell recording and two-photon dendritic Ca^{2+} imaging, Grienberger et al. demonstrated that complex spike bursts *in vivo* can be evoked by the activation of voltage-gated dendritic Ca^{2+} channels at multiple basal and apical dendrites following NMDA-dependent dendritic depolarization (Grienberger et al 2014). At the same time, the dendritic electrogenesis is regulated by inhibitory synaptic inputs. For example, optogenetically silencing somatostatin interneurons that targeted the dendrites of CA1 pyramidal cells was able to relieve the dendritic inhibition and trigger bursting in pyramidal cells. In intact circuits, such disinhibition effect might be established by the activation of SOM-targeting parvalbumin interneurons (Lovett-Barron et al 2012, Royer et al 2012). Thus, local inhibitory network plays a critical and intricate role in tuning the timing, intensity and duration of burst firing. Apart from glutamatergic and GABAergic inputs, cholinergic afferents provide another important modulation on burst firing in CA1 pyramidal cells. *In vitro* intracellular studies show that activation of muscarinic acetylcholine receptors (mAChRs) induces sustained membrane depolarization and active ADP while decreasing spike frequency adaptation in CA1 pyramidal cells (Azouz et al 1994, Halliwell & Adams 1982, Madison & Nicoll 1984). The cholinergic depolarization results from its modulation of multiple ion conductances, including the inhibition of M-currents (Halliwell & Adams 1982, Madison et al 1987) and the blockage of the slow AHP mediated by slow Ca^{2+}-activated K^+ conductance (Benardo & Prince 1982, Madison et al 1987). But for a subset of the particularly bursty CA1, cholinergic activation by carbachol application or increasing acetylcholine release suppresses burst firing *in vitro* (Alroy et al 1999, Azouz et al 1994). Moreover, dual-modulation of burst probability in pyramidal cells of different base-line excitability by the synergistic action of mAChRs and glutamate metabotropic receptors has been reported *in vivo* (Graves et al 2012). Notably, the major cholinergic inputs in hippocampus via the septo-hippocampal pathways act on both pyramidal cells and interneurons through different muscarinic and nicotinic receptors (Teles-Grilo Ruivo

& Mellor 2013). Furthermore, the activities of the circuit change with behavioral states and are critically involved in hippocampal theta rhythm where spatially tuned complex spike bursts emerge transiently. Therefore, how burst firing is modulated by cholinergic inputs depends dynamically on the wiring and functional state of a neuron within its network. It is shown that a lognormal distribution of burst firing is established across hippocampal pyramidal cells population *in vivo* possibly through the preconfigured connectivity and synaptic weights, and the small group of pyramidal cells with higher burst propensity appear to be the candidate for place cells (Epsztein et al 2011, Mizuseki & Buzsáki 2013).

Understanding burst through dynamic system analysis. To comprehend the necessity and sufficiency of varied mechanisms in generating bursts, theoretical studies have modelled a burst as a fast, regenerative spiking process modulated by a slower process and evaluated the influence of certain ion currents in terms of their contribution to these two interactive processes. The framework was developed from FitzHugh's phase space analysis of nerve membrane physiological states (FitzHugh 1961). By modelling the membrane dynamics using coupled differential equations and on a phase plane, different behavior modes (resting or bursting) were defined as attractors, and the transitions between modes as bifurcation from the perspective of dynamic system. Rinzel further introduced a decomposition of the system into a fast subsystem and a slow subsystem (Rinzel 1987, Rinzel & Ermentrout 1998). The slow subsystem (e.g., a slow variable related with a slow voltage-gated conductance) evolves slowly in time while the fast subsystem—typically with the membrane potential as one of the fast variables—progressively tracks its stable states; bursting corresponds to one stable state of the fast subsystem (Izhikevich 2000, Rinzel & Ermentrout 1998).

The complex spike bursts in hippocampal pyramidal cells have been analyzed with models of two compartments or multiple compartments to address the segregation and coupling of somatic conductance with the dendritic Ca^{2+} and K^+ currents (Kepecs & Wang 2000, Traub et al 1991). In these models, the coupling strength between the somatic and dendritic ion mechanisms proves critical for the bifurcation paradigm of the models that decides a neuron to be regular spiking or bursting. The study modelling the somatic bursting of CA1 pyramidal cells in a one-compartment model further demonstrates that M-current activation is the necessary slow variable for the system to transit between resting and bursting modes and to acquire certain burst kinetics. Without the M-current, the neuron under the I_{NaP} will fire regular spikes or on a high depolarization plateau (Golomb et al 2006).

1.2.3 Functional implications of burst firing

The importance of burst firing is implicated in its special role in information coding and synaptic plasticity. Equally critical is a balanced, regulated burst propensity for an efficient and healthy brain.

Role in information coding. Signal transmission at central synapses is often unreliable, as the probability of a single presynaptic spike to elicit postsynaptic response varies widely (Thomson 2000). However, the transmission at synapses of low probability can be facilitated if two or more spikes arrive at the pre-synapse within a brief interval as within a burst, and the probability of discharging the postsynaptic neurons can be increased (Stevens & Wang 1995). Higher transmission probability of a presynaptic burst versus a single spike has been demonstrated in both pyramidal-pyramidal synapses and pyramidal-interneuron synapses in hippocampus (Csicsvari et al 1998, Miles & Wong 1987). Moreover, burst firing may encode information different from that by single spikes (Harris et al 2001, Lisman 1997, Otto et al 1991, Ranck 1973). Simulation studies show that bursts, owing to their intrinsic biophysics and temporal features, are capable of extracting features of the stimulus or inputs distinct from single spikes (Chacron et al 2004, Kepecs & Lisman 2003). Additionally, burst may function as an information unit independent of single spikes. Mice with synaptotagmin-1 knockdown and hence revoked of single spikes firing were able to attain contextual fear memory solely relying on burst firing (Xu et al 2012). Moreover, the minority of highly bursty neurons in entorhinal cortex and hippocampus are postulated to constitute an indispensable functional subgroup for information processing and transmission throughout the network (Epsztein et al 2011, Mizuseki & Buzsáki 2013).

Role in synaptic plasticity. Burst firing can exert more lasting impact on the network by inducing synaptic plasticity. Pairing presynaptic firing with post-synaptic burst allows the induction of long-term potentiation (LTP) at hippocampal pyramidal cell synapses (Paulsen & Sejnowski 2000, Pike et al 1999, Thomas et al 1998, Wittenberg & Wang 2006). A common requirement for inducing synaptic LTP is a sufficient level of postsynaptic membrane depolarization plus sufficient Ca^{2+} entry at the activated synapses (Bliss & Collingridge 1993). Bursts can satisfy these conditions through the spikes back-propagating from axon initial

segment to dendrites, which amplifies the dendritic depolarization and trigger Ca^{2+} influx (Buzsáki et al 1996, Magee & Johnston 1997, Pike et al 1999). However, the mechanism might be more integral as burst firing in CA1 pyramidal cells *in vivo* is directly accompanied by multi-dendritic NMDA-dependent Ca^{2+} spikes and synaptic depolarization (Grienberger et al 2014). Based on the Hebbian rules of synaptic plasticity, the generation of large Ca^{2+} currents in a regenerative spike-like process across basal and apical dendrites provides a temporal and spatial frame to integrate and amplify the temporally associated signals even if they are weak (Bliss & Collingridge 1993, Hebb 1949, Paulsen & Sejnowski 2000). Therefore, the function of burst firing in synaptic plasticity has significant implications for the function of the hippocampus in learning and memory. Pyramidal cells that establish place-tuned firing in a novel environment, i.e. place cells, are cells intrinsically prone to bursting (Epsztein et al 2011). In addition, place cells fire bursts in their place fields (Epsztein et al 2011, Harris et al 2001, O'Keefe & Recce 1993, Ranck 1973), during which the burst-induced LTP can be instrumental in reinforcing and stabilizing the firing map (Kentros et al 1998).

Role in homeostatic plasticity and diseases. Burst firing does not only contribute to the synaptic plasticity but also serves as an intrinsic homeostatic mechanism for a neuron's excitability. This proposition is based on the observations that the probability of initiating bursts *in vivo* is conditioned by the neuron's recent spiking history and is suppressed by single spikes (Buzsáki et al 2002, Harris et al 2001). Synaptic potentiation induced by a burst allows weak input to trigger a single spike in postsynaptic neuron which in turn prevents another induction of burst and further potentiation of the synapse. On the other hand, strong input can induce burst firing in a lately silent neuron and re-potentiate the synapse. Therefore, the competition and balance between burst firing and single spikes might be critical for both the plasticity and homeostasis of the network. Chronically depriving activities in cortical or hippocampal network led to frequent burst discharge in principal cells, which was thought to restore the network excitability but at the same time predisposed the network to epileptogenesis (Houweling et al 2005, Kim & Tsien 2008, Trasande & Ramirez 2007). Increasing the burst firing, either by expanding the proportion of bursty neurons in the population or by promoting their excitation, poses risk on the stability of network function (Jensen & Yaari 1997, Kim & Tsien 2008, Traub & Wong 1982). An early modelling study has shown that intrinsic bursting neurons can lead an excitatory network into epileptic state through entraining regular spiking neurons into synchronous population bursts (Traub & Wong 1982). In line with this prediction, excessive burst firing has

been consistently observed in the hippocampal formation in chronic and acute epilepsy models (Behr & Heinemann 1996, Benini & Avoli 2005, Sanabria et al 2001). Abnormal regulation of burst firing is also associated with other neurological disorders such as chronic pain and Alzheimer's disease (Chen 2005, Cummins et al 2007).

1.3 KCNQ3 potassium channels

The input-output properties of a neuron and the generation of firing patterns are determined by the ion channels residing on the neuronal membrane. Ion channels also regulate cellular pathways via second messengers and contribute to the cellular and network homeostasis. Not surprisingly, functional deficiency of ion channels can in some case lead to diseases in human, collectively known as "channelopathies" (Lehmann-Horn & Jurkat-Rott 1999).

The KCNQ channels are a family of voltage-gated potassium channels, comprising five members that are named KCNQ1-5 respectively. Genetic mutations in four of these five channels have been associated with different forms of channelopathies (Jentsch 2000). KCNQ1 is expressed in heart, peripheral epithelial and smooth muscle cells. Mutations in *KCNQ1* can cause cardiac arrhythmias associated with dominant long-QT syndrome and Lange-Nielsen syndrome (Neyroud et al 1997). KCNQ4 is mostly present in sensory hair cells of inner ears; its loss of function leads to dominant deafness (Kubisch et al 1999). KCNQ2, KCNQ3 and KCNQ5 are found in various cell types throughout the nervous system including sympathetic ganglion neurons and hippocampal neurons. While *KCNQ5* is not yet identified with hereditary diseases, mutations of either *KCNQ2* or *KCNQ3* are responsible for a type of neonatal epilepsy termed benign familial neonatal convulsions (BFNC) [MIM121200; MIM121201] (Biervert et al 1998, Charlier et al 1998).

1.3.1 The structure of KCNQ3 channels

All KCNQ proteins share a structure of six transmembrane domains, the fourth domain S4 acting as voltage sensor, a single P-loop serving as a pore selectivity filter and a long, highly conserved intracellular carboxyl (C) terminus (Fig. 1.4). The lack of N-terminal T1 domain and the conserved "A-domain" on C terminus distinguish KCNQ family from other Kv potassium channel families (Long et al 2005, Schwake et al 2000). According to phylogenetic analysis, KCNQ3 and KCNQ2 come into existence later than other KCNQ proteins: while KCNQ1 and KCNQ5 are already expressed in bilaterians, KCNQ3 and KCNQ2 appear only from vertebrate

genomes (Cooper 2011). The KCNQ2 and KCNQ3 proteins boast a unique ankyrin-G binding motif on their C-terminus, evolutionarily related to the myelination of axons.

KCNQ channel is formed by four pore-bearing subunits that are presumably assembled through their C termini (Schmitt et al 2000). *In vitro*, each KCNQ isoform can form homomeric channels while heteromeric channels only exist for certain combinations that are largely constrained by their C-terminal tetramerization domains (Howard et al 2007). The KCNQ3 homomers generate relatively small current compared to other KCNQ homomers, partially due to its compromised stability and trafficking (Gómez-Posada et al 2010). But when KCNQ3 is co-expressed with KCNQ2, the heteromeric channel produces a sizable current at least 10 folds of that by their homomers (Schroeder et al 1998, Wang et al 1998). The enhancement of KCNQ2/3 current is thought to result from an increased surface expression (Schroeder et al 1998). KCNQ3 can also co-assemble with KCNQ4 and KCNQ5, making it the most undiscriminating isoform among all KCNQ proteins in forming heteromers (Hadley et al 2003, Kubisch et al 1999).

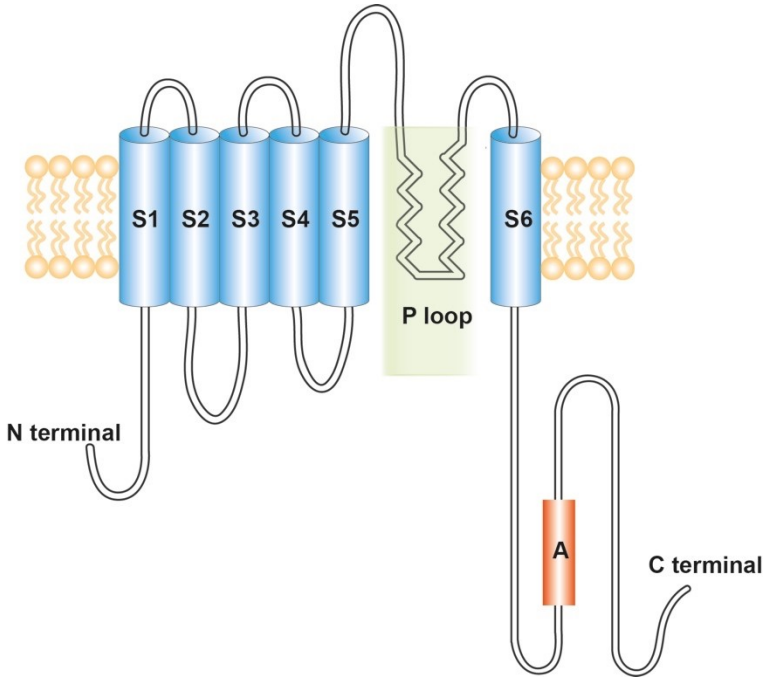

Figure 1.4: Scheme of the structure of KCNQ3 channel subunit. *KCNQ3 channel proteins have six transmembrane domains (S1–S6) and a pore-forming P-loop (green area); the long C-terminus has a highly conserved "A-domain" (orange box). Most disease-related mutations are found in residues within or adjacent to P-loop (green shade; see also Table 1).*

1.3.2 The expression of KCNQ3 channels

KCNQ3 is widely expressed in mammalian brains and overlaps considerably with KCNQ2 and KCNQ5, albeit discrepancies of their expression in certain regions and neuron types exist (Cooper et al 2001, Schroeder et al 2000). In human brains, KCNQ3 is co-localized with KCNQ2 and KCNQ5 in cortex, putamen and hippocampus (Schroeder et al 2000). In rodents, high expression of KCNQ3 is found in hippocampus, cortex and reticular thalamus among other regions (Geiger et al 2006, Tinel et al 1998). Unlike in human hippocampus, these channels display a predominant staining in axon and dendrites other than in soma. KCNQ3 shares an intense neurophil staining with KCNQ2 in CA1-CA3 area except for the mossy fiber pathway which is only labelled by KCNQ2 antibodies (Geiger et al 2006, Weber et al 2006). A comparatively weak somatic staining of KCNQ3 was detected in pyramidal cells and interneurons (Geiger et al 2006). Importantly, the expression level of KCNQ3 shows an upregulation during the maturation of the brain and is not parallel with the developmental change of the KCNQ2 expression. While KCNQ2 increases the expression swiftly within first postnatal week and remains stable until adulthood, KCNQ3 expression appears at a very low level right after birth but continuously increases into adult age (Geiger et al 2006, Tinel et al 1998). During development, KCNQ2 and KCNQ3 channels undergo a shift from a mainly somatic expression to a more neuropil one (Geiger et al 2006, Weber et al 2006). High-resolution imaging further confirms the preferred neuropil expression of KCNQ2 and KCQN3 in adult mice as the channels are found to concentrate at axon initial segments (AIS) and nodes of Ranvier in many neuron types including hippocampal pyramidal cells (Devaux et al 2004, Pan et al 2006). It is postulated that their common ankyrin-G binding motifs on the protein C-terminal end are crucial in facilitating the colocalization of KCNQ2 and KCNQ3 with the scaffold protein ankyrin-G and the voltage-gated Na^+ channels at AISs.

1.3.3 The role of KCNQ3 in neuronal excitability

The physiological functions of the KCNQ2/3 channels have been illuminated in two lines of studies: one on the functions of channel-mediated M-current and the other on transgenic mouse models with knockout or mutated KCNQ genes.

In vitro electrophysiological studies of the KCNQ2 and KCNQ3 currents in Xenopus oocytes have led to the important discovery that the expression patterns, biophysical properties and pharmacological specificity of KCNQ2/KCNQ3 heteromeric currents resemble those of a native potassium current termed “M-current” (Wang et al 1998). First identified in frog sympathetic neurons and subsequently in many other neuron types including cortical principal

cells, the M-current is a slow, non-inactivating voltage-dependent K^+ current. Its name "M" refers to the muscarinic receptors that were firstly shown to inhibit the current (Brown & Adams 1980, Delmas & Brown 2005, Jentsch 2000). The heteromeric KCNQ2/3 channels are presumably configured as two KCNQ2 subunits plus two KCNQ3s. The KCNQ2/3 currents, like native M-current, have an activation threshold around -60 mV and a slow biphasic deactivation with time constant of hundreds of milliseconds (Adams et al 1982, Selyanko et al 2001, Wang et al 1998). The slope conductance and open probability of KCNQ2/3 channels are close to those of the KCNQ3 homomeric channels while the introduction of KCNQ2 increases surface expression of the heteromers (Selyanko et al 2001). This suggests that KCNQ2 and KCNQ3 contribute complementarily to the heteromeric currents. Pharmacologically, KCNQ2/KCNQ3 channels can be blocked by specific M-current inhibitors such as linopirdine and XE991 and are sensitive to muscarinic modulations (Selyanko et al 2000, Wang et al 1998). The anti-convulsant retigabine which acts by enhancing the native M-current is shown to be a potent opener of KCNQ2/3 channels (Rundfeldt & Netzer 2000, Tatulian & Brown 2003). Besides, KCNQ5 subunits also underlie the KCNQ/M currents in varied neuron types (Schroeder et al 2000, Tzingounis et al 2010). As the KCNQ3/KCNQ5 heteromeric current has a relatively smaller magnitude than the KCNQ2/KCNQ3 current, a high amount of KCNQ5 might compete with KCNQ2 to form heteromers with KCNQ3 and down-regulate M-currents (Schroeder et al 2000). Therefore, the availability and combination of all three KCNQ subunits will determine the exact action of the M-current in the neurons.

The M-currents sustain in the range of resting membrane potential and are further activated by membrane depolarization within tens of milliseconds, much slower than the currents that generate action potentials (Brown & Adams 1980). These unique properties allow M-currents to exert a "clamping" effect on membrane potential and to restrict the neuron from repetitive discharges. In hippocampal pyramidal cells, M-currents contribute substantially to the medium after-hyperpolarization (mAHP) and facilitate the spike frequency accommodation that follow prolonged depolarization or burst firing (Gu et al 2005, Madison & Nicoll 1984, Storm 1989). When M-currents were inhibited by specific blocker XE-991 or linopirdine, the excitability of neurons increased, eliciting larger after-depolarization (ADP) and burst firing. Reversely, current opener retigabine attenuates somatic ADP and reduces bursting neurons to regular spiking in a dose-dependent manner (Gu et al 2005, Yue & Yaari 2004, Yue & Yaari 2006). Moreover, M-currents at different subcellular compartments can regulate different aspects of neuronal excitability in collaboration with other local ion currents. For instance, peri-somatic

M-currents that are activated by action potential control the size of ADP and mAHP. On the other hand, the M-currents at apical dendrites that are activated by enhanced dendritic excitation primarily serve to raise the threshold for Ca^{2+} spikes (Yue & Yaari 2006). The actions of axonal M-currents also differ from the somato-dendritic counterparts. Disrupting the KCNQ channels at AIS using ankyrin G-binding peptides decreases action potential threshold and promotes spontaneous firing, without affecting the somatic EPSP integration regulated by somatic M-currents (Shah et al 2011, Shah et al 2008). In contrast to the synergic operations of axo-somatic and dendritic M-currents in restraining excitability, axonal presynaptic M-currents appear to facilitate axonal action potentials and synaptic transmission. Blocking the currents with XE-991 at Schaffer collaterals reduced the fiber volley amplitude and glutamate release when the axons were sufficiently depolarized (Vervaeke et al 2006). Therefore, given the varied subcellular locations, different KCNQ subunits may have divergent implications for the neuronal functions and for the related pathogenesis in cases of functional deficiency.

The functional impact of M-current further derives from its modulation by a wide range of neurotransmitters and neuropeptides (Delmas & Brown 2005). M-currents were first discovered through its inhibition by the muscarinic receptors agonist as one potential pathway for cholinergic excitation (Brown & Adams 1980, Brown et al 2007). In hippocampal CA1 neurons alone, the KCNQ/M currents can be modulated by receptors for muscarine (Halliwell & Adams 1982), serotonin (Colino & Halliwell 1987), cannabinoid (Schweitzer 2000) or by peptide somatostatin (Moore et al 1988). Most of them are G-protein coupled receptors; their inhibition of the currents often involves activation of the G-proteins. The primary mechanism, as being instrumental for the muscarinic inhibition of the currents, is via the depletion of the membrane phosphatidylinositol 4,5-bisphosphate (PIP_2) by the G-protein activation. Because certain amounts of membrane PIP_2 are required for the opening as well as restoration of the KCNQ channels on neuron membrane (Suh & Hille 2002, Zhang et al 2003), the activation of the G-protein receptors induces significant reduction of the membrane PIP_2 and prevents the channels from conducting M-currents, consequentially upregulating neuronal excitability. As each KCNQ subunit has distinct affinity for PIP_2 (Li et al 2005), the neuromodulation directed through M-currents engages individual channel subunits differently.

Taken together, M-currents serve two seemingly antagonistic roles for the neurons: as a constraint on repetitive neuron firing to prevent hyper-excitability, and at the same time, as a focal point for various neuromodulators to direct a transient excitation.

1.3.4 KCNQ3 in human diseases and related animal models

KCNQ3 was first mapped as a homologue gene of *KCNQ2* on human chromosome 8q24 and became one of the two gene loci identified with benign familial neonatal convulsions (BFNC) by linkage analysis (Charlier et al 1998, Leppert et al 1989, Lewis et al 1993). *KCNQ2* resides on the other loci, chromosome 20q13 (Biervert et al 1998, Singh et al 1998). BFNC is an autosomal dominantly inherited epileptic disorder that affects neonates in the first few days after birth and spontaneously remits within a few weeks or months (Ronen et al 1993). The syndromes are of partial or generalized seizures which manifest tonic-clonic seizures, apnea and other autonomic features. Although the disease is generally regarded as benign, up to ~15% of the patients can experience recurring seizures later in life and there are increasing reports of cognitive deficits associated with BFNC (Miceli et al 2015, Steinlein et al 2007). To date, eight mutations in *KCNQ3* gene have been found in BFNC pedigrees (Table 1). All are missense mutations in pore loop of the protein or its adjacent domains (S5 to S6). Mutations commonly lead to a reduction of the heteromeric KCNQ2/3 currents. It is estimated that a modest reduction (about ~25%) of the currents is sufficient to raise the network excitability to epileptogenic levels in newborns (Schroeder et al 1998). Other *KCNQ3* missense mutations, mostly affecting the protein C-terminal, have been associated with other early onset epilepsies including benign familial infantile seizures (BFIS) and Rolandic epilepsy (RE) (Fusco et al 2015, Neubauer et al 2008, Zara et al 2013). However, more severe forms of neurological diseases such as epileptic encephalopathy and myokymia which have been linked to *KCNQ2* mutations have so far not been segregated with *KCNQ3* gene variants (Maljevic et al 2008). Apart from mutations, gene truncating, single nucleotide polymorphisms and epigenetic modification of *KCNQ3* gene have been associated with autism spectrum disorders and bipolar disorders (Gilling et al 2013, Kaminsky et al 2015).

To study the cellular and pathophysiological consequences of *KCNQ* mutations, several *Kcnq* transgenic mouse models have been developed. Models directly involving *Kcnq3* gene consist of a constitutive knockout (Tzingounis & Nicoll 2008), a knock-in with a missense mutation of G311V (Singh et al 2008) and a conditional knockout from cortical pyramidal cells (Soh et al 2014). Models targeting *Kcnq2* gene should also been reckoned with since the deficiency of the KCNQ2 channels also affects the expression of KCNQ3 (Selyanko et al 2001, Soh et al 2014). Depletion *of Kcnq2* in the earliest BFNC model caused homozygous mice to die in perinatal stage and increased the susceptibility to induced seizures in heterozygous mice. Homozygous KCNQ3 knockout mice, on the other hand, grew normally into adulthood

(Watanabe et al 2000). It is bewildering that *in vitro* studies find no reduction of M-current or of the medium AHP that the current mediates in the CA1 pyramidal cells of these mice, leading to the hypothesis that KCNQ2 and/or KCNQ5 channels may compensate the loss of KCNQ3 (Tzingounis & Nicoll 2008). To directly compare the functions of KCNQ2 and KCNQ3 and bypass the lethality of *Kcnq2* constitutive knockout, a conditional knockout model was devised to restrict the depletion of *Kcnq2* or *Kcnq3* gene in cortical pyramidal cells (Soh et al 2014). The model confirmed the necessity of KCNQ2 in generating M-current and mAHP in response to intensified current injection. In contrast, conditional knockout of *Kcnq3* had no effect on mAHP or spike adaptation despite causing a reduction of M-currents in CA1 pyramidal cells recorded from hippocampal slices. Increased neuronal excitability with reduced after-hyperpolarization was observed in another viable *Kcnq2* mutant model where a dominant negative *Kcnq2* mutation was conditionally expressed (Peters et al 2005). However, it should be noted that mice from this model showed behavioral hyperexcitability, spontaneous seizures and impaired spatial memory which was inconsistent with the clinical phenotypes of human. Stark phenotype differences were also found between the mouse models carrying *Kcnq2* disease-causing mutations and those of *Kcnq3*. Singh et al. generated knock-in mice carrying the *Kcnq2* A306T mutation or the *Kcnq3* G311V mutation, using two different mouse lines, C57BL/6J and FVB/NJ (Singh et al 2008). Both *Kcnq2* and *Kcnq3* homozygous mutants developed early-onset spontaneous seizures. Following seizures, *Kcnq2* homozygous mutants died prematurely, regardless of genetic background. But the survival of *Kcnq3* homozygous mutants was background-dependent: none from FVB/NJ background, but the majority of B6, were spared from premature death. In all *Kcnq2* and *Kcnq3* homozygous and heterozygous mutants, hippocampal pyramidal cells produced an attenuated M-current. The survived *Kcnq3* mutants, despite recurrent seizures, exhibited no neuron loss or mossy fiber sprouting in their hippocampus which is usually associated with seizures of temporal lobe origin, suggesting a very different model for epileptogenesis.

Affected protein/ gene region	Gene variant	Molecular defect	Clinical outcome	Reference
Missense mutation				
S5	V279F	Reduced KCNQ2/3 currents by ~88% in XO	BFNC	(Maljevic et al 2016)
S5 and pore region linker	E299K	Reduced KCNQ2/3 currents in XO	BFNC, RE	(Hahn & Neubauer 2009, Neubauer et al 2008)
Pore region	D305G	Reduced KCNQ2/3 currents by ~40% in XO	BFNC	(Singh et al 2003)
	W309R	Reduced KCNQ2/3 currents by ~60% in HEK 293 cells	BFNC	(Hirose et al 2000)
	G310V	Reduced KCNQ2/3 currents	BFNC	(Charlier et al 1998)
	I317T	Reduced KCNQ2/3 currents in CHO cells	BFNC, cognitive impairment, febrile seizure	(Soldovieri et al 2013)
Pore region and S6 linker	R330C	n.d.	BFNC	(Fister et al 2013, Li et al 2008)
	R330H	n.d.	BFNC	(Allen Nicholas et al 2014)
	R330L	Reduced heteromeric currents	Recurrent seizures, intellectual disability	(Miceli et al 2015)
C terminal	R364H	n.d.	BFIS, RE	(Fusco et al 2015)
	A381V	No effect on KCNQ2/3 currents in XO	RE	(Hahn & Neubauer 2009, Neubauer et al 2008)
	P574S	No reduction of KCNQ2/3 currents, reduced KCNQ3/5 currents in XO	RE without neonatal seizure, Childhood autism with no seizures;	(Gilling et al 2013, Hahn & Neubauer 2009, Neubauer et al 2008)
	R780C	n.d.	BFIS	(Zara et al 2013)
Chromosome abnormality or epigenetic alteration				
Exon1	Truncation, de novo t(3;8) (q21;q24) translocation		Childhood autism	(Gilling et al 2013)
Exon 11	Decreased DNA methylation	Reduced KCNQ3 expression	Bipolar disorder	(Kaminsky et al 2015)

Table 1: KCNQ3 channelopathies in human.

BFNC: benign familial neonatal convulsions; RE: Rolandic epilepsy; BFIS: benign familial infantile seizures. XO: Xenopus oocytes; CHO cells: Chinese hamster ovary cells. n.d.: no data.

1.4 *In vivo* extracellular electrophysiology

Empirical research of neuronal activities examines signals of different kinds: electrical, chemical or optical. Electrophysiological studies exploit the electrical nature of the neurons. By measuring the electric currents and voltages, neuronal activities can be examined in a wide range of scales, from detecting the currents through a single ion channel on the neuron's membrane by patch clamp to mapping the whole brain dynamics using electroencephalogram (EEG). To approach the cellular scale, techniques of extracellular, intracellular and juxtacellular recordings have been developed. While all these techniques can be applied *in vivo* to record neurons under physiological conditions, extracellular recording is so far the most common option for *in vivo* investigations (Chorev et al 2009). The manipulation of electrodes like wires or silicon probes is relatively simple compared to the intracellular setting like patch clamp. The improvement and miniaturization of the electrodes, such as the use of silicon probe, has significantly reduced the damage to the recorded tissue (Blanche et al 2005, Buzsaki 2004). The extracellular recording is able to capture both field (population) potentials and electrical activities of single neurons (Buzsáki et al 2012, Nádasdy et al 1999, Petsche et al 1984).

1.4.1 Recording extracellular field potentials

Transmembrane currents of the neurons give rise to the extracellular and intracellular potentials in the brain. At a given point within a conductive medium, a potential derived from the superposition of all electric currents upon this point can be detected. The potentials can be measured by electrodes placed in the extracellular space and is referred as local field potential (LFP) (Buzsáki et al 2012, Petsche et al 1984). Synaptic currents, both excitatory and inhibitory, are generally regarded as the main current source for the LFP. But currents of other origins, such as Ca^{2+} spikes, intrinsic membrane resonance, spikes and their after-potentials, also contribute to the field potentials. Importantly, the geometry of the current sources, the temporal relations between sources such as synchrony, and the conductance of the brain tissues together influence the potential measured at the targeted location (Buzsáki et al 2012, Herreras 2016). Therefore, it is difficult to accurately attribute the features of LFP to its physical substrates, unless one can assess the underlying sources with high-density recording and tools like cell-type, pathway specific optogenetics to identify the responsible neurons and cellular events. Even with such reductionist approach, great caution has been advised in the interpretation of the LFP due to its complex nature (Herreras 2016).

Nonetheless, recording extracellular LFP remains a highly informative practice in the study of the hippocampus. The elongated, parallel aligned apical dendrites of pyramidal cells serve

as efficient dipoles to generate measurable electric field. The confined laminar organization of somata, dendrites and afferents of the pyramidal cells optimize the conditions for the superposition of current flows. When the activities of a group of neurons reach a substantial level of synchrony, field potentials become sizable and generate varied patterns including population bursts, periodically fluctuating waves or large irregular activity. The laminar structure also endows some of these patterns with salient, reproducible and lamina-dependent features. One typical example is the voltage-depth profile of the theta rhythmic LFP (Buzsáki 2002). Another is the segregation of slow and fast gamma oscillations in stratum radiatum and stratum lacunosum moleculare (Colgin et al 2009). These distinct LFP features are important aids for researchers to identify and examine the synchronized neuronal activities in relation with the firing of single neurons as well as the global brain states.

1.4.2 Unitary recordings

An electrode in extracellular space also records fast voltage defections caused by action potentials, if the electrode is placed very close to the neuron and its impedance is sufficiently high (Hubel 1957, Ranck 1973). The extracellular action potential is typically biphasic: the initial large negative dip reflects the fast Na^+ influx of the action potential which would appear as a large upward peak if recorded intracellularly. Dual intracellular and extracellular recordings demonstrate that the waveform of an extracellular spike corresponds to certain intracellular features of the action potential, such as the width and amplitude (Henze et al 2000). Unlike intracellular recording, extracellular recording does not reveal detailed membrane dynamics or subthreshold synaptic activities of a neuron. Instead, it provides information of the neuron's output such as the rate and temporal patterns of the neuronal discharge.

After recording, one has to discriminate spikes that are emit by different neurons since a single electrode picks up the currents from any cells in its vicinity. It has been demonstrated in rat cortex that an electrode can detect the signal of a neuron within a radius of 140μm, which amounts to a space for ~1000 neurons (Henze et al 2000). There are currently two strategies for "spike sorting". The first one relies on extracting and discriminating features of spike waveforms (Abeles & Goldstein 1977). The other exploits the triangulation of signals from multiple electrodes that surround the same neuron (McNaughton et al 1983b). The multiple electrodes help to identify single neuron based on the temporal coherence of the signals across electrodes. The present spike sorting algorithm integrates both strategies (Hazan et al 2006). By applying component analysis or factor analysis, the waveforms of a unit on all available

electrodes are represented as a point in a feature vector space. Spikes with relatively close distances are grouped and assigned to one putative neuron—a unit—a process referred as "cluster cutting". A semi-automatic approach of combining automatic clustering with a manual adjustment is shown to be most reliable (Harris et al 2000).

Although unitary recordings provide valuable access to the activities of single neurons and led to important discoveries such as hippocampal place cells (O'Keefe & Recce 1993), the technique has its inherent limitations. First, recording spikes but no subthreshold events incurs apparent sampling bias. Given a limited amount of recording time, only active neurons that receive above-threshold excitation would be recorded. Secondly, the process of clustering in vector space presumes a limited variability of spike waveforms of a single neuron but in reality, the back-propagating action potentials and spikes within complex burst can vary considerably for the same neuron (Herreras 2016, Nádasdy et al 1999). Lastly, at times of synchronized population discharges, recorded units will have overlapping waveforms that confound their discrimination.

2 Methods

2.1 Animals

Twenty-two male mice were used in this study, all at the age of 10–18 weeks; all animals weighed more than 23 g. Animals were housed at 22 ± 2 °C with 12 h light-dark cycle and with access to food and water ad libitum.

Kcnq3 constitutive knockout (*Kcnq3*$^{-/-}$) and *Kcnq3* conditional knockout (Emx1-Δ*Kcnq3*) mice were generated using the Cre/loxP system by the laboratory of Prof. Thomas Jentsch in Leibniz-Forschungsinstitut für Molekulare Pharmakologie (FMP), Berlin. The expression of Cre-recombinase enables the recombination of two loxP sites to excise the intervening gene sequence. The floxed mice carried loxP sites that flanked the exon 3 of the *Kcnq3* gene. Crossing them with the Cre recombinase expressing "deleter" mice deleted the floxed exon and caused a frame-shift and a premature stop codon insertion of *Kcnq3*. Southern blot, RT-PCR and Western blot analysis confirmed the inactivation of *Kcnq3* and the loss of KCNQ3 protein (S.Schutze, unpublished data). *Kcnq3* cortex-specific conditional knockout mice (Emx1-Δ*Kcnq3*) were generated by crossing the *Kcnq3* floxed mice with Emx1-ires-Cre mice, which targeted the expression of Cre recombinase in neocortex and hippocampus.

2.2 Electrophysiology

2.2.1 Electrodes

Three types of electrodes were used in this study:

1. Tungsten wire array. Tungsten wires (40 μm, angular cut, California Fine Wire Company) were fabricated and guided with 70 μm silica tubes assembled in an array; individual wire differed in length thus recording signal from different depths. The ends of the wires outside the brain were connected to the pins of Omnetics connector (Omnetics Connector Corporate, MM, USA). Tungsten wires were used to record local field potentials.

2. Linear silicon probes (CM32, NeuroNexus Technologies, Ann Arbor, MI, USA). Each probe has 32 recording sites with vertical spacing of 50 μm (Fig. 2.1C). These probes capture the depth profile of local field potential.

3. Buzsaki32 silicon probes (B32, NeuroNexus Technologies, Ann Harbor, USA) have 32 electrode sites: four shanks, each with eight sites. The “octrode” configuration spans 100 µm vertically with 20 µm spacing of sites on each shank and 200 µm inter-shank spacing (Fig. 2.1A, B). The length of a shank enables up to 10 mm penetration and the thickness of the shanks (15 µm) allows to record spiking activity of individual neurons from densely packed cell areas without massive tissue or cell damage. Mounted with a lab-built microdrive, the probe moves about 300 µm with one full rotation of the screw.

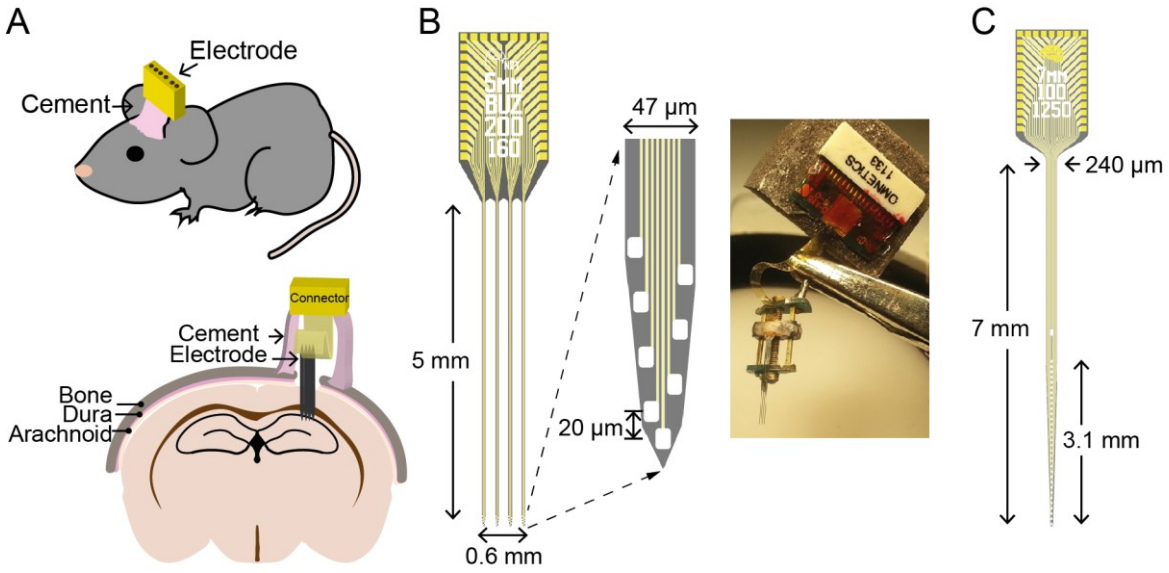

Figure 2.1: In vivo electrophysiology. *(A) Illustrations of electrode implantation. Upper: a mouse implanted with an electrode that is fixated on the head through dental cement and is only connected to recording system during the recordings. Bottom: the placement of the electrode on the mouse skull; a small hole was created through the layers of tissue underneath the skull, allowing the electrode to access the targeted hippocampal area. (B) B32 silicon probe for unitary recordings. Left: scheme of the electrode and an amplified scheme of one of the four shanks; white rectangles indicate recording sites at the tip of each shank. Right: photo of a reused B32 probe mounted on a customer micro-drive. (C) Scheme of the linear silicon probe for local field potential recording.*

2.2.2 Surgical implantation

Surgeries of implanting electrodes were conducted under isoflurane anesthesia. The mice were head fixed in a stereotactic frame (Kopf instruments, USA). 1% isoflurane was continuously supplied via nasal cone to maintain anesthesia. Depth of the anesthesia was controlled by checking pain reflex on the hind paws. Eye gel was applied to prevent corneal drying. Before the incision of the scalp, local anesthesia (10 % lidocaine, Xylocaine® Pumpspray, AstraZeneca

GmbH, Germany) was applied over the scalp. After a midline incision on the scalp, both bregma and lambda were exposed. The temporal and neck muscles were scraped aside, and the skull surface was cleaned and kept moist with saline solution. Locations for implants were marked on the skull and holes were drilled accordingly with a dental drill (OmniDrill 35, WPI, USA). The size of craniotomy and size of the drilling bits varied depending on the exact target locations and the implants desired.

Before the implantation of silicon probes and tungsten wire arrays, the impedance of recording sites was tested and sites with cross-talks were excluded from analysis. To target the dorsal hippocampal CA1 area, the implantation coordinates were set at AP–1.94 mm, L–1.4 mm, V–1.4 mm in accordance with "The Mouse Brain in Stereotaxic Coordinates" (Paxinos & Franklin 2004). Tungsten wires and linear probes were targeted at CA1 str. pyramidale and B32 probes were targeted above str. pyramidale followed by gradual advancing towards the pyramidal layer.

2.2.3 Data acquisition

Signals from the electrodes were first pre-amplified by operational amplifiers (HS-8, Neuralynx, Bozeman, Montana USA or Noted B.T., Pecs, Hungary) next to the headset to eliminate cable movement artifacts and further fed to the 128-channel recording system (Digital Lynx, Neuralynx, USA). Signals were differentially amplified, band-pass analogue filtered (1 Hz–10 kHz) and digitalized at 32 kHz. LFP was obtained off-line by down-sampling of the wide-band signal to 1250 Hz using Neurophysiological Data Manager (NDManager, http://neurosuite.sourceforge.net/).

2.2.4 Behavioral paradigms

Recordings of hippocampal LFP and neuronal firing were performed when animals were in a home-cage (25×15×18cm, with food and water) or were exploring an open field in a grey wooden rectangular box ("Arena", 50×30×18cm) or on a circular track ("Track", Ø60 cm, 10cm wide). Experiments usually started after the animals had been habituated in all arenas for two days. Each session on exploratory arenas ("Arena" or "Track") lasted about 10 min; between sessions, mice rested for at least 30 min. Each recording in the home-cage lasted 30 min. To track the animal's position during exploration, a light-emitting diode was attached to the headset and recorded at 25 frames per second in the darkness.

2.3 Analysis of *in vivo* electrophysiological data

Electrophysiological signals were processed using Neurophysiological Data Manager (NDManager, http://neurosuite.sourceforge.net/) (Hazan et al 2006), and analyzed by custom-written MATLAB algorithms (The MathWorks, Inc., Natick, Massachusetts, United States). The methods for detecting and analyzing the local field potential and spikes are documented below.

2.3.1 Local field potential analysis

Local field potential was obtained by low-pass filtering of the digitalized wide band EEG signal and down-sampling it to 1250 Hz. The LFP in dorsal hippocampal CA1 has a characteristic laminar profile: theta waves are coherent in phase and increase in amplitude from above the cortex to the pyramidal cell layer of the hippocampus; ripples occur in the pyramidal cell layer with the concurrent negative sharp waves in the stratum radiatum. These serve as the depth reference to position the tip of a movable silicon probe (B32, mounted on a microdrive). Oscillatory patterns of LFP were defined as theta (5–12 Hz), gamma (35–120 Hz), ripples (140–200 Hz) for detection.

Theta epochs were detected by calculating the power ratio of theta (5–12 Hz) and delta (2–4 Hz) frequency bands with a two-second moving window and 50% overlap. Fast Fourier Transform was used to compute the power spectra. A ratio of >=6 automatically marked the periods of theta epochs; the beginning and end of an epoch were marked when the ratio fell below 3. This was followed by a manual adjustment to exclude spurious epochs.

To detect ripples, wide-band EEG was first band-pass filtered (120–250 Hz), rectified and smoothed with a 3-ms window. Ripples were detected when the amplitude of the filtered signal exceeded the threshold of seven standard deviations above the background mean.

Power spectral density of LFP was computed using multitaper-based time-frequency spectra analysis. The recordings were first chunked with a moving window of 2048 samples and an overlap of half-window length. For each segment of data, multi-taper periodogram (power spectrum) was computed. Tapers were the first five Slepian sequences generated from a time half bandwidth product of 3; the tapered periodogram was calculated based on Fast Fourier Transform (FFT). Power spectral density was derived from averaging the power spectra of all time segments. The power of the oscillatory signal was computed as the integral power in the specified frequency range. The percentage of this integral power to the total power over the

whole frequency range was used to compare the power of the oscillation between animals and groups.

2.3.2 Spike sorting

There were three steps in attaining the spiking sequences of each neuron. First, spikes were detected from the voltage traces. After digitally high-pass filtering the wideband signal (cutoff frequency of 800 Hz), the root mean square power of the filtered signal was computed with a moving window of 0.2 ms (Csicsvari et al 1998). Spikes were detected when the power was more than five times the standard deviation from the baseline mean. In the second step, spike features were extracted. The detected spikes were up-sampled. The original and reconstructed waveforms were realigned along their peaks. Principal component analysis (PCA) was applied here to compress each waveform into the first three principal components (Abeles & Goldstein 1977). Each spike was featured with 33 parameters and projected as a 33-dimensional vector. These two steps were performed in NDManager where spike events and feature vectors were stored in ".spk" files and ".fet" files respectively. The last step was to cluster spikes based on their feature vectors and assign them to individual units. This was first performed by an automatic clustering program KlustaKwik (K.D. Harris, http://klustakwik.sourceforge.net) and followed by manual adjustment and classification of the units. The quality of a cluster was estimated by the isolation distance of the units that was the Mahalanobis distance from the cluster center within which the number of spikes from the specified cluster equals to the number of spikes from other clusters (Harris et al 2001). The manual part was aided by the graphical interface "Klusters" that displayed spike waveforms, distributions of principal component vectors, auto-correlogram (ACG) and cross-correlograms (CCG) (Fig. 2.2A). Single units were those with a clear refractory period of 2 ms shown in their ACGs. CCGs of unit pairs closely resembling the individual ACGs suggested that the two units were from the same neuron. Potentially mergeable clusters were also suggested by the color-coded error matrix which indicated the similarity of pairs of clusters based on the mean probability of the spikes in the first cluster being actually from the second cluster. Further, if the two clusters overlapped in their projections on the two dimensional spaces of any two waveform feature vectors but separated when time was selected as one of the projection dimension, they were judged to emanate from a single cell and were merged to one. Single units with slow firing rate (<3 Hz) and an ACG that showed a peak at 3–5 ms followed by a fast exponential delay (Fig. 2.2B) were classified as putative pyramidal cells. Single units with a firing rate above 7 Hz were

classified as putative interneurons. Units that could not be classified were excluded from analysis.

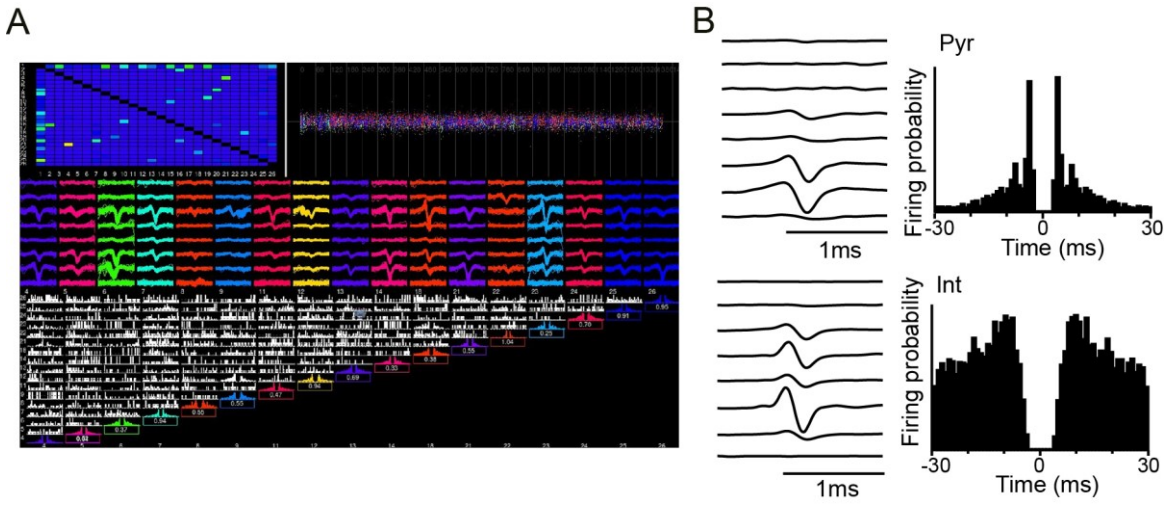

Figure 2.2: Spike sorting and unit detection. *(A) Snapshots of the semiautomatic spike sorting of a recording from a shank of B32 probe. Top, left: matrix of mean identification error probability (color-coded: blue–minimal, yellow–maximal). Top right: plot of time (x axis) against one of the principal components for all clusters obtained. Middle: average waveforms of isolated units, 8 channels from one single shank are shown. Bottom: auto-correlations of simultaneously isolated single pyramidal cells (colored diagrams, 17 single units) and their cross-correlations (white diagrams). Multi-unit clusters are not shown. (B) Examples of isolated putative pyramidal cell (Pyr) and fast spiking interneuron (Int), single units. Left: average spike waveforms recorded using a silicon probe; right: the corresponding auto-correlograms. Bin width, 1 ms.*

2.3.3 Characterization of recorded units

The firing rate of the putative neuron was computed by dividing the number of spikes over the duration of the recording. For each putative neuron, intervals between spike times, i.e. inter-spike intervals (ISIs), were calculated. The frequency distribution of ISIs was represented by the normalized ISI histogram with bin width of 2ms. For each genotype, the normalized ISI histograms were averaged at each bin across units. Spike activities were classified into two types: single spike and burst. A burst event was defined as a sequence of two or more spikes with ISI less than 15ms. Spikes that were not part of a burst were single spikes. A burst index of a unit was defined as the proportion of spikes in bursts to all spikes. Complex spike burst index was a restricted version of burst index where only bursts with spike amplitude

accommodation were included as real burst events. The time stamp of the first spike in a burst was considered as a time stamp of the burst.

The probability of burst firing following varied length of preceding silence was computed as a histogram of the ISIs that preceded the first spike of each burst event. To examine the effect of burst firing on the cell's subsequent excitability, the spiking probability as a function of the time elapsed after a burst event was calculated as a histogram of the ISIs that followed a burst and precede a single spike.

2.3.4 Analysis of burstiness

To compare the burst probability of neurons between two genotypes, I first characterized the burstiness of individual neurons based on their inter-spike interval (ISI) histograms. For each putative pyramidal cell, the first 100 milliseconds of ISIs were binned in 4-ms bins and normalized to the area, generating a firing probability distribution for each neuron. Principal component analysis was applied on the matrix of ISI probability distributions of all recorded neurons within one genotype to identify components that account for most variances in the ISIs ("pca" function in MATLAB, MathWorks). 2D plots of the first components and 3D plots the first three components aided to inspect the distribution of the neurons in components' spaces.

Putative pyramidal cells represented by their first three components were partitioned into two clusters using a k-means clustering algorithm ("kmeans" function, MATLAB). The maximal number of iteration of each run was 100 and the clustering was repeated 50 times, each with randomly assigned initial conditions. The final clusters were determined by the best fit, which had the minimal sum of squared from points to their centroid. The preset k-value of 2 was selected based on a cluster evaluation function $f(K)$ (Pham et al 2005). The function relies on the measure of within-cluster distortion I_j and the sum of distortions from all clusters S_K:

$$I_j = \sum_{t=1}^{N_j} [d(x_{jt}, W_j)]^2$$

$$S_K = \sum_{j=1}^{k} I_j$$

where W_j is the center of the cluster j, N_j is the number of object assigned to cluster j, x_{jt} is the tth object assigned to the cluster j and d is the distance between x_{jt} and W_j. The evaluation function $f(K)$ is defined as:

$$f(K) = \begin{cases} 1 & if\ K = 1 \\ \dfrac{S_K}{a_K S_{K-1}} & if\ S_{K-1} \neq 0, \forall\ K > 1 \\ 1 & if\ S_{K-1} = 0, \forall\ K > 1 \end{cases}$$

$$a_K = \begin{cases} 1 - \dfrac{3}{4N_d} & if\ K = 2\ \ and\ N_d > 1 \\ a_{K-1} + \dfrac{1 - a_{K-1}}{6} & if\ K > 2\ and\ N_d\ > 1 \end{cases}$$

where N_d is the number of dimensions. The term $a_K S_{K-1}$ estimates the S_K through the value of S_{K-1} with the assumption that the data have a uniform distribution. The search for the lowest $f(K)$ value, i.e. the optimal cluster number, was implemented using R (r-project, "kselection" package, function "kselection").

The statistical significance of splitting the neuron population into two clusters was tested using "SigClust" method in R (r-project, "sigclust" package, function "sigclust") (Huang et al 2015, Liu et al 2008). This approach models a cluster as a subset of data sampled from a single multivariate Gaussian distribution. The test null hypothesis H_0 states that the data are from a single Gaussian distribution against the alternative hypothesis H_a that the distribution is non-Gaussian. The test statistic is the cluster index CI, i.e. the ratio of within-cluster sum of squares about the mean to the total sum of squares about overall mean, defined as:

$$CI = \frac{\sum_{k=1}^{2} \sum_{j \in C_k} \left\| x_j - \bar{x}^{(k)} \right\|^2}{\sum_{j=1}^{n} \left\| x_j - \bar{x} \right\|^2}$$

where C_k is the *k*th cluster and $\bar{x}^{(k)}$ is the mean of the *k*th cluster; the smaller the CI, the larger the amount of overall variance is explained by the clustering. The null distribution of CIs was then approximated using a Monte Carlo simulation.

After assigning putative neurons to either cluster, Fisher linear discriminant analysis (FDA) was applied to the first three principal component scores of the ISI probability matrix. The analysis was implemented by custom MATLAB codes and followed the original Fisher's method that does not assume the clusters as normally distributed nor with equal covariance (Fisher 1936). In the case of two clusters, the FDA finds the linear combination of features that best discriminate the clusters by maximizing the objective function

$$J(w) = \frac{w^T S_B w}{w^T S_W w}$$

where *w* is the vector for linear combination. S_B is the between-cluster scatter matrix and S_W is the within-cluster scatter matrix, defined through:

$$S_B = (\mu_1 - \mu_2)(\mu_1 - \mu_2)^T$$

$$S_W = \sum_c \sum_{i \in c} (x_i - \mu_c)(x_i - \mu_c)^T$$

Where c denotes the index for the clusters; μ_1 and μ_2 are the means for each cluster respectively. The maximum separation J occurs when

$$\vec{w} \propto {S_W}^{-1}(\overrightarrow{\mu_2} - \overrightarrow{\mu_1})$$

The resulted vector $\vec{w}$ represents the linear combination of the features that best discriminate the two clusters. The distribution of the data from different clusters can be completely separated or partially overlapped, indicative of how well the clusters are separated from each other.

2.3.5 Cross-correlation of unit pairs

Cross-correlation histograms (CCH) of pyramidal cell pairs recorded simultaneously were computed to explore the temporal correlation of their spikes. CCHs were constructed with 10-ms bin and lags of up to ± 250 ms. The lag τ at τ = 0 corresponds to ± 5 ms. The CCH at lag τ was the count from the two spike trains that satisfies:

$$c(\tau) = \sum_{i=1}^{N_1} \sum_{j=1}^{N2} 1\{\tau - 5ms < T_{2,j} - T_{1,i} < \tau + 5ms\},$$

where $T_{2,j}$ was the timestamp of the *j*th spike of neuron 2 and $T_{i,ij}$ the timestamp of the *i*th spike of neuron 1.

2.3.6 Place cell analysis

The resolution of the firing maps was set with one pixel covering 2 × 2 cm^2 in physical space. Firing maps of place cells were computed by dividing the number of spikes in a given pixel by the time the animal spent in this pixel. Periods of immobility were excluded from the analysis. A Gaussian window of width 3 was used to smooth the firing maps. Peak firing rate was defined as the maximum firing rate over all pixels in the environment. Place fields were detected as spatially continuous areas where the firing rate exceeded 1 Hz or, for place fields constructed by spikes from bursts, 0.2 Hz.

The measured properties of a place field included its field size, coherence, sparsity and spatial information. Place field size was defined as the size of the largest place field for each cell. Coherence, a measure of the local smoothness of the firing profile (Muller & Kubie 1989), was computed as the Fisher z-transform of the Pearson's correlation between the rate in a given pixel and the average rate in its eight first-order neighbors. Sparsity, which measures how diffuse the spikes of a unit are, was computed as

$$Sparsity = \frac{(\sum_{i=1}^{n} p_i \cdot f_i)^2}{\sum_{i=1}^{n} p_i \cdot f_i^2}$$

where p_i is the occupancy probability of the *i*th bin: $p_i = t_i / \sum_{i=1}^{n} t_i$, and f_i is the firing rate of the unit in the *i*th bin. Spatial information measures the amount of information about the animal's position carried by the spike train of the place cell, based on the information theory (Skaggs et al 1996):

$$Spatial\ information = \sum_{i=1}^{n} p_i \frac{f_i}{f} log_2 \frac{f_i}{f}$$

where $\sum_{i=1}^{n} p_i \cdot f_i$, i.e. the overall mean firing rate. The unit of spatial information is bits per spike. It can be understood as such: if a unit fires spikes evenly in all bins, the spatial information is 0 bit and the sparsity would be 1; if the unit discharges spikes evenly in half of the bins and keeps silent in the other half, the spatial information is 1 bit while the sparsity gets to 0.5.

Burst and single spike firing maps were constructed using spike trains that consisted of only spikes in bursts and of only single spikes respectively.

2.3.7 Theta phase and phase precession analysis

Theta oscillation phase was derived from the Hilbert transform of the band-pass filtered (5–12Hz) LFP. Peaks were assigned as 0° and 360° of a theta cycle while troughs as 180°. Phase histograms of individual spike trains were computed and normalized by the total number of events. The mean of the phases of all spikes was calculated for each unit as its preferred phase in theta oscillations. Circular uniformity test (Rayleigh test) was applied, and a $p<0.01$ suggested the unit being significantly theta modulated. Such analysis was also performed for either only single spikes or only spike in bursts for each putative cell to estimate the theta modulation of the two firing modes. The discharge probability histograms of individual cells were convolved with the Gaussian kernel function of size 2 SD (Csicsvari et al 1999) . Histograms of mean phases of all theta-modulated units were computed to describe the preferred discharge phases of cells in each genotype.

The phase precession during successive theta cycles was estimated using a circular-linear fit method (Kempter et al 2012). For each cell, each spike was characterized by its phase ϕ and its timestamp *x*. Since the phase values are periodic, *n* spikes were projected onto a cylinder as (ϕ_1, x_1), (ϕ_2, x_2), …, (ϕ_n, x_n). A linear model of $\emptyset_i = 2\pi a x + \emptyset_0$ was fitted where *a* and ϕ_0

denote the slope and the phase offset respectively. The value of the slope a was estimated by maximizing mean resultant length R:

$$\mathrm{R} = \sqrt{[\frac{1}{n}\sum_{j=1}^{n}\cos(\emptyset_j - 2\pi a x_j)]^2 + [\frac{1}{n}\sum_{j=1}^{n}\sin(\emptyset_j - 2\pi a x_j)]^2}.$$

The estimate of the slope $\hat{a} = \arg max_a R(a)$ was restricted to the interval of $[-2\pi, 2\pi]$ and the ϕ_0 is estimated following:

$$\widehat{\emptyset_0}(\mathrm{a}) = arctan^* \frac{\sum_j \sin(\emptyset_j - 2\pi a x_j)}{\sum_j \cos(\emptyset_j - 2\pi a x_j)}.$$

To quantitatively examine the relationship of phase precession and firing dynamics, instantaneous firing rate of each spike was calculated from the number of spikes in the two full theta cycles centered at the spike of interest. Low instantaneous firing rates corresponded to 1 spike per 2 cycles (i.e. 4 Hz if the concurrent theta frequency is 8 Hz) while high firing rate was defined when ≥ 3 spike emitted per 2 cycle. In a spike train that spanned several (≥5) theta cycles, the "onset" segment was the accelerating part of the spike train where the number of spikes increased in consecutive cycles; the "offset" segment was the cessation part of spike train where the intra-cycle spike number decreased monotonically. The temporal derivative of the firing rate for each cycle was calculated by linear regression of the number of spikes against the cycle number. To compare the phases of the spikes, Watson-Williams test was used for one factor ANOVA; two-factor circular ANOVA was performed with Harrison-Kanji test using the "CircStat" MATLAB toolbox (Berens 2009).

3 Results

3.1 Firing rate of *Kcnq3*$^{-/-}$ pyramidal cells

The extracellular action potentials of neurons in hippocampal CA1 area were recorded using movable silicon probes while animals were freely behaving. In total, 458 putative pyramidal cells were recorded and sorted. The average firing rate of pyramidal cells in knockout mice was significantly lower than in the wild type (average firing rate: *Kcnq3*$^{+/+}$, 1.45 ± 0.07 Hz; *Kcnq3*$^{-/-}$, 1.08 ± 0.03 Hz; $p < 0.0001$, Mann-Whitney-U-Test. Fig. 3.1).

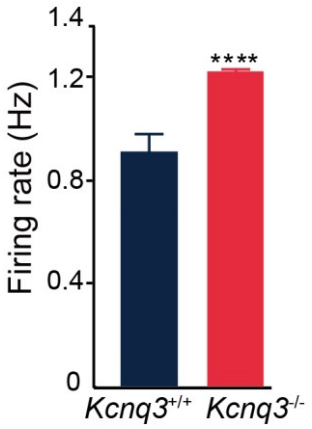

Figure 3.1: Average firing rate of CA1 pyramidal cells. *Kcnq3*$^{-/-}$*: n = 377 cells, Kcnq3*$^{+/+}$*: n = 81 cells; ****: p < 0.0001, Mann-Whitney-U-Test.*

3.2 The burst firing of *Kcnq3*$^{-/-}$ pyramidal cells

3.2.1 Increased burst firing and diminished frequency accommodation

To examine the temporal dynamics of spike trains, I computed the auto-correlograms (ACG) of spike timing and the histograms of inter-spike intervals (ISI) of individual putative pyramidal neurons. In ACGs, peaks indicate the time intervals where the firing probability is highest after or before another spike. The averaged ACG from wild-type putative pyramidal cells showed a pair of symmetrical peaks within ± 10 ms, typical of pyramidal cells firing complex spike bursts. For the knockout, the peaks on the ACG occurred at the same interval and were higher (Fig. 3.2A). From the wild-type ISI histogram, a peak was prominent at ISI of 4–6 ms and followed by an exponentially decreasing probability for longer ISIs. The ISI histogram of *Kcnq3*$^{-/-}$ pyramidal cells showed a peak at the same interval and a similar exponential tail, but the peak was twice higher than that in the wild type (Fig. 3.2B). Given that spikes within bursts give rise to ISIs of 3 to 15 ms, the higher ACG peaks from the *Kcnq3*$^{-/-}$ pyramidal cells suggested a more frequent occurrence of burst firing.

To determine whether these cells indeed discharged more bursts, I calculated for each putative pyramidal cells the complex spike index (CSI). Pyramidal cells typically fire complex spike bursts which include a group of 2–6 spikes with short ISIs (i.e. up to 15 ms) and accommodating amplitudes. The CSI represents the proportion of spikes that emit in complex spike bursts. The complex spike index was higher in pyramidal cells from the knockout, in agreement with the indication of increased burst firing by the ISIs and ACGs (Fig. 3.2C). Moreover, bursts in *Kcnq3*$^{-/-}$ cells were longer than in the wild-type, consisting of more spikes per burst (*Kcnq3*$^{-/-}$, 2.65 ± 0.003 spikes per burst, n= 377 cells; *Kcnq3*$^{+/+}$, 2.39 ± 0.004 spikes per burst, n=81 cells; two-way nested ANOVA with factors "genotype" and "unit (genotype)": main effect of

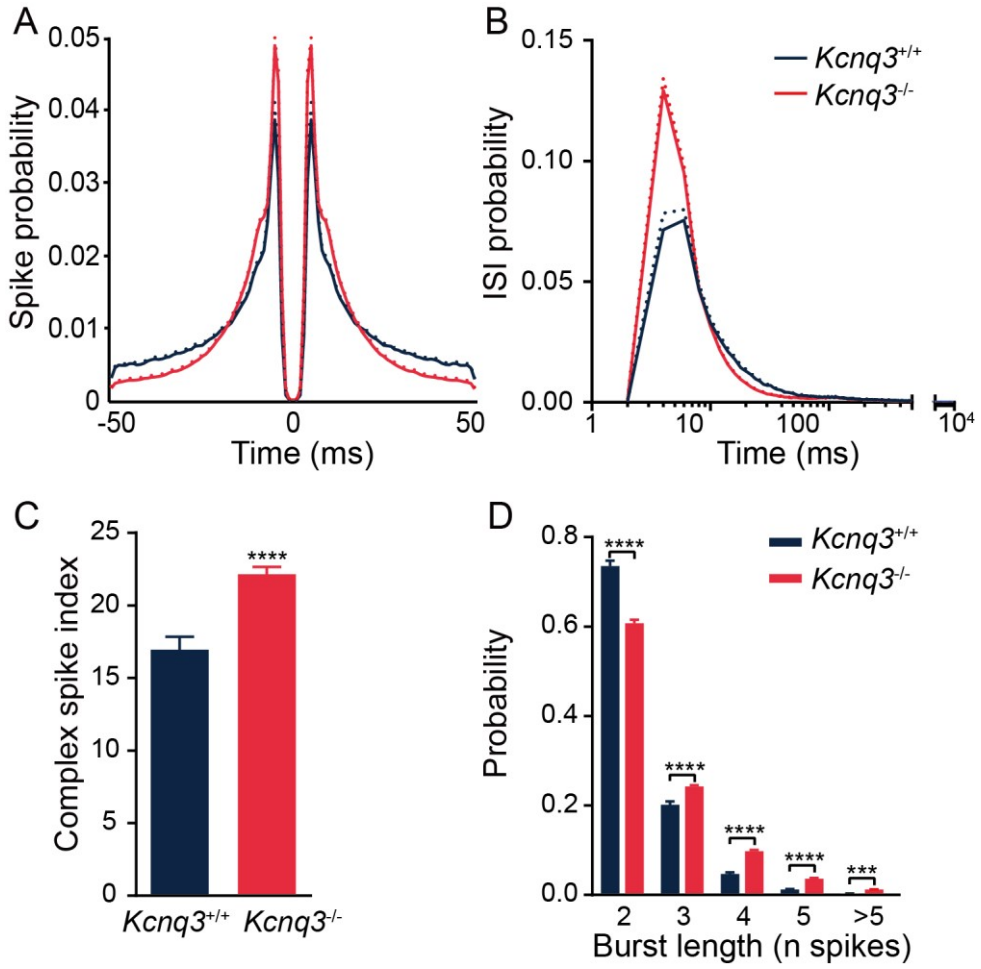

Figure 3.2: Ablation of KCNQ3 increased burst firing of CA1 pyramidal cells in vivo. *(A) Auto-correlograms of spike timestamps averaged across pyramidal cells. (B) Average inter-spike interval histograms of CA1 pyramidal cells, Kcnq3*$^{-/-}$*: n = 377 cells, Kcnq3*$^{+/+}$*: n = 81 cells. (C) Complex spike index, **** p < 0.0001, Mann-Whitney-U-Test. (D) Average probability of bursts of different length (number of spikes in a burst). **** p < 0.00001, *** p < 0.0001, Mann-Whitney-U-Test, Bonferroni adjusted alpha levels of 0.01 (0.05/5). Data are presented as mean + SEM.*

"genotype", $F_{(1.138005)}$=1704.9, $p < 0.0001$; Fig. 3.2D). Their bursts were also, on average, faster with shorter intra-burst ISIs (average intra-burst ISI: *Kcnq3*$^{-/-}$, 6.66 ± 0.02 ms, n = 377 cells; *Kcnq3*$^{+/+}$, 7.90 ± 0.09 ms, n = 81 cells. Two-way ANOVA with factors "genotype" and "burst length": main effect of "genotype", $F_{(1.5615)} = 288.93$, $p < 0.0001$; effect of interaction, $F_{(4.5615)} = 9.23$, $p < 0.0001$; Fig. 3.3C).

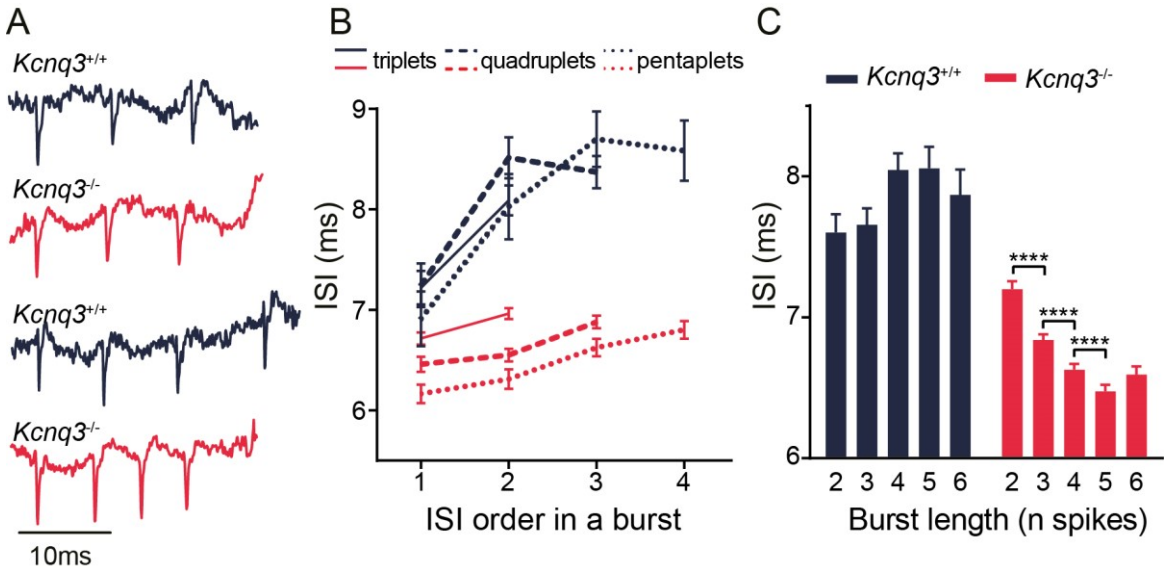

Figure 3.3: Kcnq3$^{-/-}$ pyramidal cells showed reduced frequency accommodation during burst firing. *(A) Signal traces showing representative bursts, consisting of 3 and 4 spikes. Note the shorter intra-burst spike intervals and reduced frequency accommodation in the recordings from Kcnq3$^{-/-}$ putative pyramidal cells. (B) Spike frequency accommodation: ISIs averaged according to the order of sequential spikes in bursts of different length that contained 3, 4 or 5 spikes (triplets, tetraplets and pentaplets). Kcnq3$^{-/-}$: n = 377 cells; Kcnq3$^{+/+}$: n = 81 cells. The first order spike accommodation rate was defined as* $R_{accom} = (2_{nd}\,ISI - 1_{st}\,ISI)/1_{st}\,ISI$, *where* $1_{st}\,ISI$ *and* $2_{nd}\,ISI$ *were the first and the second inter-spike intervals within the same burst, respectively.* R_{accom} *was lower in Kcnq3$^{-/-}$ than in the wild-type; two-way ANOVA ("genotype"× "burst length"), effect of "genotype":* $F_{(1,50098)} = 66.46$, $p < 0.0001$, *effect of interaction:* $F_{(2,50098)} = 5.33$, $p = 0.0048$. *(C) Average intra-burst ISI of bursts of varied lengths. Kcnq3$^{-/-}$: 6.66 ± 0.02 ms, n = 377 cells; Kcnq3$^{+/+}$: 7.90 ± 0.09 ms, n=81 cells. Two-way ANOVA ("genotype"× "burst length"): effect of "genotype":* $F_{(1,5615)} = 288.93$, $p < 0.0001$, *effect of interaction:* $F_{(4,5615)} = 9.23$, $p = 0.0048$. *The average ISIs of bursts was progressively shorter with increasing burst length in Kcnq3$^{-/-}$ but not in controls (Kcnq3$^{-/-}$: 2- vs. 3- spikes, 3- vs. 4-spikes, and 4- vs. 5-spikes:, **** $p < 0.0001$, 5- vs. 6-spike bursts: $p=0.92$, Mann-Whitney-U-tests). Data are presented as mean ± SEM.*

Another significant change of bursts in the knockout was the lack of frequency accommodation during a burst. In the wild-type, bursts of various lengths showed a frequency accommodation such that the first three spikes in a burst occurred with progressively longer ISIs (Fig. 3.3A, B). This intra-burst frequency accommodation was largely diminished in

pyramidal cells from the knockout (Fig. 3.3B). In addition, the first intra-burst ISI in the knockout was on average shorter in the long bursts (quadruplets and pentaplets) than the shorter bursts (i.e. triplets), while both short and long bursts in the wild-type exhibited similar ISI at their first intra-burst interval (Fig. 3.3B). Combined with the lack of the intra-burst frequency accommodation, this led to a higher intra-burst spike frequency in long bursts than short bursts in *Kcnq3*$^{-/-}$ pyramidal cells. In contrast, the average intra-burst ISI in the wild-type increased with longer bursts (Fig. 3.3C).

3.2.2 Recent spiking reduced burst probability

According to the hypothesis that bursts function as "conditional synchrony detectors", the probability of burst firing is presumably constrained by the neuron's recent spiking activity (Harris et al 2001). To examine whether burst firing in *Kcnq3*$^{-/-}$ pyramidal cells was subject to the regulation of previous spiking events, I compared the burst probability after varied length of the neuronal inactivity. In wild-type, neurons tended to fire a single spike instead of a burst if the preceding firing was very recent, i.e. of up to 50 ms ago. The probability of initiating a burst increased as the preceding silence prolonged and reached the maximum at ISI of ~100 ms (Fig. 3.4A). This indicated that recent spiking suppressed burst firing while the longer period of silence promoted it. Such dynamics for burst initiation was also preserved in the knockout group while the probability of initiating a burst in these neurons was generally higher regardless

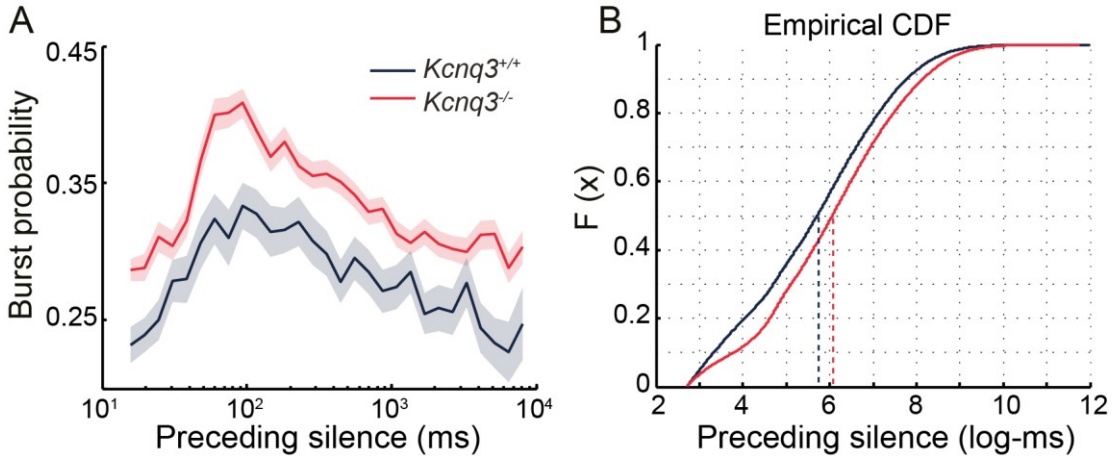

Figure 3.4: Burst generation depends on recent firing history. *(A) The probability of next spiking event being a burst as a function of preceding silence, averaged over all putative pyramidal cells from each genotype. Kcnq3*$^{-/-}$*: n=377 cells, Kcnq3*$^{+/+}$*: n=81 cells. Data are presented as mean ± SEM. (B) The empirical cumulative distributions of the length of pre-burst silence of all burst events from each genotype. Dashed lines show the median ISIs that precede burst firing in either genotype: Kcnq3*$^{-/-}$*,* $e^{6.06}$ *= 472.95 ms, Kcnq3*$^{+/+}$*,* $e^{5.71}$ *= 302.60ms; p < 0.0001, two-sample Kolmogorov-Smirnov test.*

of the length of the preceding ISI. However, the period of silence before bursts was considerably longer in *Kcnq3*$^{-/-}$ neurons which was consistent with a reduced average firing rate (Fig. 3.4B).

3.2.3 The distribution of burst probability in the pyramidal cells

Recent large-scale unit recordings have revealed a lognormal distribution of discharge rate and firing pattern in hippocampal pyramidal population that may be preconfigured by the connectivity and synaptic weights (Grosmark & Buzsáki 2016, Mizuseki & Buzsáki 2013). How would the knockout of *Kcnq3* affect such distribution of firing properties? And does the increased bursting in *Kcnq3*$^{-/-}$ pyramidal cells result from a homogenous upregulation of burst discharge in most neurons or alternatively from an increased proportion of highly bursty neurons?

First, I examined whether the pyramidal cells in the wild-type were similar or heterogeneous in their burst probability. ISI histograms below 100 ms of individual neurons were binned in 4–8 ms bins and were normalized to the area of the histograms, thus obtaining for each neuron its ISI probability distribution. Since the ISI probability at different time bins correlated, principal component analysis (PCA) was applied on the matrix of ISI probability distributions of all neurons to extract components that account for the variance in the original data and are uncorrelated with each other. The first three components explained 96.92% of the variance of the ISIs (Fig. 3.5A, 82.0% of the variance explained by 1st PC, 11.6% by 2nd PC and 3.3% by 3rd PC). Notably, the coefficient of the 1st component was highest at the time bin of 4–8 ms ($Coefficient_{PC1,Bin\ 2:\ WT}$ = 0.95) while the 2nd and the 3rd components both have highest coefficient at the bin of 0–4ms ($Coefficient_{PC2,Bin\ 1:WT}$ = 0.66; $Coefficient_{PC3,Bin\ 1:WT}$ = 0.69). Both time bins correspond to spike intervals within bursts. Therefore, much of the variance in a neuron's burst probability has been captured in the first three PCs. On the 3D-plot of the first three component scores, the *Kcnq3*$^{+/+}$ pyramidal cells did not show a single centroid of aggregation. Instead, they showed a tendency of segregating into two clusters, especially along the first component (Fig. 3.5B).

To identify potential subgroups in the wild-type population, neurons were subjected to a k-means clustering algorithm and partitioned into two clusters in the space of the first three PCs. The selection of k = 2 as the optimal cluster number was based on a clustering evaluation function which estimated how well the k-means clustering captured the aggregation of the data (for details see Method 2.3.4). The statistical significance of the 2-way clustering was tested using the "SigClust" method (for details see Method 2.3.4). The test defines a cluster as a

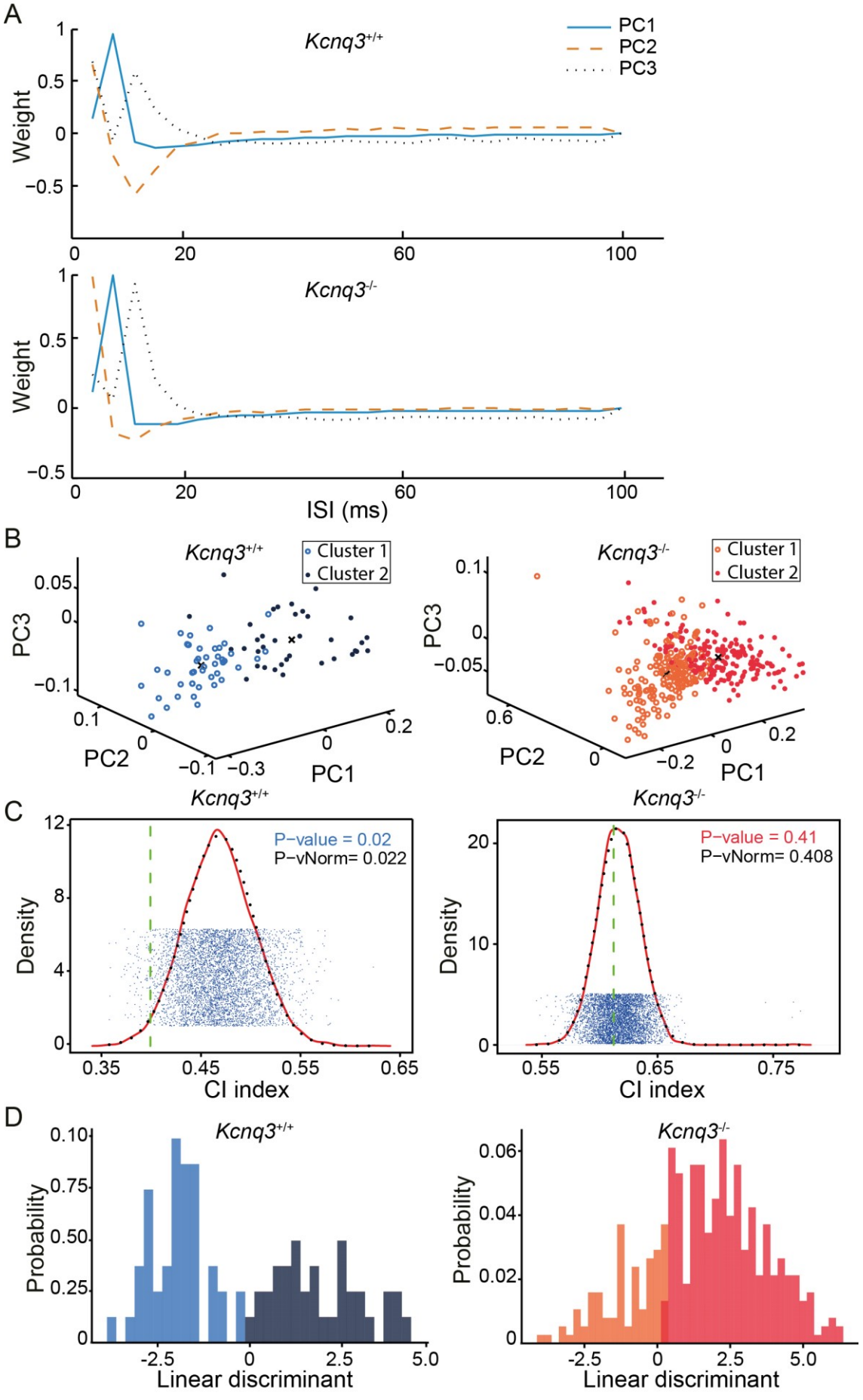
A
Kcnq3+/+
PC1
PC2
PC3
Weight
1
0.5
0
−0.5
0
20
60
100
Kcnq3-/-
Weight
ISI (ms)
B
Kcnq3+/+
Cluster 1
Cluster 2
PC3
PC2
PC1
Kcnq3-/-
Cluster 1
Cluster 2
PC3
PC2
PC1
C
Kcnq3+/+
P−value = 0.02
P−vNorm= 0.022
Density
CI index
Kcnq3-/-
P−value = 0.41
P−vNorm= 0.408
Density
CI index
D
Kcnq3+/+
Probability
Linear discriminant
Kcnq3-/-
Probability
Linear discriminant

Figure 3.5: Distribution of burstiness of the putative pyramidal cells in hippocampal CA1 of Kcnq3$^{+/+}$ and Kcnq3$^{-/-}$ mice. *(A) The first three components (PCs) extracted from the principal component analysis based on the ISI probability distributions of individual putative neurons in Kcnq3$^{+/+}$ (up) and Kcnq3$^{-/-}$ (bottom). (B) 3D scatterplots of the first three PC scores of neurons from each genotype clustered into two subgroups using k-means clustering algorithm. Left: Kcnq3$^{+/+}$ pyramidal cell; right: Kcnq3$^{-/-}$ pyramidal cells. (C) "Sigclust" test suggested the statistical significance of the 2-way clustering in Kcnq3$^{+/+}$ neurons but not in knockout. The dots present the CIs (cluster index, the ratio of within-cluster sum of squares about the mean to the total sum of squares about overall mean) simulated based on the null hypothesis and using the covariance estimate of the original data. (D) Projection of neurons onto the linear discriminant (LD) based on the ISI probabilities, indicating the distribution of burstiness. Left: distribution of the Kcnq3$^{+/+}$ pyramidal cells on the LD that best separated the "high bursty" subgroup from "low bursty" subgroup; right: distribution of Kcnq3$^{-/-}$ pyramidal cells on the LD trained by the wild-type neuron population.*

sample from a single Gaussian distribution and formulates the null hypothesis as that the data come from a single multivariate Gaussian distribution. Under the "SigClust" test, the clustering of the *Kcnq3*$^{+/+}$ neurons into 2 subgroups was significant ($p = 0.02$ at the significance level $\alpha = 0.05$; Fig. 3.5C). Fisher linear discriminant analysis was applied to attain the linear combination of the temporal features of the ISI distributions that best distinguished the two subgroups. The projection of the neurons on the linear discriminant showed a clear bimodal distribution with no overlap between two subgroups (Fig. 3.5D). Accordingly, the two subgroups of pyramidal cells from wild-type were labeled as "low bursty" and "high bursty" respectively.

Next, I applied the same analysis to the putative pyramidal cells from the knockout. The first three principal components from the PCA explained 98.1% of the variance in the ISI distributions (Fig. 3.5A, 59.7% of the variance explained by 1st PC, 34.3% by 2nd PC and 3.1% by 3rd PC). As in the wild-type, the first component had highest coefficient at time bin of 4–8 ms ($Coefficient_{PC1,Bin\ 2:KO} = 0.96$). However, the 2nd PC, which was highly correlated with the time bin of 0–4 ms, explained more variance of the ISIs in knockout than in wild-type ($Coefficient_{PC2,Bin\ 1:KO} = 0.94$). When the first three PCs of the putative pyramidal cells in the knockout were subject to the k-mean clustering, the separation of the neurons into two clusters was not significant according to "SigClust" test ($p = 0.41$ with significance level $\alpha = 0.05$; Fig. 3.5C). This suggested that the clustering of *Kcnq3*$^{+/+}$ neurons in their propensity to fire bursts was absent in *Kcnq3*$^{-/-}$ pyramidal cells. In fact, the distribution of the ISI probability in the knockout neuron population differed significantly from that of the wild-type (non-parametric Cramer test of the ISI probabilities: $p < 0.0001$ at significant level $\alpha = 0.05$; *Kcnq3*$^{-/-}$, n = 377 cells; *Kcnq3*$^{+/+}$, n = 81 cells.).

As the Fisher's linear discriminant analysis finds the linear function that best discriminates the "low bursty" pyramidal cells from the "high bursty" ones in the wild-type, we can use this linear discriminant to examine whether the *Kcnq3*$^{-/-}$ pyramidal cells resemble any subgroups in the wild-type. When their ISI histograms were projected on the linear discriminant that used the *Kcnq3*$^{+/+}$ pyramidal cells as a training sample, the fraction of *Kcnq3*$^{-/-}$ pyramidal cells classified as "high bursty" was higher than wild-type (ratio of "high bursty" neurons to "low bursty": *Kcnq3*$^{+/+}$, 36/45; *Kcnq3*$^{-/-}$, 289/88; $p < 0.0001$, χ^2 (1,N = 458) = 33.58, Chi-squared test; Fig. 3.5D). Moreover, the score of individual neuron in the discriminant function corresponded to the position of the neuron on the axis from "least bursty" to "highest bursty" and therefore could be taken as an index of the neuron's "burstiness". The "burstiness" of the pyramidal cells in the knockout classified as "high bursty" by the linear discriminant was comparable with the wild-type counterparts (two-sample Kolmogorov-Smirnov test: $p = 0.13$). In contrast, the knockout neurons classified as "low bursty" were more bursty than the "low bursty" group from the wild-type (two-sample Kolmogorov-Smirnov test: $p < 0.0001$). This revealed a general shift towards high burstiness in the *Kcnq3*$^{-/-}$ neuron population, which was translated into a significantly altered distribution of burst probability in the neuron population. While the wild-type neuron population comprised subgroups of low-bursty and high-bursty neurons, high burstiness became a feature of the majority of pyramidal cells in the knockout.

3.2.4 Decreased dependence of burst firing on the network state

The propensity of a neuron to fire bursts has been associated with the functional states of the neural network. For the pyramidal cells in CA1, the increased burst probability occurs during awake immobility versus running (Csicsvari et al 1998, Sneider et al 2006). To examine the dependence of burst firing on the network state in *Kcnq3*$^{-/-}$ mice, I drew references from the local field potential in the hippocampus CA1 whereby the firing of the neurons was compared between theta oscillations associated with locomotion or REM-sleep and the non-theta, large irregular activity (LIA) during awake immobility or slow-wave sleep.

To prevent the bias from the extremely sparse-firing neurons, only cells that emitted ≥ 20 firing events in both states were included in this analysis. In both wild-type and knockout, the propensity of bursting, measured by the fraction of burst events in total firing events, displayed a strong correlation between theta and non-theta states in individual neurons (Fig. 3.6A, B; *Kcnq3*$^{+/+}$, n = 73 cells, r = 0.84, $p < 0.0001$; *Kcnq3*$^{-/-}$, n =271 cells, r = 0.82, $p < 0.0001$). Nonetheless, the pyramidal cells of *Kcnq3*$^{+/+}$ mice exhibited a significantly higher propensity

for burst firing during LIA than during theta (Fig. 3.6A; theta vs. non-theta: $p = 0.04$, paired t-tests). More importantly, only the "high bursty" subgroup of *Kcnq3*$^{+/+}$ pyramidal cells increased their bursting with the LIA (Theta vs. non-theta: "low bursty", $p = 0.64$, n = 45 cells; "high bursty", $p < 0.0001$, n = 36 cells; paired t-tests). On the other hand, *Kcnq3*$^{-/-}$ pyramidal cells were deprived of the state-dependent shift of burst probability (Fig. 3.6A; theta vs. non-theta: $p = 0.81$, paired t-tests). At times of LIA versus theta, wild-type neurons also tended to emit

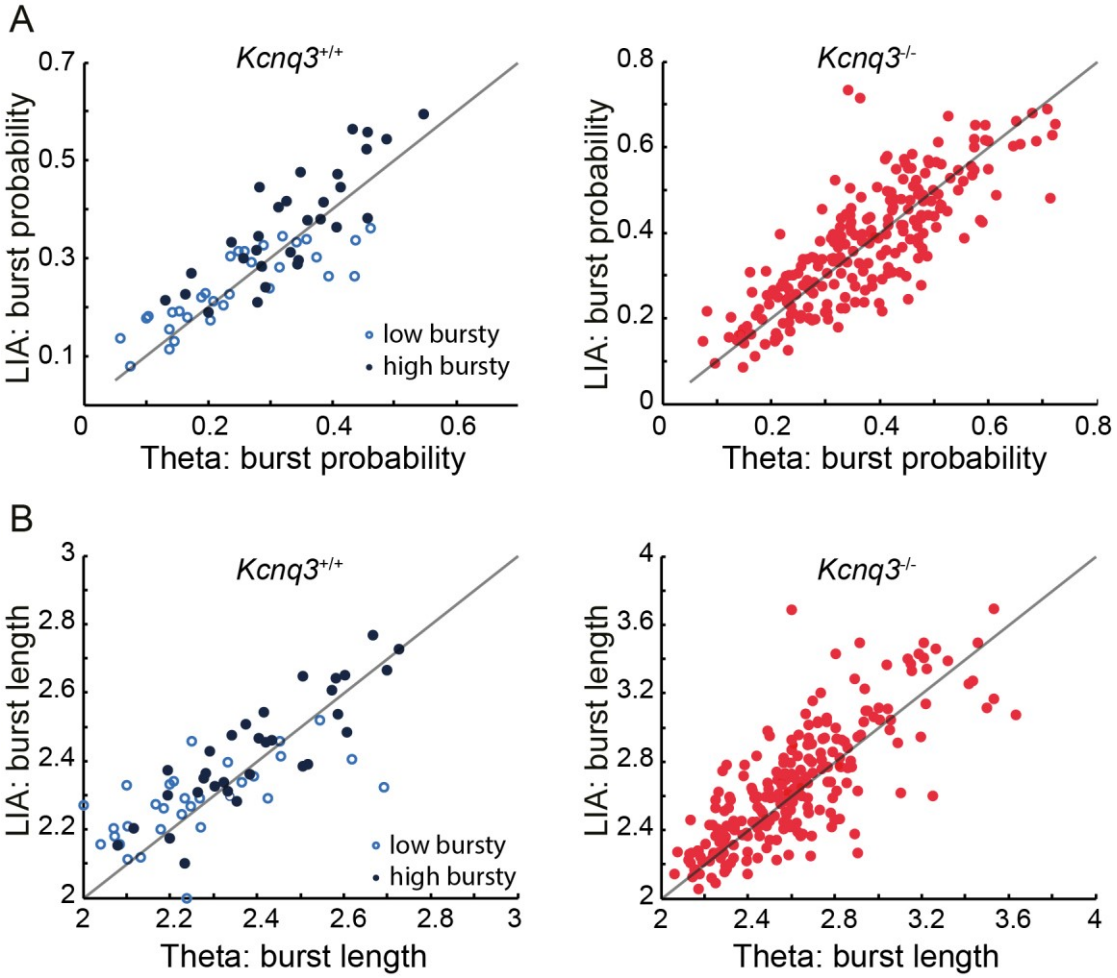

Figure 3.6: Burst probability and lengths during theta versus large irregular activity (LIA) of hippocampal LFP. *(A) Scatterplots of burst probability during theta versus burst probability during LIA. In wild-type "high bursty" but not "low bursty" nor Kcnq3*$^{-/-}$ *pyramidal cells, propensity to burst increased during LIA compared to theta (Kcnq3*$^{+/+}$*: "low bursty", p = 0.64, n = 45 cells, "high bursty", p <0.0001, n = 36 cells; Kcnq3*$^{-/-}$*, p = 0.81, n = 377 cells; paired t-test). (B) Scatterplots of average burst lengths during theta versus during LIA. For both wild-type "high bursty" and Kcnq3*$^{-/-}$ *pyramidal cells, bursts tend to be longer, with more spikes during LIA. (Kcnq3*$^{+/+}$*, "low bursty", p = 0.12, n = 45 cells, "high bursty", p = 0.03, n = 36 cells; Kcnq3*$^{-/-}$*, p = 0.002, n = 377 cells; paired t-test). Dots represent individual putative pyramidal cell; for plots of Kcnq3*$^{+/+}$ *neurons, hollow and filled dots indicate subgroups of "low bursty" and "high bursty" pyramidal cells respectively.*

bursts that comprised more spikes (Fig. 3.6B; theta vs. non-theta: $p = 0.04$, paired t-tests). The potentiation of bursts was only significant for "high bursty" subgroup (Theta vs. non-theta: "low bursty", $p = 0.12$, n = 45 cells; "high bursty", $p = 0.03$, n = 36 cells; paired t-tests). For *Kcnq3*$^{-/-}$ pyramidal cells, bursts during non-theta LIA were also longer than during theta (Fig. 3.6B; theta vs. non-theta: p = 0.002, paired t-tests). From theta to LIA state, the "high bursty" wild-type neurons became more likely to discharge in bursts and with more spikes in a burst, while the "low bursty" subgroup did not change their burst firing accordingly. In contrast, *Kcnq3*$^{-/-}$ pyramidal cells were less sensitive to different functional states; while most of them were bursty, the probability of firing a burst did not vary with the ongoing LFP states.

3.3 The neuronal firing during theta oscillations

During locomotion and REM sleep, theta oscillations dominate the hippocampal LFP. It is postulated that theta rhythms provide a temporal mechanism to coordinate neuron assemblies for collective information transfer (Buzsáki & Moser 2013). The phases at which neurons fire in relations to the ongoing theta cycle can serve as the timing of the spikes to encode information (Singer 1993). In light of this hypothesis, I examined the firing of neurons during theta oscillations, focusing on two aspects: 1) the theta modulation of burst firing; 2) the patterns and conditions of theta phase precession.

3.3.1 The theta modulation of burst firing

Previous studies have shown that pyramidal cells, despite considerable individual variability, tend to fire on the negative phases of the theta waves (O'Keefe & Recce 1993, Ranck 1973) . As expected, pyramidal cells in *Kcnq3*$^{+/+}$ mice mostly generated bursts close to the trough of the theta cycles and less frequently at other phases (Fig. 3.7A). In contrast, the pyramidal cells from knockout mice did not show a consensus of theta phases that favored burst firing (Fig. 3.7A). To estimate the phase preference of neurons at a population level, I computed the distribution of preferred phases across neurons within each genotype. The analysis recruited only pyramidal cells that exhibited strong phase preference during theta. The significance of a putative neuron preferring to fire bursts at certain phase over other phases was assessed by the Rayleigh test. 42% (33 out of 79) of pyramidal cells from wild-type and 52% (175 out of 339) from knockout showed significant phase preference ($p < 0.05$, under Rayleigh test), suggesting that for both genotypes, around half of the recorded pyramidal cells were strongly modulated

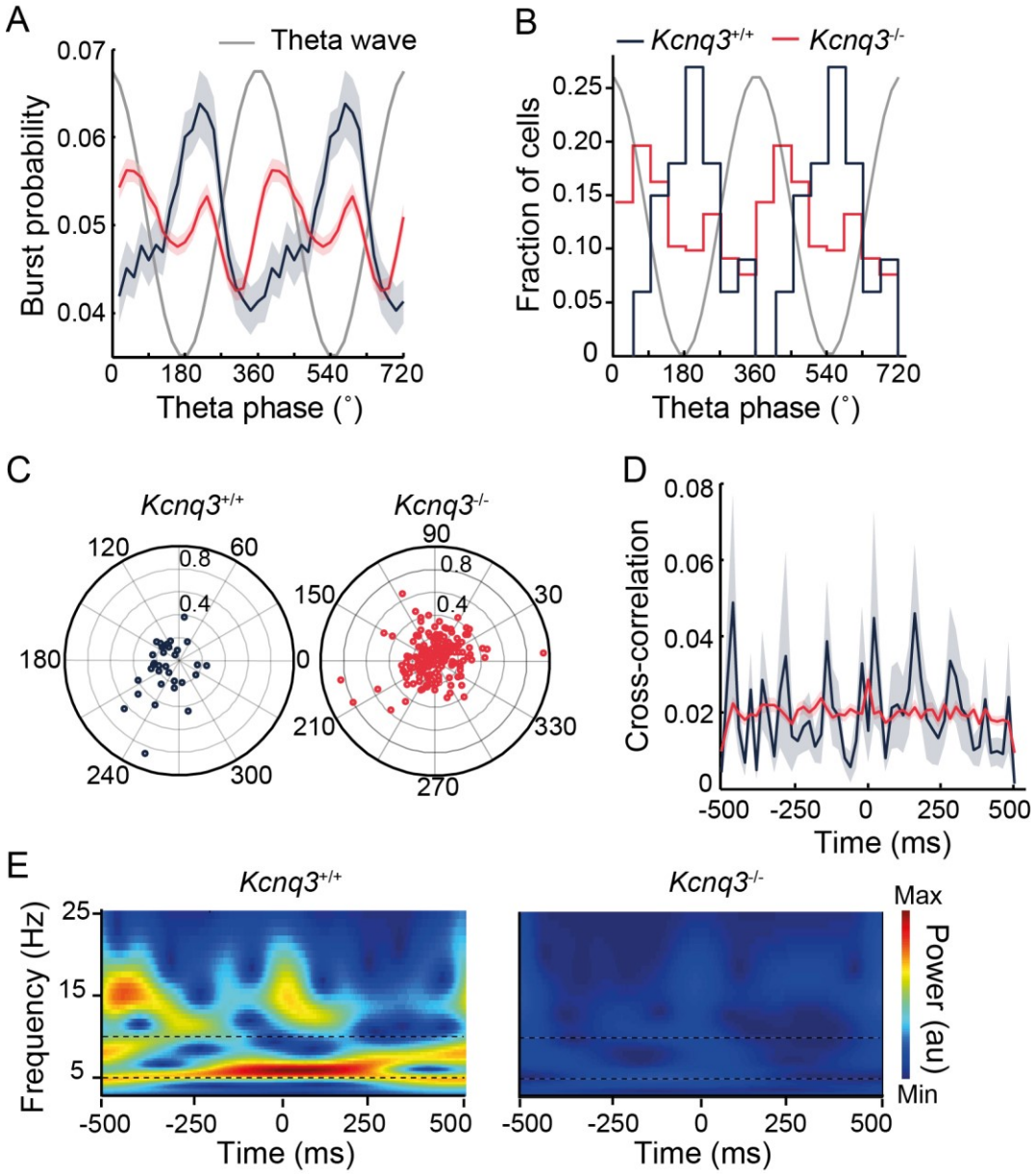

Figure 3.7: The theta modulation of burst firing altered in Kcnq3$^{-/-}$ pyramidal cells. *(A) Burst probability as a function of theta oscillation phase. Kcnq3$^{+/+}$, n=79 cells; Kcnq3$^{-/-}$, n=339 cells; grey line represents reference oscillation cycle. (B) Preferred theta phases of burst discharge in theta-modulated pyramidal cells. Kcnq3$^{-/-}$: n = 175 cells, Kcnq3$^{+/+}$: n = 33 cells; population preferred phases differed between knockout and wild-type (p = 0.002, Mardia-Watson-Wheeler test); grey line represents reference oscillation cycle. (C) Polar scatter plots of theta phase preference of the pyramidal cells. Each dot shows the preferred phase (0° and 360° for theta peak, 180° for theta trough) and modulation depth (mean resultant length, represented by the distance from the center of the plot) of each putative neuron. (D) Cross-correlation of burst timestamps between pairs of pyramidal cell during theta oscillations; Kcnq3$^{-/-}$: n = 1168 cell pairs, Kcnq3$^{+/+}$: n = 37 cell pairs. (E) Spectrograms of average cross-correlations shown in (D); color scale applies to both spectrograms, which shows theta-rhythmic coordination of burst firing in Kcnq3$^{+/+}$, but not Kcnq3$^{-/-}$; dotted lines indicate theta band (5-10 Hz). Data are presented as mean ± SEM.*

by theta oscillations. However, the distributions of preferred phases of the neurons were very different between wild-type and knockout. While the majority of the *Kcnq3*$^{+/+}$ pyramidal cells had preferred phases at the trough of theta cycle, the distribution in *Kcnq3*$^{-/-}$ was broader without single mode (Fig. 3.7B, C). Notably, 35% of pyramidal cells in knockout mice emitted most of their bursts in the vicinity of theta peak whereas only ~5% of wild-type cells preferred to fire bursts around theta peak.

The relative timing of discharge between pyramidal cells can also be theta-modulated (Skaggs et al 1996). To examine how *Kcnq3*$^{-/-}$ pyramidal cells coordinated their burst firing during theta, I computed the cross-correlation of spike timestamps during LFP theta from pairs of pyramidal cells that were recorded simultaneously. The CCGs averaged across all wild-type pairs showed a periodic increase in the correlation strength. Applying continuous wavelet transform on the averaged CCG revealed a dominant frequency component of ~7 Hz. In contrast, the rhythmic correlation of firing was completely abolished in *Kcnq3*$^{-/-}$ neuron pairs (Fig. 3.7D, E).

3.3.2 The patterns and condition of theta phase precession

Although a neuron may have preferred phase during theta where it is more likely to fire, the exact phases at which individual spike events occur often vary. Importantly, the phase variation between spikes is not altogether random; in some cases, it exhibits consistent pattern. One intriguing example is the theta phase precession in which spikes fired by a neuron advance unidirectionally towards earlier phases from one theta cycle to the next. Theta phase precession was first reported in hippocampal place cells when the animal transversed the "place field" of a "place cell" (O'Keefe & Recce 1993). Subsequently, it was also demonstrated in non-spatial contexts and indeed related with transiently intensified firing (Harris et al 2002, Huxter et al 2008). Will the phase precession persist in the *Kcnq3*$^{-/-}$ neurons of a differed theta phase preference?

Firstly, I examined the relations between the instantaneous firing rates of the spikes and their phases in theta cycles. The instantaneous rate for a spike was derived from counting the number of spikes in the two theta cycles that centered at the inquired spike event. The instantaneous firing rate of a spike was classified as "low rate" (of one spike per 2 cycles) or "high rate" (of $\geq$ 3 spikes per 2 cycles). In both *Kcnq3*$^{+/+}$ and *Kcnq3*$^{-/-}$ pyramidal cells, the average phase of spikes at high firing rate was more advanced in theta cycle than phases at

low firing rate: in *Kcnq3*$^{+/+}$ neurons, mean phase advanced from 164° ± 13° at low rate to 146° ± 15° (Fig. 3.8A, B; circular mean ± 95% confidence interval; "low rate": n = 1676 events, "high rate": n = 2703 events; $p < 0.0001$,Watson-Williams test for circular data) while in the knockout group, from 130° ± 7° at low rate to 116° ± 7° at high rate (Fig. 3.8A, B; circular mean ± 95% confidence interval; "low rate": n = 9178 events, "high rate": n = 13920 events; $p < 0.0001$, Watson-Williams test for circular data). Moreover, *Kcnq3*$^{-/-}$ putative cells fired consistently at earlier theta phases than wild-type (Harrison-Kanji test for two-way classification of circular data with factors "genotype" and "rate level": the effect of "genotypes", χ^2 (2, N = 27477) = 28.80, $p < 0.0001$; the effect of "rate level", χ^2 (2, N = 27477) = 12.82, $p < 0.01$). This result confirms the phase-rate correlation in the firing of pyramidal cells during theta as reported in previous studies. Furthermore, it suggests that such spike-phase dynamic is preserved in the knockout hippocampus while the exact phases, compared to wild-type, are systematically advanced.

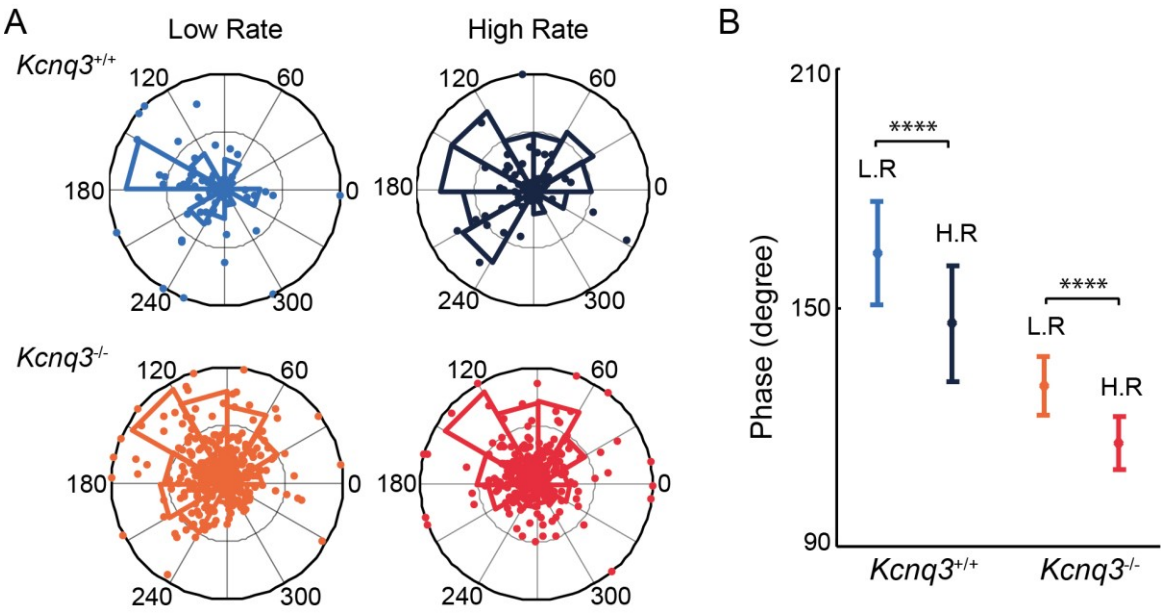

Figure 3.8: Spike theta phases in relation to instantaneous firing rate and the rate's derivative. *(A) Polar histogram plots and scatter plots of the firing of CA1 pyramidal cells in reference to the phases of theta oscillation in CA1 LFP. Each dot shows the mean phase (0° and 360° for theta peak, 180° for theta trough) and modulation depth (mean resultant length, represented by the distance from the center of the plot) of the spikes from each putative neuron at low (1 spike per 2 cycles) or high (≥ 3 spikes per 2 cycles) firing rate. Histograms show the distributions of mean phases sorted in 12 bins. (B) Firing advanced to earlier phase of theta at high rate compared to low rate in both genotypes. Plots represent circular mean ± 95% confidence interval. In Kcnq3$^{-/-}$: "low rate": n = 9178 events, "high rate": n = 13920 events, p < 0.0001; in Kcnq3$^{+/+}$: "low rate": n = 1676 events, "high rate": n = 2703 events, p < 0.0001; Watson-Williams test for circular ANOVA.*

Next, I examined the firing events spanning multiple adjoining theta cycles. Although theta phase precession is often studied in association with the transversal of place field in place cells, phase precession also occurs during non-spatial behavioral states and the phase advancement can be measured by phase-position correlation and phase-time correlation (Harris et al 2002, O'Keefe & Recce 1993). To examine the change of spike phase in all recorded units and irrespective of behavioral states, I adopted the phase-time correlation. In both *Kcnq3*$^{+/+}$ and *Kcnq3*$^{-/-}$ pyramidal cells, firing events with systematic advanced theta phases could be observed (Fig. 3.9A, B). But not all spiking sequences during theta showed phase precession (Fig. 3.9A, B). A circular-linear fit of phase and spike timing was applied to estimate the strength and slope of phase-time correlation. For both groups of neurons, more than half of the events were with negative phase-time slopes which indicated an advancement in the spike phases (63% of events in *Kcnq3*$^{+/+}$ and 54% of events in *Kcnq3*$^{-/-}$; the analysis included only events with mean vector length >= 0.3 in the circular–linear fit of phases and timestamps). The average slope of these phase-advanced spike events in the wild-type was significantly steeper than in knockout (mean ± SEM: *Kcnq3*$^{-/-}$: -0.02 ± 0.02, n = 552 events; *Kcnq3*$^{+/+}$: -0.13 ± 0.04, n = 99 events; $p < 0.01$, student t-test; Fig. 3.9C, D). These results suggested that theta phase precession existed in *Kcnq3* knockout pyramidal cells, but the extent of advancement was less pronounced than in wild-type.

Another approach to estimate the phase shift along multiple theta cycles is by comparing the phases between spikes from the onset of a theta firing sequence and those from the offset (Harris et al 2002). When phase precession was examined in the context of the place field transversal in previous studies, the acceleration of a place cell firing during theta (i.e. the "onset") correlated with the entry of its place field while the "offset" where the firing rate decreased corresponded to the exit of the field. The phase shift can be thus revealed from the phase difference between "onset" and "offset", irrespective of the strict point-wise correlation between phases and timestamps. I first detected firing events that exhibited transient acceleration and deceleration across multiple (>= 5) theta cycles. For each such firing sequence, the segment of spike train that monotonically accelerated along consecutive theta cycles was assigned as the "onset" while the "offset" was defined the cessation part of the firing where the number of spikes in each theta cycles decreased to zero. The mean phase of the spikes was 199° ± 38° during the onset and at the offset, 99° ± 22° in *Kcnq3*$^{+/+}$ pyramidal cells (circular mean ± 95% confidence interval). For spikes from *Kcnq3*$^{-/-}$ cells, mean phase of the onset spikes was 148° ± 31° and of the offset, 90° ± 10° (Fig. 3.10A, B). In both genotypes, the spike phases of

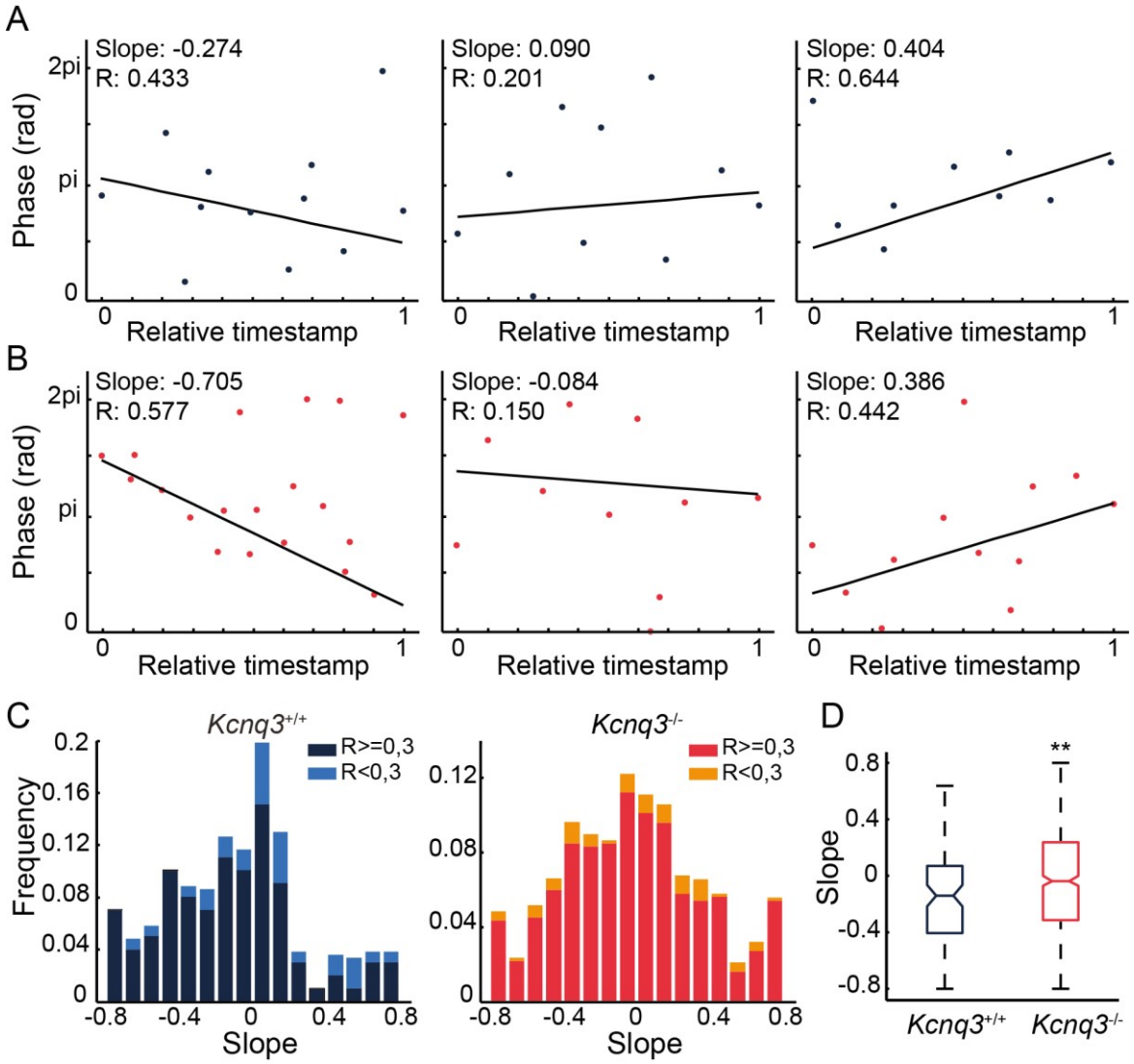

Figure 3.9: Single-trial phase precession. *Examples of phase variation over successive theta cycles from wild-type (A) and from Kcnq3$^{-/-}$ cells (B). Each dot represents one spike and the inset values show the slope and mean resultant length (R) of circular-linear regression on phases against spike timestamps. Examples on left column show significant negative phase-time correlation, suggesting phase precession. (C) The distribution of phase slopes for all spiking events that spanned multiple theta cycles. Lighter (light blue for Kcnq3$^{+/+}$, orange for Kcnq3$^{-/-}$) versus darker (dark blue for Kcnq3$^{+/+}$, red for Kcnq3$^{-/-}$) colors differentiate events of weaker correlation (R < 0.3) from those of stronger correlation (R ≥ 0.3). (D) Comparing the slopes of spike phases during theta cycles between two genotypes; **, p < 0.01, student t-test.*

the pyramidal cells during theta cycles advanced considerably from onset to offset (Fig. 3.10B; *Kcnq3*$^{-/-}$: $p < 0.0001$, n = 452 events; *Kcnq3*$^{+/+}$: $p < 0.0001$, n = 97 events; Watson-Williams test for circular data). Moreover, during the acceleration of the firing, the extent of phase advancement in both *Kcnq3*$^{+/+}$ and *Kcnq3*$^{-/-}$ pyramidal neurons were correlated with the

derivative of firing rate (Fig. 3.10C, D): the faster the firing of a neuron accelerated, the further the phases of spikes advanced (Pearson's linear correlation between the slope of mean phases over the theta cycles and the derivative of firing rate: *Kcnq3*$^{-/-}$: r = -0.24, $p < 0.0001$, n = 257 events; *Kcnq3*$^{+/+}$: r = -0.27, $p = 0.04$, n = 57 events).

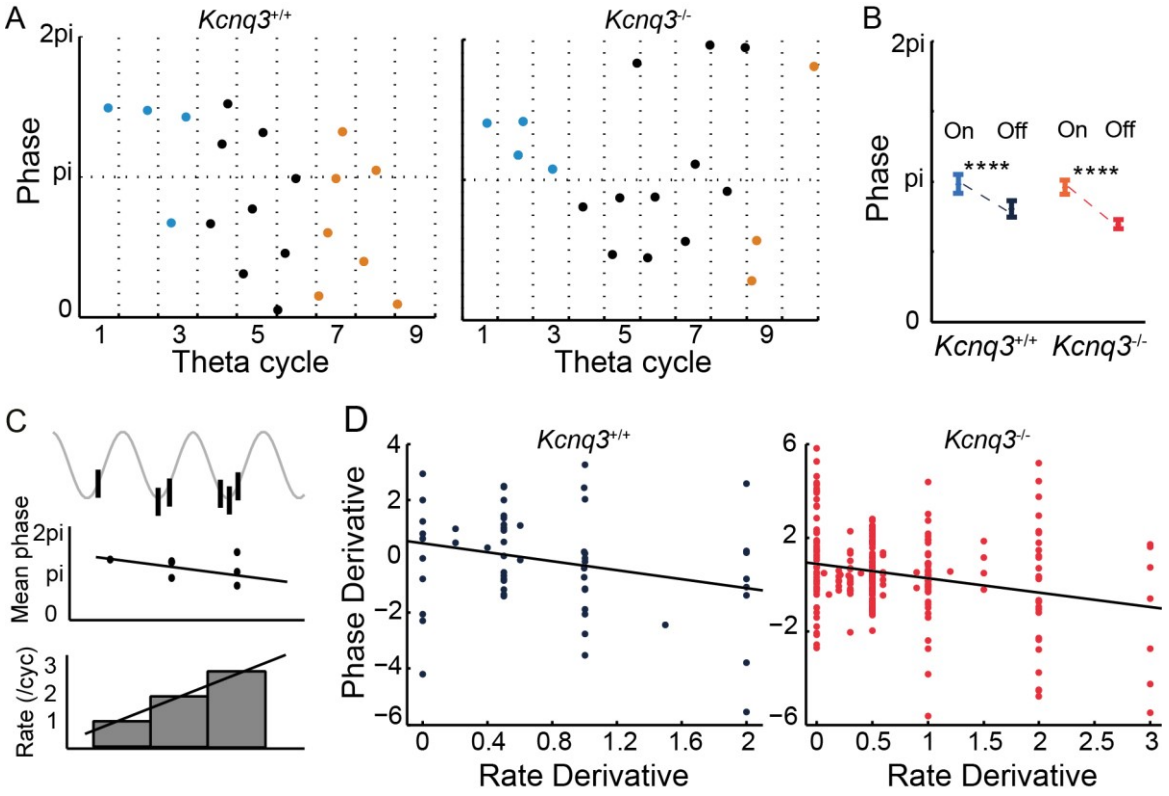

Figure 3.10: Advancement of theta phases along successive theta cycles. *(A) Example spike trains from Kcnq3*$^{+/+}$ *and Kcnq3*$^{-/-}$ *units during theta. Subsets of spikes were defined as occurring at the onset (blue) or at the offset (yellow) of successive theta cycles (selection criteria seen in method). (B) Comparison of the theta phases of spikes at the onset versus offset in each genotype. The circular mean phase and 95% confidence interval were calculated for all spikes defined as occurring at onset (blue) or at the offset (yellow), in both Kcnq3*$^{+/+}$ *and Kcnq3*$^{-/-}$ *pyramidal cells. Kcnq3*$^{-/-}$*: ****$p < 0.0001$, *n = 452 events; Kcnq3*$^{+/+}$*: $p < 0.0001$, n = 97 events; Watson-Williams test for circular data. (C) Calculation of the firing rate derivative. Upper: theta oscillations (grey line) and the timestamps of spikes (black ticks); bottom: the derivative of firing rate calculated by linear regression of spike counts against the theta cycle sequence. (D) Slope of mean phase over successive theta cycles as a function of the firing rate's derivative in both genotypes. Pearson's linear correlation between the slope of mean phases over theta cycles and the derivative of firing rate: Kcnq3*$^{-/-}$*: r = -0.24, $p < 0.0001$, n =257 events; Kcnq3*$^{+/+}$*: r = -0.27, $p = 0.04$, n = 57 events).*

3.4 Spatial signaling by bursts and single spikes

In hippocampus, a subset of pyramidal cells display spatially selective firing which means they discharge predominantly at a certain location of the space where animal explores. Extensive studies have attributed a range of characteristics to the "place cell" that involve properties like firing rate, propensity for burst firing, temporal interplay between firing modes and theta phase preference (Grosmark & Buzsáki 2016, Harris et al 2001, Mizuseki & Buzsáki 2013, O'Keefe & Recce 1993). In the *Kcnq3* knockout mice, many of the firing properties were shown to depart considerably from those in the wild-type. Will that affect the spatial signaling in *Kcnq3*$^{-/-}$ hippocampus?

To answer this question, I recorded the neuron firing activities while animals explored in two different enclosures: one is a rectangular arena which represented a conventional open-field two-dimensional environment and the other, a circular track where animals were confined to move on a rather linear trajectory. In both environments, a few *Kcnq3*$^{-/-}$ pyramidal cells did turn out to have place-selective firing (Fig. 3.11A). But these place cells did not have the same quality as the wild-type ones when assessed by the place field size and the field coherence (Fig. 3.11B, C; Table 2 in Appendix). On the circular track, the place fields in *Kcnq3*$^{-/-}$ mice were significantly smaller than in *Kcnq3*$^{+/+}$. In the 2-D arena, place fields also tended to be smaller in the knockout but not significantly (Fig. 3.11B). Spatial coherence, as an estimate of the firing field quality, was computed through z-transformation of the correlation of the firing rate in each bin of the place field with the firing rate in its neighboring 8 bins and serves an estimate of the "local orderliness" (Muller & Kubie 1989). The spatial coherence of the 2-D place fields showed a reduction in knockout (coherence in "Arena": *Kcnq3*$^{-/-}$: 0.56 ± 0.03, n = 70 cells; *Kcnq3*$^{+/+}$: 0.83 ± 0.08, n = 20 cells, $p < 0.0001$, student t-test; Fig. 3.11C).

To further inspect the contribution of bursts and single spikes in spatial signaling, I computed the firing maps separately from single spikes and from spikes in bursts. In both the track and the arena, the sizes of place fields constructed by burst spikes were similar between two genotypes. In contrast, the single-spike place fields from the knockout were of smaller size than those from the wild-type in both enclosures (Fig. 3.12A). The information density of burst spikes and single spikes were also computed to measure the amount the spatial information carried by each type of spikes. In both *Kcnq3*$^{+/+}$ cells and *Kcnq3*$^{-/-}$ place cells, burst spikes had a higher information density over single spikes regardless of the enclosure types (Fig. 3.12B; Table 2 in Appendix). For either genotype, the information density of bursts remained

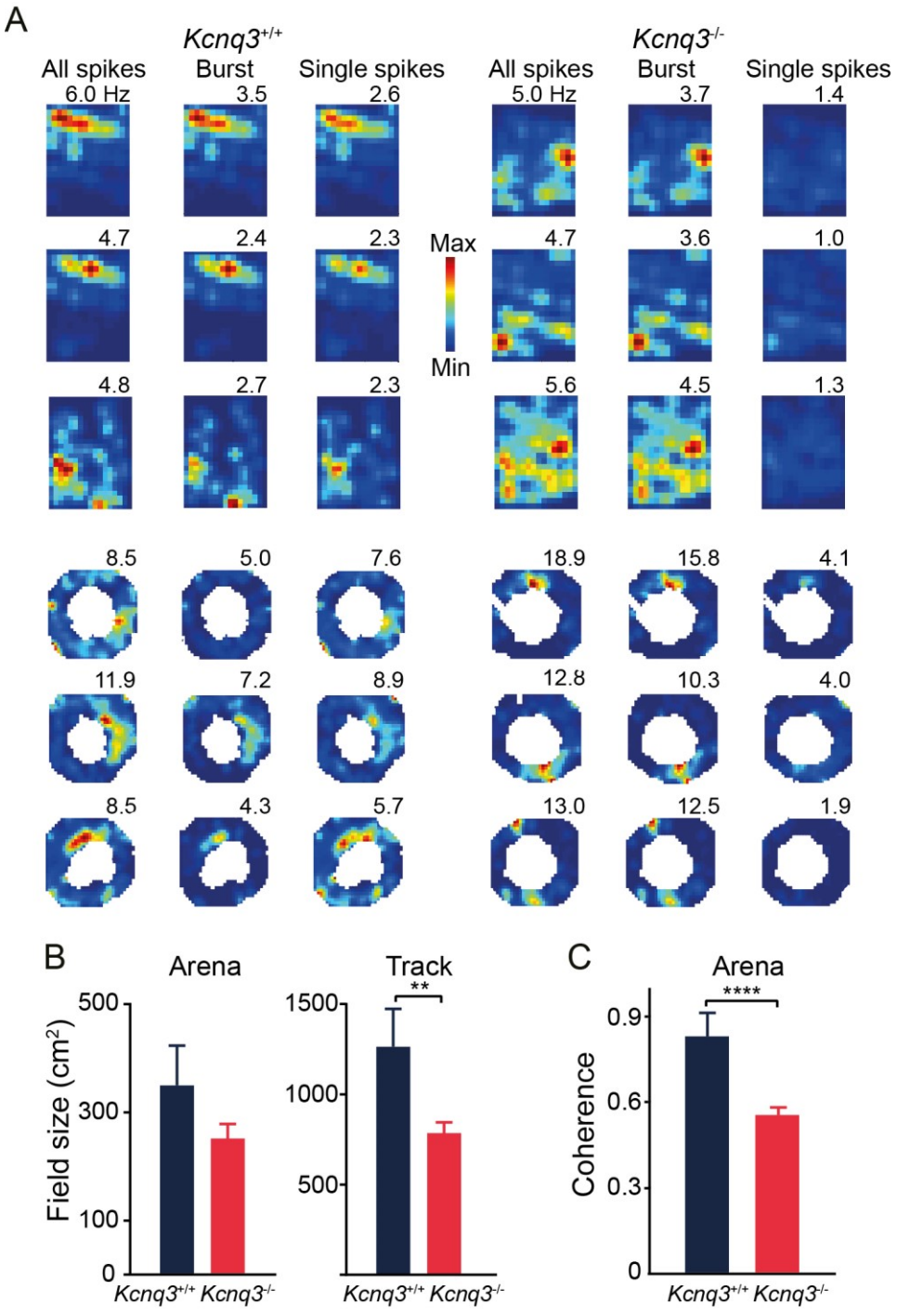

Figure 3.11: Place cells in Kcnq3$^{+/+}$ and Kcnq3$^{-/-}$ mice. *(A) Firing maps of CA1 pyramidal cells recorded during navigation in a rectangular arena (top), and on a circular track (bottom). For each place cell, three firing maps were constructed: using all spikes (left), spikes fired in bursts (middle) and only single spikes (right). The peak rate of each map is indicated, color scales match across burst and single-spike firing maps in each cell. (B) Size of place fields in the rectangular arena (Arena, Kcnq3$^{-/-}$: n = 70 cells, Kcnq3$^{+/+}$: n = 20 cells) and on the track (Track, Kcnq3$^{-/-}$: n = 58 cells, Kcnq3$^{+/+}$: n = 11 cells), ** p = 0.005, Mann-Whitney-U-Test. (C) Coherence of place fields in the rectangular arena. ****p < 0.0001, student t-test. Data are presented as mean + SEM.*

comparable between 1-D track and 2-D arena. The single spikes of the wild-type place cells also showed same level of information density across both environments. In contrast, the spatial information density of the single spikes in the knockout significantly decreased in the 2-D arena compared to that on the circular track (Fig. 3.12B).

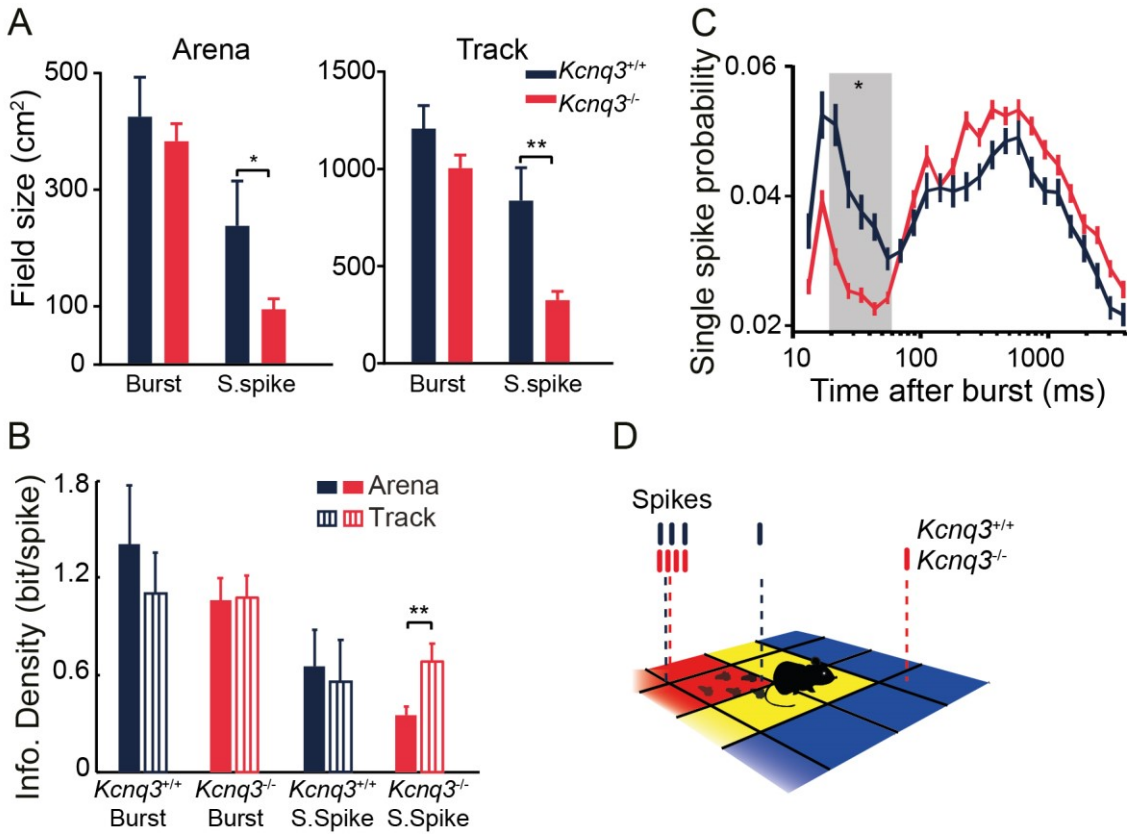

Figure 3.12: Place coding through bursts and single spikes in Kcnq3$^{+/+}$ and Kcnq3$^{-/-}$ mice. *(A) Sizes of place fields constructed by bursts and single spikes respectively. In the rectangular arena (Arena), Kcnq3$^{-/-}$: n = 70 cells, Kcnq3$^{+/+}$: n = 20 cells, and on the track, Kcnq3$^{-/-}$: n = 58 cells, Kcnq3$^{+/+}$: n = 11 cells, * p < 0.05, ** p < 0.01, Mann-Whitney-U-Test. (B) Information density of burst spikes and of single spikes in the arena and on the circular track. ** p < 0.01, Mann-Whitney-U-Test. (C) Probability of a single spike emission as a function of the silence duration after a burst. For each time bin under grey shade, * p < 0.002, student t-test, Bonferroni adjusted alpha levels of 0.002 (0.05/25) per test; Kcnq3$^{-/-}$: n = 153 cells, Kcnq3$^{+/+}$: n = 63 cells. (D)A scheme illustrating how delayed firing of single spikes after vigorous bursting impairs concordant spatial representations by bursts and single spikes in Kcnq3$^{-/-}$ mice. Data are presented as mean ± SEM.*

Normally, place cells fire both bursts and single spikes within the corresponding place fields. Especially at the second half of the field transversal, place cells become more likely to fire single spikes than bursts due to strong dendrite inhibition by the increased activation of somatostatin interneurons (Harris et al 2002, Lovett-Barron et al 2012, Royer et al 2012). However, the firing of single spikes following a burst event was further suppressed in *Kcnq3$^{-/-}$* pyramidal cells in the time-window of 20–70 ms (Fig. 3.12C). The change in the temporal

relation between burst and single spikes may underlie the reduced contribution of single spikes in spatial coding, resulting in the smaller and patchier place fields in *Kcnq3* knockout (Fig. 3.12D).

3.5 Reduced gamma and ripple oscillations in Emx1-Δ*Kcnq3* mice

We further examined whether the lack of KCNQ3 channels in pyramidal cells would disrupt the hippocampal oscillations. Since constitutive knockout of *Kcnq3* will also affect interneurons and alter their firing behaviors that are responsible for the network oscillations in hippocampus, we used the Emx1-Δ*Kcnq3* mice to restrict the deletion of *Kcnq3* in cortical pyramidal cells (see Method 2.1.1)[2]. This conditional mutation has been shown to reduce the M-current in CA1 pyramidal cells by ~50% (Gorski et al 2002).

During exploratory behaviors, prominent theta (5–12 Hz) and gamma (35–120 Hz) were observed in the LFP of hippocampal CA1 in both wild-type and Emx1-Δ*Kcnq3* mice (Fig. 3.13A). Theta power (cumulative power of 5–12 Hz) and the frequency of theta rhythms did not differ between genotypes (see the inset in Fig. 3.13B). However, the power spectra indicated a significant reduction of gamma power (35–120 Hz cumulative power) in Emx1-Δ*Kcnq3* mice (Emx1- Δ *Kcnq3*: N = 4 mice, $Kcnq3^{+/+}$: N = 5 mice, $p < 0.05$, student t-test; Fig. 3.13B).

Ripple is another high frequency oscillatory pattern that occurs in the LFP of CA1 pyramidal layers mainly during immobility and non-REM sleep. Putative ripple events were first detected using threshold criteria and for each event, power spectrum was computed using a multi-taper method. To sufficiently distinguish ripples from gamma oscillations, only events that exhibited peak power at 140–220 Hz were defined as ripples. The leading frequencies—the frequency of the peak power of the oscillatory event—of the ripple events in both genotypes followed similar distribution. However, the occurrence of ripple events was significantly less frequent in Emx1-Δ*Kcnq3* mice (mean ± SEM: Emx1-Δ*Kcnq3*: 0.35 ± 0.11 $second^{-1}$, N = 4 mice; $Kcnq3^{+/+}$: 0.90 ± 0.09 $second^{-1}$, N = 5 mice; $p < 0.01$, student t-test; Fig. 3.13C, D).

These results suggest that KCNQ3 channels in pyramidal cells play an important role in maintaining high frequency network oscillations such as gamma and ripples in hippocampal CA1 area.

[2] The recording data of local field potentials in Emx1-Δ*Kcnq3* mice was contributed by Dr. Tatiana Korotkova.

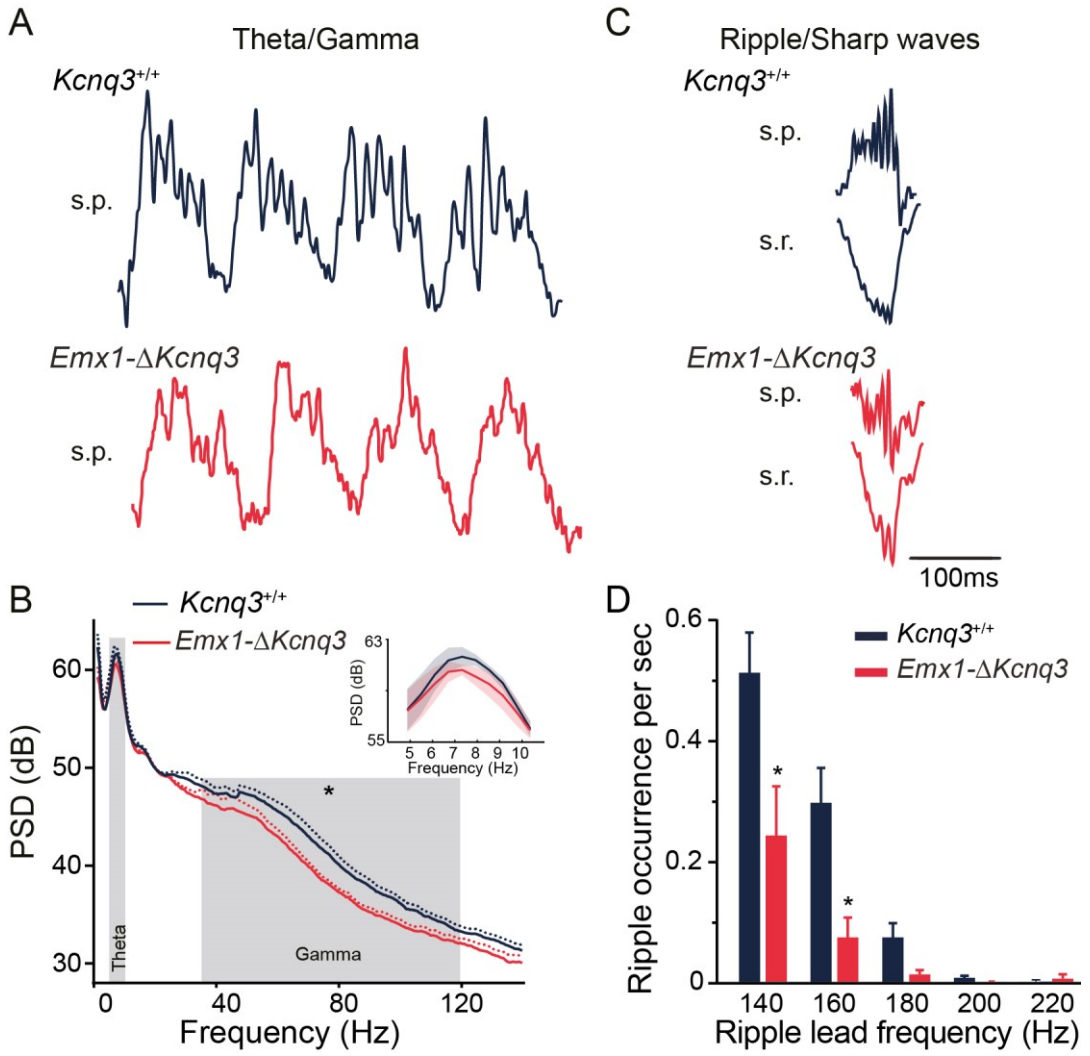

Figure 3.13: Impaired fast network oscillations in Emx1-ΔKcnq3 mice. *(A) Representative LFP signals (1–250 Hz) showing theta (5–10 Hz) and gamma (35–120 Hz) oscillations during running (left traces, recordings from CA1 str. pyramidale) in Kcnq3$^{+/+}$ mice and Emx1-ΔKcnq3 mice. (B) Power spectral density (PSD) of LFP during theta oscillations. The inset shows the PSD in the frequency range of theta. Emx1-ΔKcnq3: N=4 mice, Kcnq3$^{+/+}$: N = 5 mice. Cumulative gamma power, * p < 0.05, t-test. (C) Example LFP traces of ripple oscillations (140–220 Hz, right traces, CA1 str. pyramidale) with concurrent sharp-waves (str. radiatum) during immobility in the two genotypes. (D) Occurrence rate of ripple oscillations of different leading frequencies. Ripple events were binned (5 bins in 140–220 Hz with 20 Hz interval) based on their leading frequencies; for ripples of leading frequencies of ~140 Hz and of ~160 Hz, * p < 0.05, Emx1-ΔKcnq3: N = 4 mice, Kcnq3$^{+/+}$: N = 5 mice, student t-test. Data are presented as mean ± SEM.*

4 Discussion

Using *in vivo* electrophysiological recordings in *Kcnq3* knockout mice, the present study reveals the indispensable role of KCNQ3-containing potassium channels in regulating the neuronal excitability of pyramidal cells in the hippocampus. The firing of the *Kcnq3*$^{-/-}$ pyramidal cells displayed several features that were distinct from the wild-type: 1) *Kcnq3* knockout neurons were more bursty, showing increased burst probability, higher propensity to emit long bursts and diminished within-burst frequency accommodation. 2) A general shift toward high burstiness was shared by the majority of knockout pyramidal cells which significantly altered the distribution of neuronal burstiness in the population: the subgroups of "low bursty" versus "high bursty" neurons observed in the wild-type population became indistinguishable in knockout. 3) Unlike the high bursty pyramidal cells in the wild-type, the more bursty *Kcnq3*$^{-/-}$ pyramidal cells did not exhibit the dependence of burst probability on the behavior states differentiated by the theta versus non-theta rhythms of the hippocampal LFP. The altered firing properties motivated us to look into the spike phase during theta and the rate map of place cells as they are assumed to respectively represent the temporal coding and the rate coding operated by hippocampus network. The rate coding of space was largely preserved in the knockout but it was mainly carried out by the bursts of the place cells than jointly by bursts and single spikes as in the wild-type.

These results are unexpected, given the rather minor role of KCNQ3 in controlling neuronal excitability proposed in former studies (Soh et al 2014, Tzingounis & Nicoll 2008). In the following, I will discuss our findings in the light of our current knowledge about the functions of KCNQ2/3 channels as well as the functional implications of hippocampal *in vivo* electrophysiology.

4.1 The implications of increased burstiness of *Kcnq3*$^{-/-}$ pyramidal cells

Previous studies have consistently reported a substantial loss of M-currents in *Kcnq3* transgenic mice (Singh et al 2008, Soh et al 2014). The burst phenotype in our knockout mice reveals the functional consequence of the M-current insufficiency. Blocking M-current pharmacologically has promoted complex spike bursts in pyramidal cells in conditions that normally only induced single spike (Gu et al 2005, Yue & Yaari 2004). M-currents blockage also led to changes in the features of *in vitro* bursts such as increased burst lengths and diminished intra-burst spike

adaptations (Gu et al 2005, Madison & Nicoll 1984, Storm 1989). However, in studies with genetic models, increased neuronal excitability was only detected in those involving mutations of *Kcnq2* but not *Kcnq3* (Peters et al 2005, Soh et al 2014). It should be pointed out that these studies mainly relied on current injection of neurons *in vitro* to examine the neuronal excitability. To my knowledge, the electrophysiology of neurons with KCNQ3 deficiency had not been examined under *in vivo* condition up to now.

The increased burst firing in *Kcnq3*$^{-/-}$ pyramidal cells was not anticipated by the *in vitro* studies where pyramidal cells with the deletion of *Kcnq3* showed normal ADP and neuronal excitability. The inconsistence might reflect different mechanisms of generating bursts *in vivo* versus *in vitro*. ADPs underlying bursts *in vivo* in hippocampal pyramidal cells are induced by synaptic excitation and require NMDA receptor activation in contrast to the somatic current-induced ADP measured *in vitro* (Grienberger et al 2014). Owing to the constant synaptic inputs and an increased membrane conductance, the intrinsic properties of pyramidal cells such as the integrative properties of synaptic inputs *in vivo* can also differ qualitatively from *in vitro* condition (Prescott et al 2008).

In addition, unlike the wild-type neurons that increased burst firing during non-theta, pyramidal cells in the knockout fired bursts largely independent of the concurrent network states. This can be due to an inadequate cholinergic modulation through M-currents. Increased burst firing in hippocampal pyramidal cells can be induced by septal cholinergic afferents through the activation of mAChRs which act to inhibit KCNQ/M currents (Graves et al 2012). KCNQ3 dysfunction might disrupt this pathway for modulating burst plasticity. There might also involve change of the intrinsic electrical properties such as the theta resonance as KCNQ/M currents are responsible for a form of subthreshold theta resonance at depolarized potentials that modulates neuronal response to theta rhythmic inputs (Hu et al 2002, Peters et al 2005).

At the population level, we showed that wild-type pyramidal cells had a heterogeneous distribution in their burst propensity. Subpopulations of pyramidal cells in CA1 with distinct firing properties have been reported in a few recent works that suggested an unambiguous segregation resulted from either morphological and electrophysiological differences (Graves et al 2012) or the neurons' positions along the superficial–deep CA1 sublayers (Mizuseki et al 2011). However, whether the subgrouping of low bursty and high bursty *Kcnq3*$^{+/+}$ pyramidal cells can be explained by any of these sources of variation remains inconclusive as no measurements of the neurons' morphology nor their relative depth have been made in this study. It should be noted that little gap was found between the edges of the two subgroups on the linear

discriminant, which argued against a rigid dichotomy of CA1 pyramidal cells based on their firing patterns. In contrast, a general increase of burst probability of the pyramidal cells in the knockout obscured the subgrouping shown in the wild-type neurons. The effect resembled what was achieved *in vitro* by raising the extracellular potassium concentration from the physiological 3.5 mM to 7.5 mM (Jensen et al 1994, Jensen & Yaari 1997) or by depolarizing the membrane of pyramidal cells *in vivo* (Grienberger et al 2014). Taken together, our results share the view that all pyramidal cells in CA1 in principle can fire bursts and the burst propensity of individual neuron is to some degree adjustable (Grienberger et al 2014, Jensen et al 1994).

4.2 The discrepancy between *in vitro* and *in vivo* findings regarding the functions of KCNQ3 channels

In contrast to previous *in vitro* studies that found no significant effect of KCNQ3-containing channels on neuronal excitability, the loss of KCNQ3, when examined *in vivo*, has elevated burst probability, abolished within-burst spike frequency adaptation and decreased the conditional regulation of firing modes in CA1 pyramidal cells. The discrepancy might originate from two kinds of dynamics that *in vitro* studies are unable to capture. First, cortical neurons in intact brain have very different electrophysiological profiles than *in vitro* on parameters such as membrane conductance, resting membrane potential and input integrative behavior (Destexhe et al 2003, Prescott & Sejnowski 2008). These properties are critical in determining the relative contributions of various ion currents in forming after-potentials, spike adaption currents and membrane oscillations. Therefore, the functional weight of KCNQ/M currents *in vivo* can be very different from *in vitro*. If a much smaller amount of M-currents is active *in vitro* than *in vivo*, the significance of the current will be underestimated by *in vitro* studies. Indeed, an increase in KCNQ/M currents has been demonstrated in *in vivo*-like conditions and associated with the quantitative change in the input-output behaviors of pyramidal cells (Prescott & Sejnowski 2008). *In vitro* settings also leave out the activity-dependent modulation of the currents. Under physiological conditions, KCNQ/M currents can be modulated by the action of numerous neurotransmitters or neuropeptide receptors. More importantly, different KCNQ subunits engage in the modulation to a considerably varied degree, depending on their kinetics and their affinity for the regulatory messengers downstream of the receptors (Li et al

2005). For example, among all subunits, KCNQ3 has the highest affinity for PIP_2, the key messenger shared by several M-current modulatory pathways. Our *in vivo* results show that in the absence of KCNQ3, the conditional modulation of burst firing in states of theta versus non-theta, became indiscriminate. This suggests an important role of KCNQ3 in the activity-dependent function of the KCNQ/M currents.

4.3 The relevance of KCNQ3 channels for the functions of hippocampus

4.3.1 Enabling spatial representation in both bursts and single spikes

For hippocampus, the group of pyramidal cells with low spike threshold and high burst propensity are thought to be the candidate for "place cells" which constitute the hippocampal spatial maps (Epsztein et al 2011). What will be the effect of a general upregulation of burst firing on the formation of firing maps? Can place cells still emerge in *Kcnq3*$^{-/-}$ hippocampus to encode spatial memory?

Some pyramidal cells in the hippocampus of the *Kcnq3*$^{-/-}$ mice did turn out as place cells when animals explored 1-D or 2-D enclosures. Moreover, the spatial firing in *Kcnq3*$^{-/-}$ place cells depended more on burst spiking while their single spikes contributed significantly less to forming the place fields. The essential role of burst firing in establishing hippocampal firing maps supports the hypothesis that burst can function as an independent unit for information coding (Lisman 1997). The higher information density of burst spikes observed in both genotypes also suggests that bursts prevail over single spikes in coding spatial information. In line with our findings, a recent study demonstrated that information transferred through burst-mediated synaptic transmission alone is sufficient for the acquisition of contextual fear memory in the hippocampus when synaptic transmission evoked by single spikes was selectively obstructed by the knockdown of synaptotagmin-1 (Xu et al 2012).

In contrast to bursts, single spikes discharge downstream neurons unreliably yet with high temporal precision, thus presenting a very different coding strategy (Branco & Staras 2009, Varshney et al 2006). Although their relative functional significance in hippocampal spatial memory is yet to dissect, the study with synaptotagmin-1 knockdown by Xu et al. showed that the depletion of single spike transmission impaired the precision of fear memory, causing the mice unable to distinguish altered spatial context (Xu et al 2012). In the *Kcnq3* knockout, the reduced participation of single spikes in spatial coding might have similar adverse

consequences. To test this hypothesis, more discriminating behavioral paradigms, for example testing memory accuracy in varied environments, will be required.

4.3.2 Controlling theta phase preference but not phase precession

The timing of neuronal firing in relation with the network oscillations provides a mechanism for temporal coding (Huxter et al 2008, Sejnowski & Paulsen 2006). For hippocampal CA1 pyramidal cells, two timing features are repeatedly observed: phase preference and a systematic phase advancement at times of intense firing such as place field transversal (Harris et al 2002, Mizuseki et al 2009, O'Keefe & Recce 1993).

Similar to the wild-type, half of the *Kcnq3*$^{-/-}$ pyramidal cells exhibited significant phase preference during theta. But instead of concentrating around the trough of theta wave as the wild-type neurons, the preferred phases of *Kcnq3*$^{-/-}$ pyramidal cells formed a wide distribution. The result would at first seem incompatible with the reduced dependence of firing pattern on LFP states i.e. during theta versus non-theta and a possible loss of M-current-mediated theta resonance. However, apart from the M-currents providing theta resonance at depolarized potentials, other currents such as the cation current I_h and the persistent Na^+ current can also supply the intrinsic theta resonance albeit at different potential ranges (Hu et al 2002). It is also important to recognize that the varied resonance-generating conductances are modulated differently, sometimes antagonistically, by various neuromodulators such as acetylcholine (Halliwell & Adams 1982, Pape 1996). Therefore, the lack of KCNQ/M currents might not simply cancel the intrinsic theta resonance but alter it in its voltage dependence and modulation. In support of this hypothesis, the preferred phases of strongly theta-modulated neurons in the knockout formed a very different distribution than the one in the wild-type. While most wild-type pyramidal cells preferred burst firing around the trough of field theta when the overall inhibition on pyramidal cells became low, the phase prevalence in the knockout was replaced by a wide-spread distribution of phases across theta cycles.

Nonetheless, theta phase precession appeared to persist in the *Kcnq3* knockout mice when the spike timing of individual neuron was tracked across successive theta cycles. The theta phase variation in both *Kcnq3*$^{+/+}$ and *Kcnq3*$^{-/-}$ pyramidal cells reproduced the observations made by Harris et al. that: 1) the timing of an action potential within theta cycle is correlated with the instantaneous firing rate, with spikes at high rate advancing towards earlier theta phases relative to those at low rate; 2) unidirectional phase precession occurs when a neuron transiently intensifies its firing during theta cycles. These results support the “soma-dendritic interference”

model of phase precession which postulates that the spike phase is set by the interplay between an oscillatory inhibition near the soma and the dynamic excitatory inputs which drives the phase precession (Harvey et al 2009, Kamondi et al 1998, Mehta et al 2002). As the firing probability of CA1 pyramidal cells at a certain theta phase is shown to depend on the relative strength of CA3 and EC afferents which have contrasting phase preference (Fernández-Ruiz et al 2017), the spike phase precession of the pyramidal cells in CA1 would continue to exist if the knockout of *Kcnq3* did not cause significant change in the phase contrast between entorhinal cortex and CA3 or in their dynamic control on the CA neurons. It is also likely that the phases in hippocampal pyramidal cells are updated from cycle to cycle by extra-hippocampal inputs, as suggested in experiments where phase precession persists after hippocampal activities were temporarily disrupted (Zugaro et al 2005).

In addition to the phase advancement, *Kcnq3* knockout pyramidal cells consistently initiated spiking at phases more advanced than wild-type, when compared at similar firing rate level, and away from theta trough. Normally, the spike phase precession of a pyramidal cell occurs during the transversal of place field when the phases of spikes advance from the ascending phase of theta before entering the place field and via the trough of theta to the descending phase of theta after leaving the place field (Dragoi & Buzsáki 2006, O'Keefe & Recce 1993, Skaggs et al 1996). Intracellular recordings of place cells *in vivo* have suggested the phase advancement is associated with a ramp-like membrane depolarization and an augmented intracellular theta oscillation that is phase shifted from field theta (Harvey et al 2009). According to computational predictions, the peri-threshold activation of the M-current can enhance intrinsic theta resonance at depolarization membrane potential and at the same time provide adaptation that improve spike-timing reliability (Ermentrout et al 2001, Hu et al 2002, Prescott et al 2008, Prescott & Sejnowski 2008). In *Kcnq3*$^{-/-}$ pyramidal cells, the deficiency of M-currents might affect the theta resonance in such a way that favors the initiation of spikes at more hyperpolarized phases of theta oscillations.

4.3.3 Contributing to local high frequency oscillations

Due to the exclusive expression of Emx1 in cortical principal neurons, hippocampal interneurons in Emx1- Δ*Kcnq3* mice were spared from the excision of the *Kcnq3* gene thus allowing us to examine to what extent the KCNQ3 channels of pyramidal cells contribute to the hippocampal oscillations *in vivo*.

The field theta oscillations recorded from CA1 remained unaffected in the mutants, suggesting that the knockout of *Kcnq3* and the resulted change of firing properties in pyramidal cells did not interfere the generation nor the maintenance of theta rhythms. However, high frequency oscillations in CA1, including gamma and ripples, were impaired by the loss of KCNQ3 channels in pyramidal cells. Both groups of oscillations are generated in CA1 pyramidal cells by synchronized discharge of local inhibitory interneurons. What then, is the role of M-currents in pyramidal cell in this process? In the case of gamma, the extracellular field oscillations consist of a slow (30–80 Hz) and a fast (60–100 Hz) frequency components, each corresponding to the synchronized, gamma-phase-timed activation of interneurons driven by afferents from CA3 and from medial entorhinal cortex (MEC) respectively (Colgin et al 2009). The level of synchronization between local interneurons, reflected in the power of gamma, is inherited from the synchronization of the upstream structures through either direct excitatory drive or indirect inhibitory mechanisms (Fuchs et al 2007, Wang & Buzsáki 1996). In *Kcnq3* knockout mice, the impact of a deficient M-current on CA3 might resemble the effect of pharmacological blockage of M-current that corrupt the phase coupling of CA3 pyramidal cells and cause the reduced gamma amplitude (Leão et al 2009). As demonstrated in computational models with coupled pyramidal cells, spike frequency adaptation provided by KCNQ/M currents is instrumental for the coupling behavior and the strength of synchrony among excitatory neurons (Crook et al 1998, Ermentrout et al 2001).

The possibly decreased synchrony in CA3 can be more detrimental for the CA1 ripple oscillations, since the sharp-wave-ripple (SPW-R) events occur at times of low subcortical and entorhinal inputs while population bursts in CA3 are the major drive of the massive dendritic depolarization on CA1 pyramidal cells manifested as the sharp waves in stratum radiatum and the synchronizing discharge of CA1 basket cells that lead to the ripple-rhythmic perisomatic IPSPs on pyramidal cells (Buzsaki et al 1992, Ylinen et al 1995). Higher CA3 synchrony predicts a larger ripple amplitude in CA1 (Csicsvari et al 2000). Additionally, pre-synaptic KCNQ/M channels at Schaffer collaterals play a specific role in facilitating synaptic transmission (Vervaeke et al 2006). The lack of KCNQ3 channels may result in a sluggish CA3-CA1 transmission that does not favor ripples.

4.3.4 Implications for protection against over-excitability

Despite no signs of spontaneous epilepsy nor other behavioral abnormalities, the *Kcnq3* knockout animals have a strikingly low threshold to induced epilepsy as we demonstrated in

our previous study (Gao 2013). A single ipsilateral microinjection of kainic acid in dorsal CA1, that only induced acute status epilepticus in wild-type animals, caused recurrent epileptiform EEGs in the knockout mice and a swift intractable progress towards generalized, lethal seizures. The augmented burst firing and the altered regulation of firing patterns observed in the present study provide a link between the inadequate KCNQ/M current and the predisposition to epileptogenesis that has been associated with KCNQ3 deficiency (Singh et al 2008, Soh et al 2014). Both theoretical study and experiment models of limbic epilepsy have suggested a critical role of intrinsic bursting neurons in epileptogenesis (Jensen & Yaari 1997, Sanabria et al 2001, Traub & Wong 1982). For instance, the acute epilepsy model using high K^+ treatment showed that depolarization of intrinsic bursting neurons initiated the primary focal bursts and recruited other neurons to generate a larger population discharges manifested as interictal spikes on the EEG. And as the population discharge continued to excite and synchronize more neurons, a massive, self-sustained ictal event would occur. Similar process might well exist for the *Kcnq3* knockout mice, as we also observed the prevalence of ultrafast oscillations of 200–500 Hz near the sites of intrahippocampal injection in our previous study that might indeed reflect the population discharges.

Apart from the general upregulation of burst firing, the loss of KCNQ3 channels can also result in a lack of regulatory leverage mediated by KCNQ/M currents that is normally required to impede the pathological network response to convulsants. In normal hippocampus, treatment of kainic acid induces a transcriptional upregulation of *Kcnq2* and *Kcnq3* (Zhang & Shapiro 2012). Meanwhile, ihKA and the resultant status epilepticus (SE) can drive the network to adapt via both synaptic and intrinsic mechanisms (Sperk et al 2009). In the course of SE, the expression level of many neurotransmitters changes accordingly which include modulators of M-currents such as somatostatin and dynorphin (Delmas & Brown 2005, Moore et al 1988). Considering the low open probability of KCNQ/M channels under normal physiological states, the requirement of an upregulated M-current may explain why the otherwise near-normal *Kcnq3*$^{-/-}$ hippocampus becomes so susceptible to epilepsy.

Furthermore, the swift transition from hippocampal epilepsy to generalized seizures in *Kcnq3* knockout suggests a possible contribution of M-current not only in epileptogenic process but also during the ictogenesis. Since our constitutive model introduced a systematic knockout of *Kcnq3* across brain regions, the M-current deficiency might also significantly alter the functions of certain microcircuits or long-range projections that critically control the propagation of the epileptiform activities and the seizures generalization (Paz & Huguenard 2015). Therefore, the

abnormal neuronal firing and ultrafast oscillations in the hippocampus may not be sufficient to explain the seizure phenotype of the *Kcnq3* knockout mice. Future work is needed to disambiguate the role of KCNQ/M current in epileptogenic and ictogenic circuits.

4.4 Different roles of KCNQ2 and KCNQ3 in the neuronal excitability

The altered burst firing properties of *Kcnq3*$^{-/-}$ pyramidal cells *in vivo* provide a critical update to the existing view that mainly regarded KCNQ2 subunits as the most indispensable components in generating M-currents. While jointly functioning as heteromeric channels, KCNQ2 and KCNQ3 may play divergent roles in shaping the actions of KCNQ/M currents and their modulation of neuronal excitability.

First, the two subunits define different properties of the heteromeric currents. KCNQ2/3 heteromers create currents more than ten times of KCNQ2 homomers while the KCNQ3 homomers do not even produce currents above background levels (Wang et al 1998). The heteromerization primarily increases the surface expression of the channels which is largely attributed to the C-terminus on KCNQ2 (Etxeberria et al 2004, Schwake et al 2000). Thus, the absence of KCNQ2s caused by the knockout or mutation of *Kcnq2* was accompanied by a severe reduction of KCNQ3s while the depletion of *Kcnq3* caused only minor loss of KCNQ2 channels (Soh et al 2014). Moreover, KCNQ3 subunit has an alanine in its pore region that strongly prevents current flow in the homomers but this effect is canceled by the threonine at the equivalent position on KCNQ2 in the heteromeric channels (Etxeberria et al 2004). KCNQ3 subunits, on the other hand, influence the conductance of the heteromeric currents with their higher channel open probability and slope conductance (Schwake et al 2000, Selyanko et al 2001). *Kcnq3* mutations associated with BFNC or epileptic encephalopathy all involve the domains for ion conduction (Allen Nicholas et al 2014). In *Kcnq3* knockout neurons, we would therefore expect a lesser reduction of KCNQ/M currents but a considerably altered current kinetics.

Secondly, KCNQ2 and KCNQ3 differ partially in their subcellular expression. The expression of KCNQ2 is generally higher, with a primary occupation at nodes and axon initial segments (Devaux et al 2004, Tinel et al 1998, Weber et al 2006). In contrast, KCNQ3 are expressed rather diffusely. Although they often co-localize with KCNQ2, their nodal expression is relatively limited (Devaux et al 2004). How the remaining KCNQ2s distribute in *Kcnq3* knockout neurons and conversely, the remaining KCNQ3 in *Kcnq2* knockout are so far overlooked in our and others' studies. This might indeed underlie the discrepancy of the

neuronal excitability between *Kcnq2* and *Kcnq3* knockout model as M-currents at different cellular compartments might regulate different pathways of a neuron's response to its inputs. In hippocampal pyramidal cells, *in vitro* electrophysiology combined with modelling has suggested that peri-somatic KCNQ/M currents control the integration of post-synaptic EPSPs while axonal KCNQ/M currents control the resting membrane potential and action potential threshold (Shah et al 2011). Consistently, *Kcnq2* knockout neurons readily responded to somatic current injection with enlarged after-depolarization (ADP), attenuated medium after-hyperpolarization (mAHP), and increased spiking with less adaptations (Peters et al 2005, Soh et al 2014), while the pyramidal cells in mice with conditional deletion of *Kcnq3* maintained a normal membrane input resistance, action potential threshold and mAHP (Soh et al 2014).

Lastly, the developmental profile of *Kcnq3* expression does not parallel that of *Kcnq2*. It has been suggested that M-current at early postnatal stage is primarily conducted by KCNQ2 homomeric channels while the expression of KCNQ3 appears later in development when the matured neurotransmitters such as GABA take over the inhibitory actions (Geiger et al 2006, Tinel et al 1998). In line with this proposition, animal models of KCNQ2 defect consistently exhibit severe seizures that are often early-onset while restraining the expression of KCNQ2 mutation out of the early neonatal stage was able to restore normal neuronal excitability and prevent seizures in transgene animals (Marguet et al 2015, Peters et al 2005). On the other hand, the resistance to spontaneous seizures in *Kcnq3* knockout mice and their near-normal neuronal excitability *in vitro* suggests some forms of homeostatic adaptation have been acquired during development. However, such adaption would undermine the resilience of the network. When exposed to epileptogenic insults, the *Kcnq3*$^{-/-}$ hippocampus was prone to epilepsy. Therefore, while KCNQ2 channels are unambiguously important, the role of the KCNQ3 channels in regulating network excitability should not be underestimated, especially at disordered states.

4.5 Clinical implications

Despite that the mutations of *KCNQ3* gene have been associated with varied forms of early onset epilepsy in human including BFNC and RE, former electrophysiological studies failed to discern any clear effect of KCNQ3 channels deficiency on the firing behavior of the neurons in animal models. In this work, I demonstrated a significant change of the firing dynamics of hippocampal pyramidal cells *in vivo* in the absence of KCNQ3 channels. In particular, the increased burst firing of neurons and the general shift of firing pattern of the pyramidal

population provide a long-anticipated explanation for the susceptibility to epilepsy in KCNQ3-related channelopathies and animal models.

The increased burst firing in the KCNQ3 knockout has another implication. Linopirdine and XE991, two classic M-current inhibitors, are also cognition enhancing drugs (Lamas et al 1997, Zaczek et al 1998). The effects of these agents in improving attention and memory are thought to arrive via post-synaptic mechanisms caused by an increased release of acetylcholine (Aiken et al 1996). The elevated burstiness in *Kcnq3*$^{-/-}$ pyramidal cells suggests an alternative mechanism for these cognitive enhancers: a direct promotion of burst firing in cortical neurons causes a more potent and reliable release of neurotransmitters at pre-synapses and at the same time introduces a critical time-window at the post-synapses in favor of synaptic modification such as LTP (Lisman 1997). But a shift towards intrinsic bursting imperils the resilience of neural network. Just like the low seizure-threshold shown in *Kcnq3* knockout animals, high dose of linopirdine or XE991 can induce epilepsy.

4.6 Future studies

In our *Kcnq3* knockout model, increased burst probability in pyramidal cells did not translate into disease phenotypes such as spontaneous epilepsy or seizures in drug-free animals. The decreased average firing rate, the near-normal place cell rate maps and the tenacity of theta phase precession suggest that some forms of homeostatic adaptation might take place either at cellular or at the network level. First of all, we have yet to examine if and how the remaining KCNQ channels redistribute across subcellular compartments. Change of the relative weight of the functional KCNQ/M channels in different subcellular compartments could result in homeostatic adaptation of intrinsic membrane properties through, for example, the regulation of other voltage-dependent conductances. Secondly, the adaptation of other network components such as local interneurons has to be reckoned with. To this end, *in vivo* recordings of the interneuron population combined with the confirmation of their cell-types and projections by optogenetic tools would be desired.

Despite that the neural network of *Kcnq3*$^{-/-}$ animals maintains normal physiological functions under drug-free conditions, the network is far less resilient when an extreme condition such as the administration of convulsant is introduced. Here an important question has yet to be answered: is there a sizable upregulation of KCNQ/M currents demanded for the network to prevent or alleviate epileptogenic processes which requires intact KCNQ2/3 heteromeric channels. Although a multi-fold augmentation of *Kcnq2* and *Kcnq3* transcription has been

detected in wild-type animals after kainic acid administration (Zhang & Shapiro 2012), we do not know to what extent the remaining KCNQ2 channels in the absence of KCNQ3 can be upregulated in response to convulsant. Further immunohistochemistry and transcriptional studies are in call to understand the activity-dependent regulation of different KCNQ subunits in disease-related mutant or knockout animal models.

Alternatively, the significant shift of the burstiness distribution observed in the knockout may have tipped the balance of excitability and rendered the network less stable. To test this hypothesis and to determine the boundary of the network excitability within which sufficient resistance against epilepsy can be guaranteed, we would need insights from computational models.

4.7 Concluding remarks

This thesis presents a novel *in vivo* account of how the firing dynamics of hippocampal pyramidal cells changes in the absence of KCNQ3 potassium channels and how such change affects the functions of hippocampus and its resistance to epilepsy. We recognize the importance of KCNQ3 channels in regulating the neuronal excitability alongside the long appreciated KCNQ2 channels. We also demonstrate a new approach of studying channelopathies by combining animal models with *in vivo* electrophysiology, in the hope that this approach will inspire new perspective in understanding the functions of ion channels.

5 Appendix

5.1 Table 2: Properties of place cells

Arena	***Kcnq3*$^{+/+}$**			***Kcnq3*$^{-/-}$**		
	All spikes	**Burst**	**Single spikes**	**All spikes**	**Burst**	**Single spikes**
Peak rate (Hz)	5.38±0.81	2.77±0.44	3.54±0.49	4.62±0.31	3.36±0.26	2.44±0.21
In-field rate (Hz)	2.56±0.13	1.00±0.10	1.68±0.10	2.10±0.07	1.08±0.06	1.51±0.06
Sparsity	0.60±0.09	0.42±0.10	0.61±0.10	0.51±0.03	0.40±0.03	0.61±0.04
Information Density (bit/spike)	0.70±0.26	1.41±0.36	0.65±0.23	0.65±0.09	1.06±0.14	0.35±0.05
Coherence	0.83±0.08	0.73±0.07	0.75±0.08	0.56±0.03	0.50±0.02	0.52±0.05
Track	***Kcnq3*$^{+/+}$**			***Kcnq3*$^{-/-}$**		
	All spikes	**Burst**	**Single spikes**	**All spikes**	**Burst**	**Single spikes**
Peak rate (Hz)	10.89±1.56	8.31±1.70	6.25±0.84	12.68±0.95	10.76±0.90	4.40±0.29
In-field rate (Hz)	3.04±0.24	1.56±0.20	2.33±0.18	3.90±0.21	2.41±0.20	2.15±0.07
Sparsity	0.63±0.10	0.34±0.05	0.67±0.11	0.54±0.03	0.40±0.03	0.53±0.04
Information density (bit/spike)	0.49±0.18	1.10±0.25	0.56±0.26	0.47±0.11	1.08±0.14	0.68±0.11

6 References

Abeles M, Goldstein MH. 1977. Multispike train analysis. *Proceedings of the IEEE* 65: 762-73

Adams PR, Brown DA, Constanti A. 1982. M-currents and other potassium currents in bullfrog sympathetic neurones. *The Journal of Physiology* 330: 537-72

Aiken SP, Zaczek R, Brown BS. 1996. Pharmacology of the neurotransmitter release enhancer Linopirdine (DuP 996), and insights into its mechanism of action In *Advances in Pharmacology*, ed. JT August, MW Anders, F Murad, JT Coyle, pp. 349-84: Academic Press

Allen Nicholas M, Mannion M, Conroy J, Lynch Sally A, Shahwan A, et al. 2014. The variable phenotypes of KCNQ-related epilepsy. *Epilepsia* 55: e99-e105

Alonso A, Llinás RR. 1989. Subthreshold Na^+-dependent theta-like rhythmicity in stellate cells of entorhinal cortex layer II. *Nature* 342: 175-77

Alroy G, Su H, Yaari Y. 1999. Protein kinase C mediates muscarinic block of intrinsic bursting in rat hippocampal neurons. *The Journal of Physiology* 518: 71-79

Andersen P, Bliss TVP, Skrede KK. 1971. Lamellar organization of hippocampal excitatory pathways. *Experimental Brain Research* 13: 222-38

Andersen P, Morris R, Amaral D, O'Keefe J, Bliss DNT, Bliss T. 2007. *The Hippocampus Book*. New York, NY, US: Oxford University Press.

Arvanitaki A. 1939. Recherches sur la réponse oscillatoire locale de l'axone géant isolé de « Sepia ». *Archives Internationales de Physiologie* 49: 209-56

Azouz R, Jensen MS, Yaari Y. 1994. Muscarinic modulation of intrinsic burst firing in rat hippocampal neurons. *European Journal of Neuroscience* 6: 961-66

Azouz R, Jensen MS, Yaari Y. 1996. Ionic basis of spike after-depolarization and burst generation in adult rat hippocampal CA1 pyramidal cells. *The Journal of Physiology* 492: 211-23

Beck H, Yaari Y. 2008. Plasticity of intrinsic neuronal properties in CNS disorders. *Nature Reviews Neuroscience* 9: 357-69

Behr J, Heinemann U. 1996. Low Mg^{2+} induced epileptiform activity in the subiculum before and after disconnection from rat hippocampal and entorhinal cortex slices. *Neuroscience Letters* 205: 25-28

Benardo LS, Prince DA. 1982. Cholinergic excitation of mammalian hippocampal pyramidal cells. *Brain Research* 249: 315-31

Benini R, Avoli M. 2005. Rat subicular networks gate hippocampal output activity in an *in vitro* model of limbic seizures. *The Journal of Physiology* 566: 885-900

Berens P. 2009. CircStat: a MATLAB toolbox for circular statistics. *Journal of Statistical Software* 1: 1-21

Biervert C, Schroeder BC, Kubisch C, Berkovic SF, Propping P, et al. 1998. A potassium channel mutation in neonatal human epilepsy. *Science* 279: 403-06

Bird CM, Burgess N. 2008. The hippocampus and memory: insights from spatial processing. *Nature Reviews Neuroscience* 9: 182-94

Blanche TJ, Spacek MA, Hetke JF, Swindale NV. 2005. Polytrodes: high-density silicon electrode arrays for large-scale multiunit recording. *Journal of Neurophysiology* 93: 2987-3000

Bliss TVP, Collingridge GL. 1993. A synaptic model of memory: long-term potentiation in the hippocampus. *Nature* 361: 31-39

Bragin A, Jando G, Nadasdy Z, Hetke J, Wise K, Buzsaki G. 1995. Gamma (40-100 Hz) oscillation in the hippocampus of the behaving rat. *The Journal of Neuroscience* 15: 47-60

Branco T, Staras K. 2009. The probability of neurotransmitter release: variability and feedback control at single synapses. *Nature Reviews Neuroscience* 10: 373-83

Brankačk J, Stewart M, Fox SE. 1993. Current source density analysis of the hippocampal theta rhythm: associated sustained potentials and candidate synaptic generators. *Brain Research* 615: 310-27

Brown DA, Adams P. 1980. Muscarinic suppression of a novel voltage-sensitive K^+ current in a vertebrate neuron. *Nature* 283: 673-76

Brown DA, Hughes SA, Marsh SJ, Tinker A. 2007. Regulation of M(Kv7.2/7.3) channels in neurons by PIP(2) and products of PIP(2) hydrolysis: significance for receptor-mediated inhibition. *The Journal of Physiology* 582: 917-25

Burgess N, Recce M, O'Keefe J. 1994. A model of hippocampal function. *Neural Networks* 7: 1065-81

Buzsaki G. 2004. Large-scale recording of neuronal ensembles. *Nat Neurosci* 7: 446-51

Buzsáki G. 1986. Hippocampal sharp waves: their origin and significance. *Brain Research* 398: 242-52

Buzsáki G. 2002. Theta oscillations in the hippocampus. *Neuron* 33: 325-40

Buzsáki G, Anastassiou CA, Koch C. 2012. The origin of extracellular fields and currents — EEG, ECoG, LFP and spikes. *Nature Reviews Neuroscience* 13: 407-20

Buzsáki G, Csicsvari J, Dragoi G, Harris K, Henze D, Hirase H. 2002. Homeostatic maintenance of neuronal excitability by burst discharges *in vivo*. *Cerebral Cortex* 12: 893-99

Buzsaki G, Horvath Z, Urioste R, Hetke J, Wise K. 1992. High-frequency network oscillation in the hippocampus. *Science* 256: 1025-27

Buzsáki G, Lai-Wo S L, Vanderwolf CH. 1983. Cellular bases of hippocampal EEG in the behaving rat. *Brain Research Reviews* 6: 139-71

Buzsáki G, Moser EI. 2013. Memory, navigation and theta rhythm in the hippocampal-entorhinal system. *Nature neuroscience* 16: 130-38

Buzsáki G, Penttonen M, Nádasdy Z, Bragin A. 1996. Pattern and inhibition-dependent invasion of pyramidal cell dendrites by fast spikes in the hippocampus *in vivo*. *Proceedings of the National Academy of Sciences of the United States of America* 93: 9921-25

Chacron MJ, Longtin A, Maler L. 2004. To burst or not to burst? *Journal of computational neuroscience* 17: 127-36

Charlier C, Singh NA, Ryan SG, Lewis TB, Reus BE, et al. 1998. A pore mutation in a novel KQT-like potassium channel gene in an idiopathic epilepsy family. *Nature Genetics* 18: 53-55

Chen C. 2005. β-Amyloid increases dendritic Ca^{2+} influx by inhibiting the A-type K^{+} current in hippocampal CA1 pyramidal neurons. *Biochemical and Biophysical Research Communications* 338: 1913-19

Chorev E, Epsztein J, Houweling AR, Lee AK, Brecht M. 2009. Electrophysiological recordings from behaving animals—going beyond spikes. *Current Opinion in Neurobiology* 19: 513-19

Colgin LL. 2016. Rhythms of the hippocampal network. *Nature Reviews Neuroscience* 17: 239-49

Colgin LL, Denninger T, Fyhn M, Hafting T, Bonnevie T, et al. 2009. Frequency of gamma oscillations routes flow of information in the hippocampus. *Nature* 462: 353-57

Colino A, Halliwell JV. 1987. Differential modulation of three separate K-conductances in hippocampal CA1 neurons by serotonin. *Nature* 328: 73-77

Connors BW, Gutnick MJ. 1990. Intrinsic firing patterns of diverse neocortical neurons. *Trends in Neurosciences* 13: 99-104

Connors BW, Gutnick MJ, Prince DA. 1982. Electrophysiological properties of neocortical neurons *in vitro*. *Journal of Neurophysiology* 48: 1302-20

Cooper EC. 2011. Made for “anchorin": Kv7.2/7.3 (KCNQ2/KCNQ3) channels and the modulation of neuronal excitability in vertebrate axons. *Seminars in cell & developmental biology* 22: 185-92

Cooper EC, Aldape KD, Abosch A, Barbaro NM, Berger MS, et al. 2000. Colocalization and coassembly of two human brain M-type potassium channel subunits that are mutated in epilepsy. *Proceedings of the National Academy of Sciences* 97: 4914-19

Cooper EC, Harrington E, Jan YN, Jan LY. 2001. M channel KCNQ2 subunits are localized to key sites for control of neuronal network oscillations and synchronization in mouse brain. *The Journal of Neuroscience* 21: 9529-40

Cooper EC, Jan LY. 2003. M-channels: neurological diseases, neuromodulation, and drug development. *Archives of Neurology* 60: 496-500

Crook SM, Ermentrout GB, Bower JM. 1998. Spike frequency adaptation affects the synchronization properties of networks of cortical oscillators. *Neural Computation* 10: 837-54

Csicsvari J, Hirase H, Czurko A, Buzsáki G. 1998. Reliability and state dependence of pyramidal cell–interneuron synapses in the hippocampus: an ensemble approach in the behaving rat. *Neuron* 21: 179-89

Csicsvari J, Hirase H, Czurkó A, Mamiya A, Buzsáki G. 1999. Oscillatory coupling of hippocampal pyramidal cells and interneurons in the behaving rat. *The Journal of Neuroscience* 19: 274

Csicsvari J, Hirase H, Mamiya A, Buzsáki G. 2000. Ensemble patterns of hippocampal CA3-CA1 neurons during sharp wave-associated population events. *Neuron* 28: 585-94

Cummins TR, Sheets PL, Waxman SG. 2007. The roles of sodium channels in nociception: implications for mechanisms of pain. *Pain* 131: 243-57

Dan Y, Poo M-M. 2004. Spike timing-dependent plasticity of neural circuits. *Neuron* 44: 23-30

Delmas P, Brown DA. 2005. Pathways modulating neural KCNQ/M (Kv7) potassium channels. *Nature Reviews Neuroscience* 6: 850-62

Denham MJ, Borisyuk RM. 2000. A model of theta rhythm production in the septal-hippocampal system and its modulation by ascending brain stem pathways. *Hippocampus* 10: 698-716

Destexhe A, Rudolph M, Paré D. 2003. The high-conductance state of neocortical neurons *in vivo*. *Nature Reviews Neuroscience* 4: 739-51

Devaux JJ, Kleopa KA, Cooper EC, Scherer SS. 2004. KCNQ2 is a nodal K^+ channel. *The Journal of Neuroscience* 24: 1236-44

Dragoi G, Buzsáki G. 2006. Temporal encoding of place sequences by hippocampal cell assemblies. *Neuron* 50: 145-57

Eccles JC, Krnjević K. 1959. Potential changes recorded inside primary afferent fibres within the spinal cord. *The Journal of Physiology* 149: 250-73

Engel Jr J, Bragin A, Staba R, Mody I. 2009. High-frequency oscillations: what is normal and what is not? *Epilepsia* 50: 598-604

Epsztein J, Brecht M, Lee AK. 2011. Intracellular determinants of hippocampal CA1 place and silent cell activity in a novel environment. *Neuron* 70: 109-20

Ermentrout B, Pascal M, Gutkin B. 2001. The effects of spike frequency adaptation and negative feedback on the synchronization of neural oscillators. *Neural Computation* 13: 1285-310

Etienne AS, Maurer R, Séguinot V. 1996. Path integration in mammals and its interaction with visual landmarks. *The Journal of Experimental Biology* 199: 201-09

Etxeberria A, Santana-Castro I, Regalado MP, Aivar P, Villarroel A. 2004. Three mechanisms underlie KCNQ2/3 heteromeric potassium M-channel potentiation. *The Journal of Neuroscience* 24: 9146-52

Fernández-Ruiz A, Oliva A, Nagy GA, Maurer AP, Berényi A, Buzsáki G. 2017. Entorhinal-CA3 dual-input control of spike timing in the hippocampus by theta-gamma coupling. *Neuron* 93: 1213-26

Fisher RA. 1936. The use of multiple measurements in taxonomic problems. *Annals of Eugenics* 7: 179-88

Fister P, Soltirovska-Salamon A, Debeljak M, Paro-Panjan D. 2013. Benign familial neonatal convulsions caused by mutation in KCNQ3, exon 6: a European case. *European Journal of Paediatric Neurology* 17: 308-10

FitzHugh R. 1961. Impulses and physiological states in theoretical models of nerve membrane. *Biophysical Journal* 1: 445-66

Foster DJ, Wilson MA. 2007. Hippocampal theta sequences. *Hippocampus* 17: 1093-99

Fox SE. 1989. Membrane potential and impedance changes in hippocampal pyramidal cells during theta rhythm. *Experimental Brain Research* 77: 283-94

Frank K, Fuortes MGF. 1956. Unitary activity of spinal interneurones of cats. *The Journal of Physiology* 131: 424-35

Freund TF, Antal M. 1988. GABA-containing neurons in the septum control inhibitory interneurons in the hippocampus. *Nature* 336: 170-73

Freund TF, Buzsáki G. 1996. Interneurons of the hippocampus. *Hippocampus* 6: 347-470

Fuchs EC, Zivkovic AR, Cunningham MO, Middleton S, LeBeau FEN, et al. 2007. Recruitment of parvalbumin-positive interneurons determines hippocampal function and associated behavior. *Neuron* 53: 591-604

Fusco C, Frattini D, Bassi MT. 2015. A novel KCNQ3 gene mutation in a child with infantile convulsions and partial epilepsy with centrotemporal spikes. *European Journal of Paediatric Neurology* 19: 102-03

Gao X. 2013. *Hippocampal excitability and synchronization in vivo following genetic ablation of KCNQ3 voltage-gated potassium channel*. Master thesis. Charité – Universitätsmedizin Berlin, Berlin, Germany

Geiger J, Weber YG, Landwehrmeyer B, Sommer C, Lerche H. 2006. Immunohistochemical analysis of KCNQ3 potassium channels in mouse brain. *Neuroscience Letters* 400: 101-04

Gilling M, Rasmussen H, Calloe K, Sequeira A, Baretto M, et al. 2013. Dysfunction of the heteromeric KV7.3/KV7.5 potassium channel is associated with autism spectrum disorders. *Frontiers in Genetics* 4: 54

Golding NL, Jung H-y, Mickus T, Spruston N. 1999. Dendritic calcium spike initiation and repolarization are controlled by distinct potassium channel subtypes in CA1 pyramidal neurons. *The Journal of Neuroscience* 19: 8789-98

Golomb D, Yue C, Yaari Y. 2006. Contribution of persistent Na^+ current and M-type K^+ current to somatic bursting in CA1 pyramidal cells: combined experimental and modeling study. *Journal of Neurophysiology* 96: 1912-26

Gómez-Posada JC, Etxeberría A, Roura-Ferrer M, Areso P, Masin M, et al. 2010. A pore residue of the KCNQ3 potassium M-channel subunit controls surface expression. *The Journal of Neuroscience* 30: 9316-23

Gorski JA, Talley T, Qiu M, Puelles L, Rubenstein JLR, Jones KR. 2002. Cortical excitatory neurons and glia, but not GABAergic neurons, are produced in the Emx1-expressing lineage. *The Journal of Neuroscience* 22: 6309-14

Goutagny R, Jackson J, Williams S. 2009. Self-generated theta oscillations in the hippocampus. *Nature Neuroscience* 12: 1491-93

Graves AR, Moore SJ, Bloss EB, Mensh BD, Kath WL, Spruston N. 2012. Hippocampal pyramidal neurons comprise two distinct cell types that are countermodulated by metabotropic receptors. *Neuron* 76: 776-89

Green JD, Arduini AA. 1954. Hippocampal electrical activity in arousal. *Journal of Neurophysiology* 17: 533-57

Grienberger C, Chen X, Konnerth A. 2014. NMDA receptor-dependent multidendrite Ca^{2+} spikes required for hippocampal burst firing *in vivo*. *Neuron* 81: 1274-81

Grosmark AD, Buzsáki G. 2016. Diversity in neural firing dynamics supports both rigid and learned hippocampal sequences. *Science* 351: 1440-43

Gu N, Vervaeke K, Hu H, Storm JF. 2005. Kv7/KCNQ/M and HCN/h, but not KCa2/SK channels, contribute to the somatic medium after-hyperpolarization and excitability control in CA1 hippocampal pyramidal cells. *The Journal of Physiology* 566: 689-715

Hadley JK, Passmore GM, Tatulian L, Al-Qatari M, Ye F, et al. 2003. Stoichiometry of expressed KCNQ2/KCNQ3 potassium channels and subunit composition of native ganglionic M channels deduced from block by tetraethylammonium. *The Journal of Neuroscience* 23: 5012-19

Hafting T, Fyhn M, Molden S, Moser M-B, Moser EI. 2005. Microstructure of a spatial map in the entorhinal cortex. *Nature* 436: 801-06

Hahn A, Neubauer BA. 2009. Sodium and potassium channel dysfunctions in rare and common idiopathic epilepsy syndromes. *Brain and Development* 31: 515-20

Halliwell JV, Adams PR. 1982. Voltage-clamp analysis of muscarinic excitation in hippocampal neurons. *Brain Research* 250: 71-92

Hangya B, Borhegyi Z, Szilágyi N, Freund TF, Varga V. 2009. GABAergic neurons of the medial septum lead the hippocampal network during theta activity. *The Journal of Neuroscience* 29: 8094-102

Harris KD, Henze DA, Csicsvari J, Hirase H, Buzsáki G. 2000. Accuracy of tetrode spike separation as determined by simultaneous intracellular and extracellular measurements. *Journal of Neurophysiology* 84: 401-14

Harris KD, Henze DA, Hirase H, Leinekugel X, Dragoi G, et al. 2002. Spike train dynamics predicts theta-related phase precession in hippocampal pyramidal cells. *Nature* 417: 738-41

Harris KD, Hirase H, Leinekugel X, Henze DA, Buzsáki G. 2001. Temporal interaction between single spikes and complex spike bursts in hippocampal pyramidal cells. *Neuron* 32: 141-49

Harvey CD, Collman F, Dombeck DA, Tank DW. 2009. Intracellular dynamics of hippocampal place cells during virtual navigation. *Nature* 461: 941-46

Hazan L, Zugaro M, Buzsáki G. 2006. Klusters, NeuroScope, NDManager: A free software suite for neurophysiological data processing and visualization. *Journal of Neuroscience Methods* 155: 207-16

Hebb DO. 1949. *The organization of behavior: a neuropsychological theory*. Oxford, England: John Wiley.

Henze DA, Borhegyi Z, Csicsvari J, Mamiya A, Harris KD, Buzsáki G. 2000. Intracellular features predicted by extracellular recordings in the hippocampus *in vivo*. *Journal of Neurophysiology* 84: 390-400

Herreras O. 2016. Local field potentials: myths and misunderstandings. *Frontiers in Neural Circuits* 10: 101

Hirose S, Zenri F, Akiyoshi H, Fukuma G, Iwata H, et al. 2000. A novel mutation of KCNQ3 (c.925T→C) in a Japanese family with benign familial neonatal convulsions. *Annals of Neurology* 47: 822-26

Hoffman DA, Magee JC, Colbert CM, Johnston D. 1997. K^+ channel regulation of signal propagation in dendrites of hippocampal pyramidal neurons. *Nature* 387: 869-75

Hölscher C, Anwyl R, Rowan MJ. 1997. Stimulation on the positive phase of hippocampal theta rhythm induces long-term potentiation that can be depotentiated by stimulation on the negative phase in Area CA1 *in vivo*. *The Journal of Neuroscience* 17: 6470-77

Houweling AR, Bazhenov M, Timofeev I, Steriade M, Sejnowski TJ. 2005. Homeostatic synaptic plasticity can explain post-traumatic epileptogenesis in chronically isolated neocortex. *Cerebral cortex* 15: 834-45

Howard RJ, Clark KA, Holton JM, Minor DL. 2007. Structural insight into KCNQ (Kv7) channel assembly and channelopathy. *Neuron* 53: 663-75

Hu H, Vervaeke K, Storm JF. 2002. Two forms of electrical resonance at theta frequencies, generated by M-current, h-current and persistent Na+ current in rat hippocampal pyramidal cells. *The Journal of Physiology* 545: 783-805

Huang H, Liu Y, Yuan M, Marron JS. 2015. Statistical significance of clustering using soft thresholding. *Journal of computational and graphical statistics* 24: 975-93

Hubel DH. 1957. Tungsten microelectrode for recording from single units. *Science* 125: 549-50

Hunt CC, Kuno M. 1959. Properties of spinal interneurones. *The Journal of Physiology* 147: 346-63

Huxter JR, Senior TJ, Allen K, Csicsvari J. 2008. Theta phase–specific codes for two-dimensional position, trajectory and heading in the hippocampus. *Nature Neuroscience* 11: 587-94

Izhikevich EM. 2000. Neural excitability, spiking and bursting. *International Journal of Bifurcation and Chaos* 10: 1171-266

Jarsky T, Mady R, Kennedy B, Spruston N. 2007. Distribution of bursting neurons in the CA1 region and the subiculum of the rat hippocampus. *Journal of Comparative Neurology* 506: 535-47

Jensen MS, Azouz R, Yaari Y. 1994. Variant firing patterns in rat hippocampal pyramidal cells modulated by extracellular potassium. *Journal of Neurophysiology* 71: 831-39

Jensen MS, Yaari Y. 1997. Role of intrinsic burst firing, potassium accumulation, and electrical coupling in the elevated potassium model of hippocampal epilepsy. *Journal of Neurophysiology* 77: 1224-33

Jentsch TJ. 2000. Neuronal KCNQ potassium channels:physislogy and role in disease. *Nature Reviews Neuroscience* 1: 21-30

Jung R, Kornmüller AE. 1938. Eine Methodik der Ableitung Iokalisierter Potentialschwankungen aus subcorticalen Hirngebieten. *Archiv für Psychiatrie und Nervenkrankheiten* 109: 1-30

Kaminsky Z, Jones I, Verma R, Saleh L, Trivedi H, et al. 2015. DNA methylation and expression of KCNQ3 in bipolar disorder. *Bipolar Disorders* 17: 150-59

Kamondi A, Acsády L, Wang X-J, Buzsáki G. 1998. Theta oscillations in somata and dendrites of hippocampal pyramidal cells *in vivo*: activity-dependent phase-precession of action potentials. *Hippocampus* 8: 244-61

Kandel ER, Spencer WA. 1961. Electrophysiology of hippocampal neurons: II. After-potentials and repetitive firing. *Journal of Neurophysiology* 24: 243-59

Kempter R, Leibold C, Buzsáki G, Diba K, Schmidt R. 2012. Quantifying circular–linear associations: hippocampal phase precession. *Journal of Neuroscience Methods* 207: 113-24

Kentros C, Hargreaves E, Hawkins RD, Kandel ER, Shapiro M, Muller RV. 1998. Abolition of long-term stability of new hippocampal place cell maps by NMDA receptor blockade. *Science* 280: 2121-26

Kepecs A, Lisman J. 2003. Information encoding and computation with spikes and bursts. *Network: Computation in Neural Systems* 14: 103-18

Kepecs A, Uchida N, Mainen ZF. 2007. Rapid and precise control of sniffing during olfactory discrimination in rats. *Journal of Neurophysiology* 98: 205-13

Kepecs A, Wang X-J. 2000. Analysis of complex bursting in cortical pyramidal neuron models. *Neurocomputing* 32-33: 181-87

Kim J, Tsien RW. 2008. Synapse-specific adaptations to inactivity in hippocampal circuits achieve homeostatic gain control while dampening network reverberation. *Neuron* 58: 925-37

King C, Recce M, O'Keefe J. 1998. The rhythmicity of cells of the medial septum/diagonal band of Broca in the awake freely moving rat: relationships with behaviour and hippocampal theta. *European Journal of Neuroscience* 10: 464-77

Kocsis B, Bragin A, Buzsáki G. 1999. Interdependence of multiple theta generators in the hippocampus: a partial coherence analysis. *The Journal of Neuroscience* 19: 6200-12

Kramis R, Vanderwolf CH, Bland BH. 1975. Two types of hippocampal rhythmical slow activity in both the rabbit and the rat: Relations to behavior and effects of atropine, diethyl ether, urethane, and pentobarbital. *Experimental Neurology* 49: 58-85

Kubisch C, Schroeder BC, Friedrich T, Lütjohann B, El-Amraoui A, et al. 1999. KCNQ4, a novel potassium channel epressed in sensory outer hair cells, is mutated in dominant deafness. *Cell* 96: 437-46

Lamas JA, Selyanko AA, Brown DA. 1997. Effects of a cognition-enhancer, Linopirdine (DuP 996), on M-type potassium currents (IK(M)) some other voltage- and ligand-gated membrane currents in rat sympathetic neurons. *European Journal of Neuroscience* 9: 605-16

Leão RN, Tan HM, Fisahn A. 2009. Kv7/KCNQ channels control action potential phasing of pyramidal neurons during hippocampal gamma oscillations *in vitro*. *The Journal of Neuroscience* 29: 13353-64

Lee AK, Wilson MA. 2002. Memory of sequential experience in the hippocampus during slow wave sleep. *Neuron* 36: 1183-94

Lee MG, Chrobak JJ, Sik A, Wiley RG, Buzsáki G. 1994. Hippocampal theta activity following selective lesion of the septal cholinergic system. *Neuroscience* 62: 1033-47

Lehmann-Horn F, Jurkat-Rott K. 1999. Voltage-gated ion channels and hereditary disease. *Physiological Reviews* 79: 1317-72

Leppert M, Anderson VE, Quattlebaum T, Stauffer D, O'Connell P, et al. 1989. Benign familial neonatal convulsions linked to genetic markers on chromosome 20. *Nature* 337: 647-48

Lewis TB, Leach RJ, Ward K, O'Connell P, Ryan SG. 1993. Genetic heterogeneity in benign familial neonatal convulsions: identification of a new locus on chromosome 8q. *American Journal of Human Genetics* 53: 670-75

Li H, Li N, Shen L, Jiang H, Yang Q, et al. 2008. A novel mutation of KCNQ3 gene in a Chinese family with benign familial neonatal convulsions. *Epilepsy Research* 79: 1-5

Li Y, Gamper N, Hilgemann DW, Shapiro MS. 2005. Regulation of Kv7 (KCNQ) K^+ channel open probability by phosphatidylinositol 4,5-bisphosphate. *The Journal of Neuroscience* 25: 9825-35

Lisman JE. 1997. Bursts as a unit of neural information: making unreliable synapses reliable. *Trends in Neurosciences* 20: 38-43

Liu Y, Hayes DN, Nobel A, Marron JS. 2008. Statistical significance of clustering for high-dimension, low-sample size data. *Journal of the American Statistical Association* 103: 1281-93

Long SB, Campbell EB, MacKinnon R. 2005. Crystal structure of a mammalian voltage-dependent shaker family K^+ channel. *Science* 309: 897-903

Lovett-Barron M, Turi GF, Kaifosh P, Lee PH, Bolze F, et al. 2012. Regulation of neuronal input transformations by tunable dendritic inhibition. *Nature Neuroscience* 15: 423-30

Macrides F, Eichenbaum HB, Forbes WB. 1982. Temporal relationship between sniffing and the limbic theta rhythm during odor discrimination reversal learning. *The Journal of Neuroscience* 2: 1705-17

Madison DV, Lancaster B, Nicoll RA. 1987. Voltage clamp analysis of cholinergic action in the hippocampus. *The Journal of Neuroscience* 7: 733-41

Madison DV, Nicoll RA. 1984. Control of the repetitive discharge of rat CA1 pyramidal neurones *in vitro*. *The Journal of Physiology* 354: 319-31

Magee JC, Carruth M. 1999. Dendritic voltage-gated ion channels regulate the action potential firing mode of hippocampal CA1 pyramidal neurons. *Journal of Neurophysiology* 82: 1895-901

Magee JC, Johnston D. 1997. A synaptically controlled, associative signal for hebbian plasticity in hippocampal neurons. *Science* 275: 209-13

Maljevic S, Vejzovic S, Bernhard MK, Bertsche A, Weise S, et al. 2016. Novel KCNQ3 mutation in a large family with benign familial neonatal epilepsy: a rare cause of neonatal seizures. *Molecular Syndromology* 7: 189-96

Maljevic S, Wuttke TV, Lerche H. 2008. Nervous system KV7 disorders: breakdown of a subthreshold brake. *The Journal of Physiology* 586: 1791-801

Marguet SL, Le-Schulte VTQ, Merseburg A, Neu A, Eichler R, et al. 2015. Treatment during a vulnerable developmental period rescues a genetic epilepsy. *Nature Medicine* 21: 1436-44

Martin C, Beshel J, Kay LM. 2007. An olfacto-hippocampal network is dynamically involved in odor-discrimination learning. *Journal of Neurophysiology* 98: 2196-205

McCormick DA, Connors BW, Lighthall JW, Prince DA. 1985. Comparative electrophysiology of pyramidal and sparsely spiny stellate neurons of the neocortex. *Journal of Neurophysiology* 54: 782-806

McHugh TJ, Blum KI, Tsien JZ, Tonegawa S, Wilson MA. 1996. Impaired hippocampal representation of space in CA1-specific NMDAR1 knockout mice. *Cell* 87: 1339-49

McNaughton BL, Barnes CA, O'Keefe J. 1983a. The contributions of position, direction, and velocity to single unit activity in the hippocampus of freely-moving rats. *Experimental Brain Research* 52: 41-49

McNaughton BL, O'Keefe J, Barnes CA. 1983b. The stereotrode: A new technique for simultaneous isolation of several single units in the central nervous system from multiple unit records. *Journal of Neuroscience Methods* 8: 391-97

Mehta MR, Lee AK, Wilson MA. 2002. Role of experience and oscillations in transforming a rate code into a temporal code. *Nature* 417: 741-46

Metz AE, Jarsky T, Martina M, Spruston N. 2005. R-type calcium channels contribute to afterdepolarization and bursting in hippocampal CA1 pyramidal neurons. *The Journal of Neuroscience* 25: 5763-73

Miceli F, Striano P, Soldovieri MV, Fontana A, Nardello R, et al. 2015. A novel KCNQ3 mutation in familial epilepsy with focal seizures and intellectual disability. *Epilepsia* 56: e15-e20

Miles R, Wong RK. 1987. Inhibitory control of local excitatory circuits in the guinea-pig hippocampus. *The Journal of Physiology* 388: 611-29

Mizumori SJY, Perez GM, Alvarado MC, Barnes CA, McNaughton BL. 1990. Reversible inactivation of the medial septum differentially affects two forms of learning in rats. *Brain Research* 528: 12-20

Mizuseki K, Buzsáki G. 2013. Preconfigured, skewed distribution of firing rates in the hippocampus and entorhinal cortex. *Cell Reports* 4: 1010-21

Mizuseki K, Diba K, Pastalkova E, Buzsáki G. 2011. Hippocampal CA1 pyramidal cells form functionally distinct sublayers. *Nature Neuroscience* 14: 1174-81

Mizuseki K, Sirota A, Pastalkova E, Buzsáki G. 2009. Theta oscillations provide temporal windows for local circuit computation in the entorhinal-hippocampal loop. *Neuron* 64: 267-80

Moore SD, Madamba SG, Joels M, Siggins GR. 1988. Somatostatin augments the M-current in hippocampal neurons. *Science* 239: 278-80

Mountcastle VB, Davies PW, Berman AL. 1957. Response porperties of neurons of cat's somatic sensory cortex to peripheral stimuli. *Journal of Neurophysiology* 20: 374-407

Muller RU, Kubie JL. 1987. The effects of changes in the environment on the spatial firing of hippocampal complex-spike cells. *The Journal of Neuroscience* 7: 1951-68

Muller RU, Kubie JL. 1989. The firing of hippocampal place cells predicts the future position of freely moving rats. *The Journal of Neuroscience* 9: 4101-10

Nádasdy Z, Hirase H, Czurkó A, Csicsvari J, Buzsáki G. 1999. Replay and time compression of recurring spike sequences in the hippocampus. *The Journal of Neuroscience* 19: 9497-507

Neubauer BA, Waldegger S, Heinzinger J, Hahn A, Kurlemann G, et al. 2008. KCNQ2 and KCNQ3 mutations contribute to different idiopathic epilepsy syndromes. *Neurology* 71: 177-83

Neyroud N, Tesson F, Denjoy I, Leibovici M, Donger C, et al. 1997. A novel mutation in the potassium channel gene KVLQT1 causes the Jervell and Lange-Nielsen cardioauditory syndrome. *Nature Genetics* 15: 186-89

O'Keefe J. 1976. Place units in the hippocampus of the freely moving rat. *Experimental Neurology* 51: 78-109

O'Keefe J, Burgess N. 1996. Geometric determinants of the place fields of hippocampal neurons. *Nature* 381: 425-28

O'Keefe J, Dostrovsky J. 1971. The hippocampus as a spatial map. Preliminary evidence from unit activity in the freely-moving rat. *Brain Research* 34: 171-75

O'Keefe J, Nadel L. 1978. *The hippocampus as a cognitive map*. Oxford: Clarendon Press.

O'Keefe J, Recce ML. 1993. Phase relationship between hippocampal place units and the EEG theta rhythm. *Hippocampus* 3: 317-30

O'Keefe J, Burgess N. 2005. Dual phase and rate coding in hippocampal place cells: theoretical significance and relationship to entorhinal grid cells. *Hippocampus* 15: 853-66

Otto T, Eichenbaum H, Wible CG, Wiener SI. 1991. Learning-related patterns of CA1 spike trains parallel stimulation parameters optimal for inducing hippocampal long-term potentiation. *Hippocampus* 1: 181-92

Pan Z, Kao T, Horvath Z, Lemos J, Sul J-Y, et al. 2006. A common ankyrin-G-based mechanism retains KCNQ and NaV channels at electrically active domains of the axon. *The Journal of Neuroscience* 26: 2599-613

Pape HC. 1996. Queer current and pacemaker: the hyperpolarization-activated cation current in neurons. *Annual Review of Physiology* 58: 299-327

Paulsen O, Sejnowski TJ. 2000. Natural patterns of activity and long-term synaptic plasticity. *Current opinion in neurobiology* 10: 172-79

Paxinos G, Franklin KBJ. 2004. *The mouse brain in stereotaxic coordinates*. Elsevier Academic Press.

Paz JT, Huguenard JR. 2015. Microcircuits and their interactions in epilepsy: is the focus out of focus? *Nature Neuroscience* 18: 351-59

Peters HC, Hu H, Pongs O, Storm JF, Isbrandt D. 2005. Conditional transgenic suppression of M channels in mouse brain reveals functions in neuronal excitability, resonance and behavior. *Nature Neuroscience* 8: 51-60

Petsche H, Pockberger H, Rappelsberger P. 1984. On the search for the sources of the electroencephalogram. *Neuroscience* 11: 1-27

Petsche H, Stumpf C, Gogolak G. 1962. The significance of the rabbit's septum as a relay station between the midbrain and the hippocampus I. The control of hippocampus arousal activity by the septum cells. *Electroencephalography and Clinical Neurophysiology* 14: 202-11

Pham D, Dimov S, Nguyen C. 2005. Selection of K in K-means clustering. *Journal of Mechanical Engineering Science* 219: 103-19

Pike FG, Meredith RM, Olding AWA, Paulsen O. 1999. Postsynaptic bursting is essential for 'Hebbian' induction of associative long-term potentiation at excitatory synapses in rat hippocampus. *The Journal of Physiology* 518: 571-76

Popa D, Duvarci S, Popescu AT, Léna C, Paré D. 2010. Coherent amygdalocortical theta promotes fear memory consolidation during paradoxical sleep. *Proceedings of the National Academy of Sciences* 107: 6516-19

Prescott SA, Ratté S, De Koninck Y, Sejnowski TJ. 2008. Pyramidal neurons switch from integrators *in vitro* to resonators under *in vivo*-like conditions. *Journal of Neurophysiology* 100: 3030-42

Prescott SA, Sejnowski TJ. 2008. Spike-rate coding and spike-time coding are affected oppositely by different adaptation mechanisms. *The Journal of Neuroscience* 28: 13649-61

Ranck JB, Jr. 1973. Studies on single neurons in dorsal hippocampal formation and septum in unrestrained rats. I. Behavioral correlates and firing repertoires. *Experimental Neurology* 41: 461-531

Rapp PR, Gallagher M. 1996. Preserved neuron number in the hippocampus of aged rats with spatial learning deficits. *Proceedings of the National Academy of Sciences of the United States of America* 93: 9926-30

Rinzel J. 1987. A formal classification of bursting mechanisms in excitable systems In *Mathematical Topics in Population Biology, Morphogenesis and Neurosciences: Proceedings of an International Symposium held in Kyoto, November 10–15, 1985*, ed. E Teramoto, M Yumaguti, pp. 267-81. Berlin, Heidelberg: Springer Berlin Heidelberg

Rinzel J, Ermentrout B. 1998. Analysis of neural excitability and oscillations In *Methods in neuronal modeling*, ed. C Koch, S Idan, pp. 135-69. Cambridge, MA, USA: MIT Press

Ronen GM, Rosales TO, Connolly M, Anderson VE, Leppert M. 1993. Seizure characteristics in chromosome 20 benign familial neonatal convulsions. *Neurology* 43: 1355-60

Royer S, Zemelman BV, Losonczy A, Kim J, Chance F, et al. 2012. Control of timing, rate and bursts of hippocampal place cells by dendritic and somatic inhibition. *Nature Neuroscience* 15: 769-75

Rundfeldt C, Netzer R. 2000. The novel anticonvulsant retigabine activates M-currents in Chinese hamster ovary-cells tranfected with human KCNQ2/3 subunits. *Neuroscience Letters* 282: 73-76

Sanabria ERG, Su H, Yaari Y. 2001. Initiation of network bursts by Ca^{2+}-dependent intrinsic bursting in the rat pilocarpine model of temporal lobe epilepsy. *The Journal of Physiology* 532: 205-16

Schmitt N, Schwarz M, Peretz A, Abitbol I, Attali B, Pongs O. 2000. A recessive C-terminal Jervell and Lange-Nielsen mutation of the KCNQ1 channel impairs subunit assembly. *The EMBO Journal* 19: 332-40

Schroeder BC, Hechenberger M, Weinreich F, Kubisch C, Jentsch TJ. 2000. KCNQ5, a novel potassium channel broadly expressed in brain, mediates M-type currents. *Journal of Biological Chemistry* 275: 24089-95

Schroeder BC, Kubisch C, Stein V, Jentsch TJ. 1998. Moderate loss of function of cyclic-AMP-modulated KCNQ2/KCNQ3 K^+ channels causes epilepsy. *Nature* 396: 687-90

Schwake M, Pusch M, Kharkovets T, Jentsch TJ. 2000. Surface expression and single channel properties of KCNQ2/KCNQ3, M-type K^+ channels involved in epilepsy. *Journal of Biological Chemistry* 275: 13343-48

Schweitzer P. 2000. Cannabinoids decrease the K^+ M-current in hippocampal CA1 neurons. *The Journal of Neuroscience* 20: 51-58

Scoville WB, Milner B. 1957. Loss of recent memory after bilateral hippocampal lesions. *Journal of Neurology, Neurosurgery & Psychiatry* 20: 11-21

Sejnowski TJ, Paulsen O. 2006. Network oscillations: emerging computational principles. *The Journal of Neuroscience* 26: 1673-76

Selyanko AA, Hadley JK, Brown DA. 2001. Properties of single M-type KCNQ2/KCNQ3 potassium channels expressed in mammalian cells. *The Journal of Physiology* 534: 15-24

Selyanko AA, Hadley JK, Wood IC, Abogadie FC, Jentsch TJ, Brown DA. 2000. Inhibition of KCNQ1-4 potassium channels expressed in mammalian cells via M(1) muscarinic acetylcholine receptors. *The Journal of Physiology* 522: 349-55

Shah MM, Migliore M, Brown DA. 2011. Differential effects of Kv7 (M-) channels on synaptic integration in distinct subcellular compartments of rat hippocampal pyramidal neurons. *The Journal of Physiology* 589: 6029-38

Shah MM, Migliore M, Valencia I, Cooper EC, Brown DA. 2008. Functional significance of axonal Kv7 channels in hippocampal pyramidal neurons. *Proceedings of the National Academy of Sciences* 105: 7869-74

Sharp PE, Green C. 1994. Spatial correlates of firing patterns of single cells in the subiculum of the freely moving rat. *The Journal of Neuroscience* 14: 2339-56

Singer W. 1993. Synchronization of cortical activity and its putative role in information processing and learning. *Annual Review of Physiology* 55: 349-74

Singh NA, Charlier C, Stauffer D, DuPont BR, Leach RJ, et al. 1998. A novel potassium channel gene, KCNQ2, is mutated in an inherited epilepsy of newborns. *Nature Genetics* 18: 25-29

Singh NA, Otto JF, Jill Dahle E, Pappas C, Leslie JD, et al. 2008. Mouse models of human KCNQ2 and KCNQ3 mutations for benign familial neonatal convulsions show seizures and neuronal plasticity without synaptic reorganization. *The Journal of Physiology* 586: 3405-23

Singh NA, Westenskow P, Charlier C, Pappas C, Leslie J, et al. 2003. KCNQ2 and KCNQ3 potassium channel genes in benign familial neonatal convulsions: expansion of the functional and mutation spectrum. *Brain* 126: 2726-37

Skaggs WE, McNaughton BL, Wilson MA, Barnes CA. 1996. Theta phase precession in hippocampal neuronal populations and the compression of temporal sequences. *Hippocampus* 6: 149-72

Sneider J, Chrobak J, Quirk M, Oler J, Markus EJ. 2006. Differential behavioral state-dependence in the burst properties of CA3 and CA1 neurons. *Neuroscience* 141: 1665-77

Soh H, Pant R, LoTurco JJ, Tzingounis AV. 2014. Conditional deletions of epilepsy-associated KCNQ2 and KCNQ3 channels from cerebral cortex cause differential effects on neuronal excitability. *The Journal of Neuroscience* 34: 5311-21

Soldovieri MV, Boutry-Kryza N, Milh M, Doummar D, Heron B, et al. 2013. Novel KCNQ2 and KCNQ3 mutations in a large cohort of families with benign neonatal epilepsy: first dvidence for an altered channel regulation by syntaxin-1A. *Human Mutation* 35: 356-67

Solstad T, Moser EI, Einevoll GT. 2006. From grid cells to place cells: a mathematical model. *Hippocampus* 16: 1026-31

Sperk G, Drexel M, Pirker S. 2009. Neuronal plasticity in animal models and the epileptic human hippocampus. *Epilepsia* 50: 29-31

Staff NP, Jung H-Y, Thiagarajan T, Yao M, Spruston N. 2000. Resting and active properties of pyramidal neurons in subiculum and CA1 of rat hippocampus. *Journal of Neurophysiology* 84: 2398-408

Steinlein OK, Conrad C, Weidner B. 2007. Benign familial neonatal convulsions: always benign? *Epilepsy Research* 73: 245-49

Steriade M. 2000. Corticothalamic resonance, states of vigilance and mentation. *Neuroscience* 101: 243-76

Stevens CF, Wang Y. 1995. Facilitation and depression at single central synapses. *Neuron* 14: 795-802

Stewart M, Fox SE. 1990. Do septal neurons pace the hippocampal theta rhythm? *Trends in Neurosciences* 13: 163-69

Storm JF. 1987. Action potential repolarization and a fast after-hyperpolarization in rat hippocampal pyramidal cells. *The Journal of Physiology* 385: 733-59

Storm JF. 1989. An after-hyperpolarization of medium duration in rat hippocampal pyramidal cells. *The Journal of Physiology* 409: 171-90

Su H, Alroy G, Kirson ED, Yaari Y. 2001. Extracellular calcium modulates persistent sodium current-dependent burst-firing in hippocampal pyramidal neurons. *The Journal of Neuroscience* 21: 4173-82

Suh B-C, Hille B. 2002. Recovery from muscarinic modulation of M current channels requires phosphatidylinositol 4,5-bisphosphate synthesis. *Neuron* 35: 507-20

Suzuki SS, Smith GK. 1985. Burst characteristics of hippocampal complex spike cells in the awake rat. *Experimental Neurology* 89: 90-95

Takács VT, Freund TF, Gulyás AI. 2008. Types and synaptic connections of hippocampal inhibitory neurons reciprocally connected with the medial septum. *European Journal of Neuroscience* 28: 148-64

Tasaki I. 1954. Nerve impluses in individual auditory nerve fibers of guinea pig. *Journal of Neurophysiology* 17: 97-122

Tatulian L, Brown DA. 2003. Effect of the KCNQ potassium channel opener retigabine on single KCNQ2/3 channels expressed in CHO cells. *The Journal of Physiology* 549: 57-63

Taube JS, Muller RU, Ranck JB. 1990. Head-direction cells recorded from the postsubiculum in freely moving rats. I. Description and quantitative analysis. *The Journal of Neuroscience* 10: 420-35

Teles-Grilo Ruivo LM, Mellor JR. 2013. Cholinergic modulation of hippocampal network function. *Frontiers in synaptic neuroscience* 5: 2

Thomas MJ, Watabe AM, Moody TD, Makhinson M, O'Dell TJ. 1998. Postsynaptic complex spike bursting enables the induction of LTP by theta frequency synaptic stimulation. *The Journal of Neuroscience* 18: 7118-26

Thomson AM. 2000. Facilitation, augmentation and potentiation at central synapses. *Trends in Neurosciences* 23: 305-12

Tinel N, Lauritzen I, Chouabe C, Lazdunski M, Borsotto M. 1998. The KCNQ2 potassium channel: splice variants, functional and developmental expression. Brain localization and comparison with KCNQ3. *FEBS Letters* 438: 171-76

Toth K, Borhegyi Z, Freund TF. 1993. Postsynaptic targets of GABAergic hippocampal neurons in the medial septum-diagonal band of broca complex. *The Journal of Neuroscience* 13: 3712-24

Trasande CA, Ramirez J-M. 2007. Activity deprivation leads to seizures in hippocampal slice cultures: is epilepsy the consequence of homeostatic plasticity? *Journal of Clinical Neurophysiology* 24: 154-64

Traub RD, Wong RK. 1982. Cellular mechanism of neuronal synchronization in epilepsy. *Science* 216: 745-47

Traub RD, Wong RK, Miles R, Michelson H. 1991. A model of a CA3 hippocampal pyramidal neuron incorporating voltage-clamp data on intrinsic conductances. *Journal of Neurophysiology* 66: 635-50

Tzingounis AV, Heidenreich M, Kharkovets T, Spitzmaul G, Jensen HS, et al. 2010. The KCNQ5 potassium channel mediates a component of the afterhyperpolarization current in mouse hippocampus. *Proceedings of the National Academy of Sciences of the United States of America* 107: 10232-37

Tzingounis AV, Nicoll RA. 2008. Contribution of KCNQ2 and KCNQ3 to the medium and slow afterhyperpolarization currents. *Proceedings of the National Academy of Sciences of the United States of America* 105: 19974-79

van der Meer MAA, Redish AD. 2011. Theta phase precession in rat ventral striatum links place and reward information. *The Journal of Neuroscience* 31: 2843-54

Vandecasteele M, Varga V, Berényi A, Papp E, Barthó P, et al. 2014. Optogenetic activation of septal cholinergic neurons suppresses sharp wave ripples and enhances theta oscillations in the hippocampus. *Proceedings of the National Academy of Sciences of the United States of America* 111: 13535-40

Vanderwolf CH. 1969. Hippocampal electrical activity and voluntary movement in the rat. *Electroencephalography and Clinical Neurophysiology* 26: 407-18

Varshney LR, Sjöström PJ, Chklovskii Dmitri B. 2006. Optimal information storage in noisy synapses under resource constraints. *Neuron* 52: 409-23

Vervaeke K, Gu N, Agdestein C, Hu H, Storm JF. 2006. Kv7/KCNQ/M-channels in rat glutamatergic hippocampal axons and their role in regulation of excitability and transmitter release. *The Journal of Physiology* 576: 235-56

Vyazovskiy VV, Olcese U, Lazimy YM, Faraguna U, Esser SK, et al. 2009. Cortical firing and sleep homeostasis. *Neuron* 63: 865-78

Wang H-S, Pan Z, Shi W, Brown BS, Wymore RS, et al. 1998. KCNQ2 and KCNQ3 potassium channel subunits: molecular correlates of the M-channel. *Science* 282: 1890-93

Wang X-J. 2002. Pacemaker neurons for the theta rhythm and their synchronization in the septohippocampal reciprocal loop. *Journal of Neurophysiology* 87: 889-900

Wang X-J, Buzsáki G. 1996. Gamma oscillation by synaptic inhibition in a hippocampal interneuronal network model. *The Journal of Neuroscience* 16: 6402-13

Watanabe H, Nagata E, Kosakai A, Nakamura M, Yokoyama M, et al. 2000. Disruption of the epilepsy KCNQ2 gene results in neural hyperexcitability. *Journal of Neurochemistry* 75: 28-33

Weber YG, Geiger J, Kämpchen K, Landwehrmeyer B, Sommer C, Lerche H. 2006. Immunohistochemical analysis of KCNQ2 potassium channels in adult and developing mouse brain. *Brain Research* 1077: 1-6

Wilson MA, McNaughton BL. 1993. Dynamics of the hippocampal ensemble code for space. *Science* 261: 1055-58

Winson J. 1978. Loss of hippocampal theta rhythm results in spatial memory deficit in the rat. *Science* 201: 160-63

Wittenberg GM, Wang SSH. 2006. Malleability of spike-timing-dependent plasticity at the CA3–CA1 synapse. *The Journal of Neuroscience* 26: 6610-17

Wong RK, Prince DA. 1981. Afterpotential generation in hippocampal pyramidal cells. *Journal of Neurophysiology* 45: 86-97

Xu W, Morishita W, Buckmaster PS, Pang ZP, Malenka RC, Südhof TC. 2012. Distinct neuronal coding schemes in memory revealed by selective erasure of fast synchronous synaptic transmission. *Neuron* 73: 990-1001

Yaari Y, Yue C, Su H. 2007. Recruitment of apical dendritic T-type Ca^{2+} channels by backpropagating spikes underlies de novo intrinsic bursting in hippocampal epileptogenesis. *The Journal of Physiology* 580: 435-50

Ylinen A, Soltész I, Bragin A, Penttonen M, Sik A, Buzsáki G. 1995. Intracellular correlates of hippocampal theta rhythm in identified pyramidal cells, granule cells, and basket cells. *Hippocampus* 5: 78-90

Yue C, Remy S, Su H, Beck H, Yaari Y. 2005. Proximal persistent Na^{+} channels drive spike afterdepolarizations and associated bursting in adult CA1 pyramidal cells. *The Journal of Neuroscience* 25: 9704-20

Yue C, Yaari Y. 2004. KCNQ/M channels control spike afterdepolarization and burst generation in hippocampal neurons. *The Journal of Neuroscience* 24: 4614-24

Yue C, Yaari Y. 2006. Axo-somatic and apical dendritic Kv7/M channels differentially regulate the intrinsic excitability of adult rat CA1 pyramidal cells. *Journal of Neurophysiology* 95: 3480-95

Zaczek R, Chorvat RJ, Saye JA, Pierdomenico ME, Maciag CM, et al. 1998. Two new potent neurotransmitter release enhancers, 10,10-bis(4-pyridinylmethyl)-9(10H)-anthracenone and 10,10-bis(2-fluoro-4-pyridinylmethyl)-9(10H)-anthracenone: comparison to Linopirdine. *Journal of Pharmacology and Experimental Therapeutics* 285: 724-30

Zara F, Specchio N, Striano P, Robbiano A, Gennaro E, et al. 2013. Genetic testing in benign familial epilepsies of the first year of life: clinical and diagnostic significance. *Epilepsia* 54: 425-36

Zhang H, Craciun LC, Mirshahi T, Rohács T, Lopes CMB, et al. 2003. PIP(2) activates KCNQ channels, and its hydrolysis underlies receptor-mediated inhibition of M currents. *Neuron* 37: 963-75

Zhang J, Shapiro MS. 2012. Activity-dependent transcriptional regulation of M-type (Kv7) K(+) channels by AKAP79/150-mediated NFAT actions. *Neuron* 76: 1133-46

Zugaro MB, Monconduit L, Buzsaki G. 2005. Spike phase precession persists after transient intrahippocampal perturbation. *Nature Neuroscience* 8: 67-71

7 Abbreviation

ACG	auto-correlogram
ADP	after-depolarization
AIS	axon initial segment
ANOVA	analysis of variance
BFIS	benign familial infantile seizures
BFNC	benign familial neonatal convulsions
CA	cornu ammonis
CCG	cross-correlogram
CCH	cross-correlation histogram
CDF	cumulative distribution function
CHO	Chinese hamster ovary cells
CI	cluster index
CSI	complex spike index
DG	dentate gyrus
EC	entorhinal cortex
EEG	electroencephalography
EPSP	excitatory postsynaptic potential
FFT	fast Fourier transform
fMRI	functional magnetic resonance imaging
GABA	gamma-Aminobutyric acid
HD	head direction
ihKA	intra-hippocampal administration of kainic acid
IPSP	inhibitory postsynaptic potential
ISI	inter-spike intervals
KCNQ	potassium voltage-gated channel subfamily Q
LFP	local field potential
LIA	large irregular activity
mAChR	muscarinic acetylcholine receptor
mAHP	medium after-hyperpolarization
MSDB	medial septal nucleus and the nucleus of diagonal band of Broca
NMDA	N-Methyl-D-aspartic acid
O-LM	oriens-lacunosum moleculare
PC	principal component
PCA	principal component analysis
PIP_2	phosphatidylinositol 4,5-bisphosphate
PSD	power spectral density
RE	Rolandic epilepsy
REM	rapid eye movement
SE	status epilepticus
SOM	somatostatin-expressing
TLE	temporal lobe epilepsy
TTX	tetrodotoxin
UFO	ultrafast oscillation
XE-991	10,10-bis(4-Pyridinylmethyl)-9(10H)-anthracenone dihydrochloride
XO	xenopus oocyte

Selbständigkeitserklärung

Ich erkläre, dass ich die vorliegende Arbeit selbständig und nur unter Verwendung der angegebenen Literatur und Hilfsmittel angefertigt habe.

Berlin, den 10.05.2019

Xiaojie Gao